Searches for the production of *two* Higgs bosons using the CMS detector

Souvik Das on behalf of the **CMS Collaboration**

PANIC 2014, 26 August 2014

Introduction

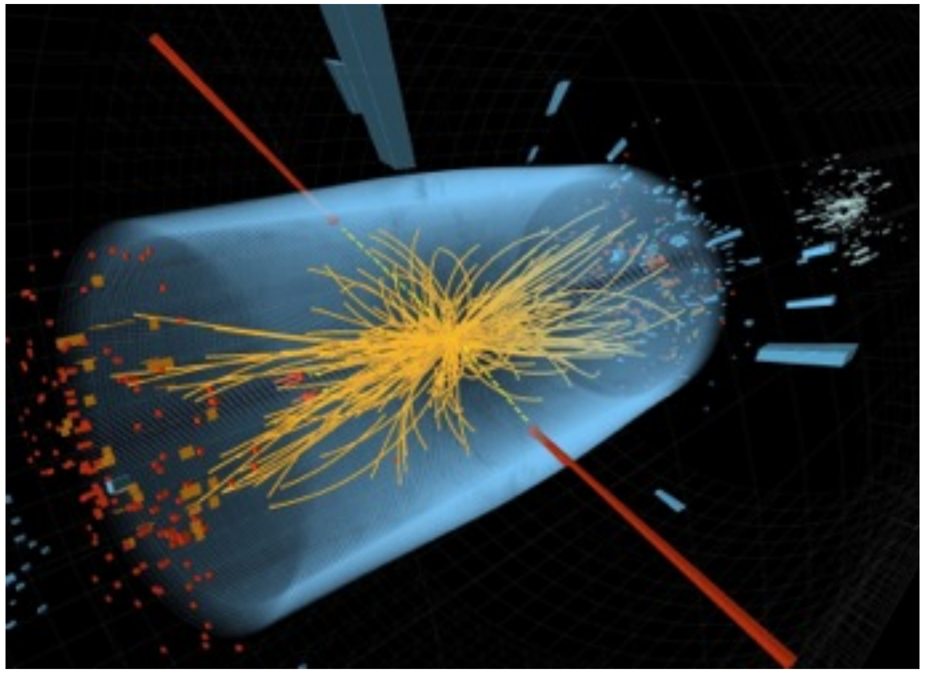

CMS and ATLAS have observed a
Standard Model-like Higgs boson

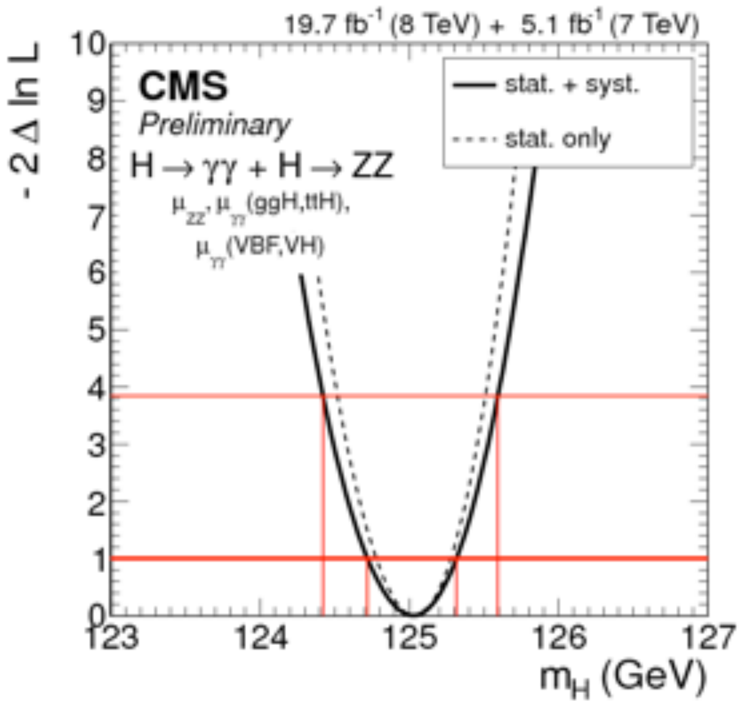

Higgs mass in expected range

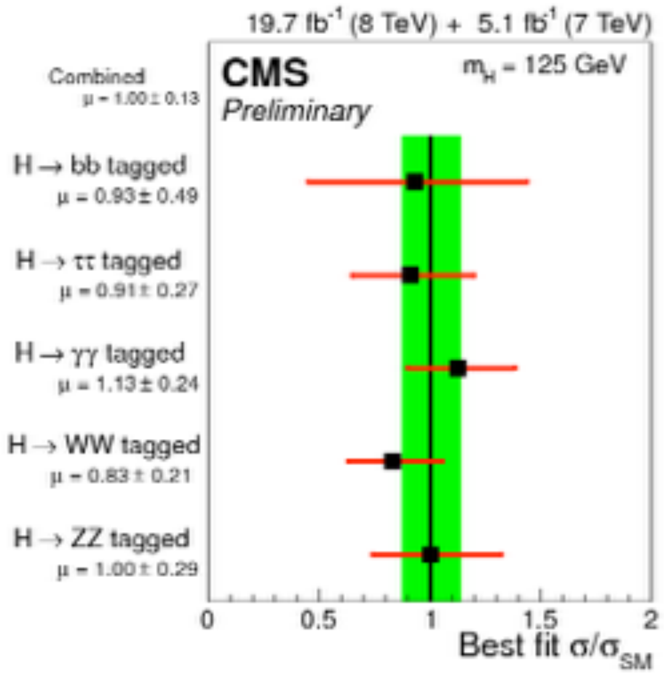

Couplings match SM predictions
Spin-parity consistent with 0^+

Introduction

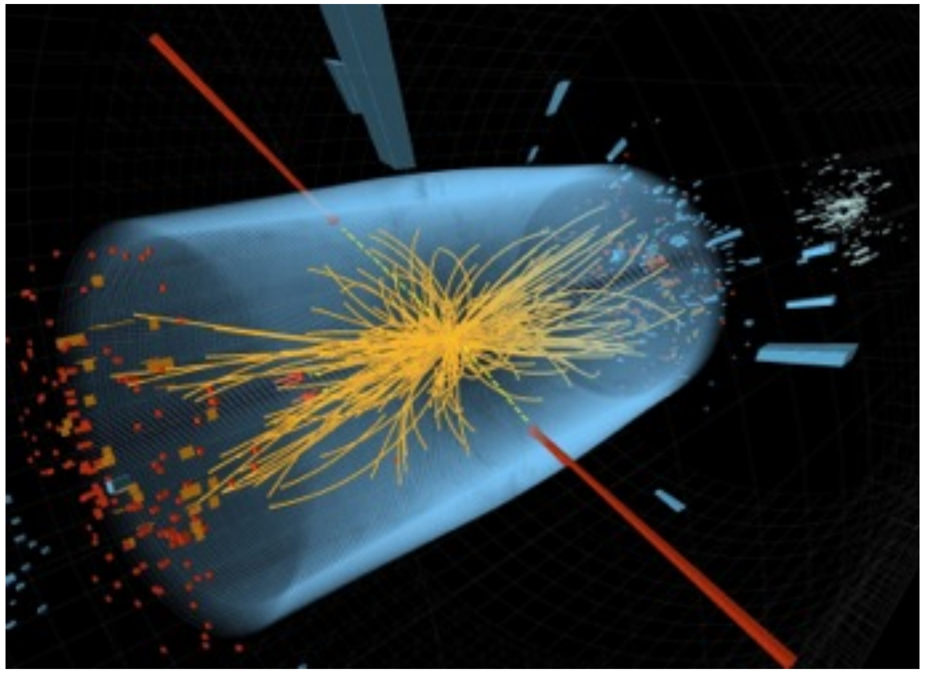

CMS and ATLAS have observed a Standard Model-like Higgs boson

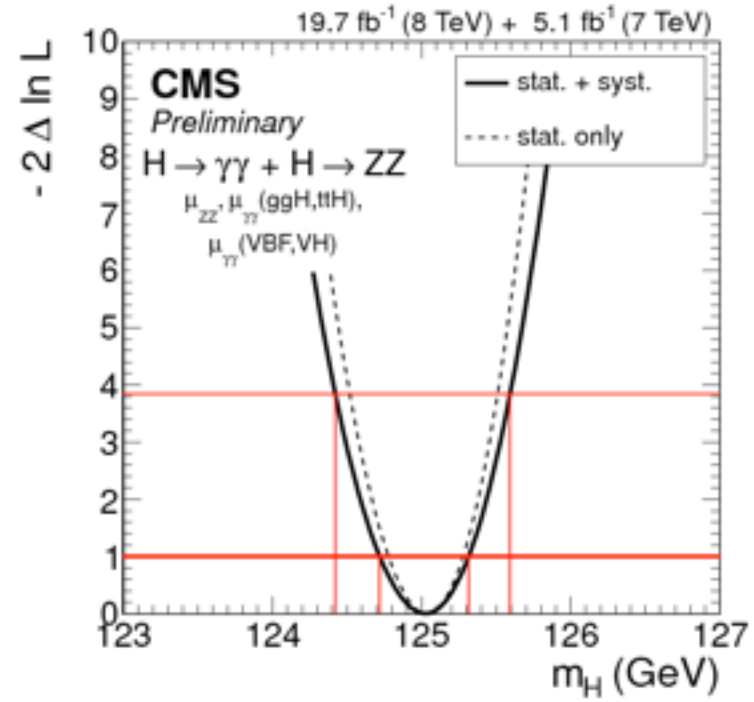

Higgs mass in expected range

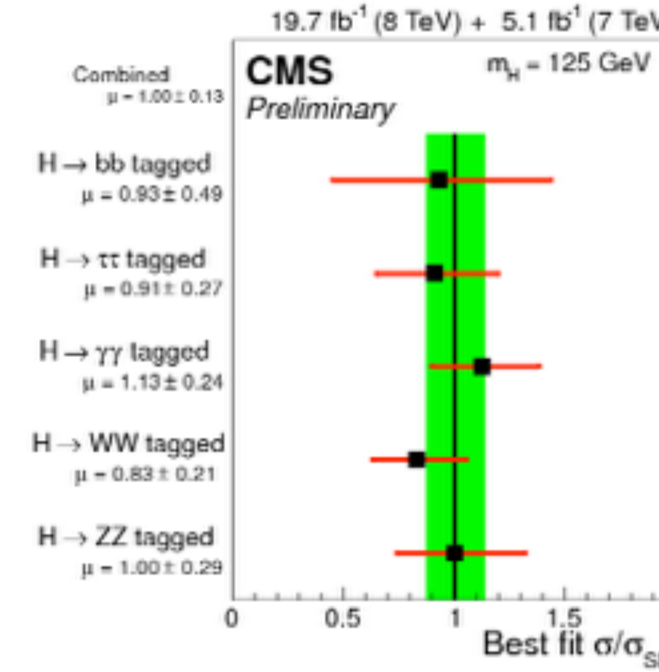

Couplings match SM predictions
Spin-parity consistent with 0^+

The **Higgs boson (H) is now a tool** for searches Beyond the Standard Model. No resonant HH production in the Standard Model. Negligible non-resonant HH production. **Experimentally feasible and important to search for HH resonances.**

Some **theoretical motivation** for resonant HH production
- 2 Higgs-doublet models
- Warped extra dimensions

Experimental searches at CMS
- Multi-leptons and Photons Final State: X→HH→(ll)(ll/γ)
- 2 Photons and 2 b-jets Final State: X→HH→(γγ)($b\bar{b}$)
- 4 b-jet Final State: X→HH→($b\bar{b}$)($b\bar{b}$)

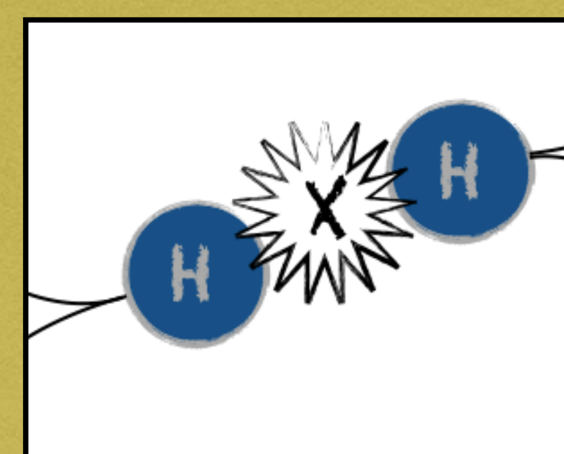

Example Theoretical Models

Example Theoretical Models

2 Higgs-Doublet Models

- Two EWK SU(2) Higgs doublets, $\mathbf{\Phi}_1$ and $\mathbf{\Phi}_2$
- 5 Higgs bosons emerge: **H**, **h**, **A**, **H⁺**, **H⁻**
- Parameters for theoretical exclusion:
  tan$\boldsymbol{\beta}$ and **cos(**$\boldsymbol{\beta}$ **- α)**, where

$$\tan\beta = \left|\frac{\langle\Phi_2^0\rangle}{\langle\Phi_1^0\rangle}\right| \qquad \begin{pmatrix} \sqrt{2}\,\mathrm{Re}(\Phi_2^0) - v_2 \\ \sqrt{2}\,\mathrm{Re}(\Phi_1^0) - v_1 \end{pmatrix} = \begin{pmatrix} \cos\alpha & \sin\alpha \\ -\sin\alpha & \cos\alpha \end{pmatrix} \begin{pmatrix} h \\ H \end{pmatrix}$$

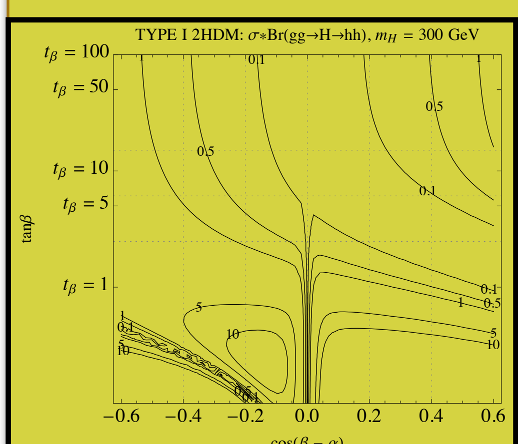

Type I 2HDM where $y_1^{u,d,e}$ = 0. Contour lines give σ(pp→H→hh) for a given tanβ and cos(β-α).

Experimental exclusion curves will be placed on such plots.

Example Theoretical Models

2 Higgs-Doublet Models

- Two EWK SU(2) Higgs doublets, $\mathbf{\Phi}_1$ and $\mathbf{\Phi}_2$
- 5 Higgs bosons emerge: **H**, **h**, **A**, **H⁺**, **H⁻**
- Parameters for theoretical exclusion:
  tanβ and **cos(β - α)**, where

$$\tan\beta = \left|\frac{\langle\Phi_2^0\rangle}{\langle\Phi_1^0\rangle}\right| \qquad \begin{pmatrix}\sqrt{2}\,\mathrm{Re}(\Phi_2^0) - v_2 \\ \sqrt{2}\,\mathrm{Re}(\Phi_1^0) - v_1\end{pmatrix} = \begin{pmatrix}\cos\alpha & \sin\alpha \\ -\sin\alpha & \cos\alpha\end{pmatrix}\begin{pmatrix}h \\ H\end{pmatrix}$$

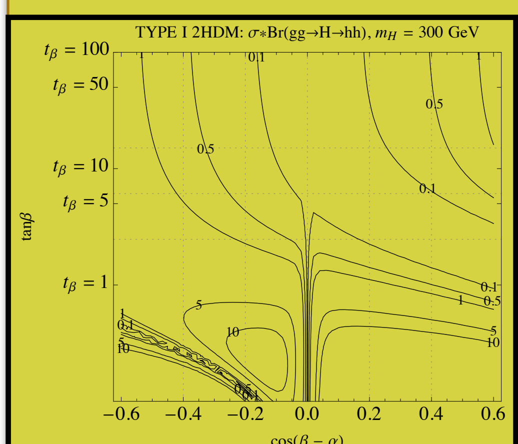

Type I 2HDM where $y_1^{u,d,e} = 0$. Contour lines give σ(pp→H→hh) for a given tanβ and cos(β-α).

Experimental exclusion curves will be placed on such plots.

Warped Extra Dimensions

- Randall Sundrum (RS1) warped extra dimension models require a scalar **radion** to stabilize the length of the extra dimension
  [Goldberger-Wise mechanism]
- A radion with mass above 250 GeV can decay to two SM Higgs
  [Radion phenomenology, Csaba Csaki et al]

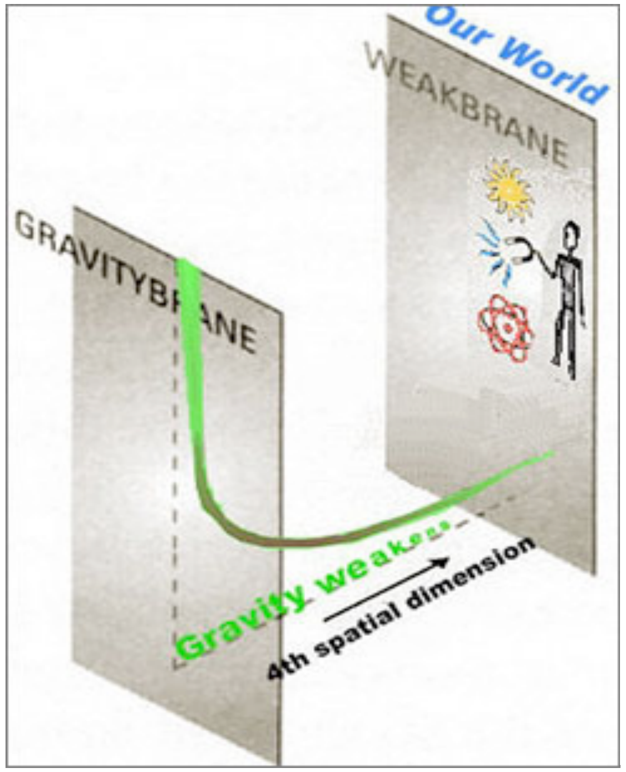

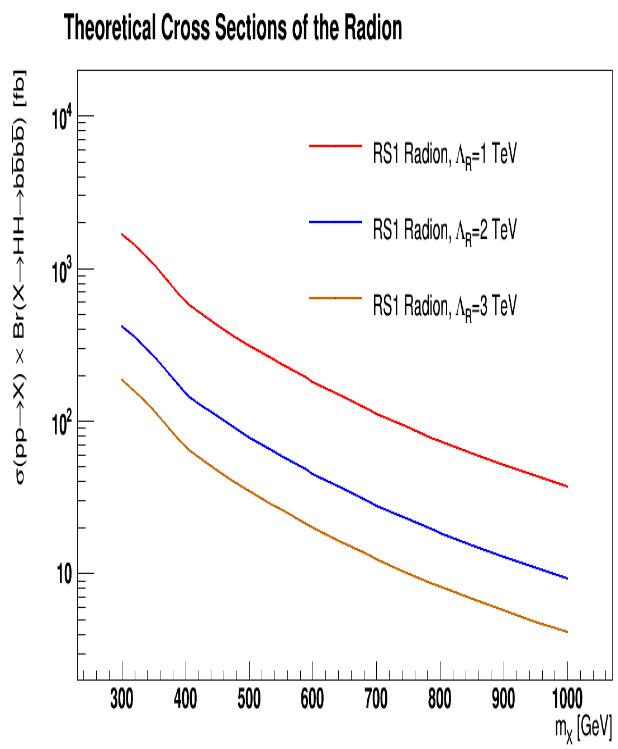

Theoretical cross section for the RS1 radion with radion decay constant Λ_R = 1, 2, 3 TeV. Experimental exclusion curves will be placed on this plot.

Multi-leptons and Photons: Search Channels

- **CMS-HIG-13-025**. Searches for H→hh (and A→Zh) within the context of 2HDM.
- Triggers: di-photon and di-lepton
- Combinations of Higgs decays

	$h \to WW^*$	$h \to ZZ^*$	$h \to \tau\tau$	$h \to bb$	$h \to \gamma\gamma$
$h \to WW^*$	✓	✓	✓	X	✓
$h \to ZZ^*$	-	✓	✓	✓	✓
$h \to \tau\tau$	-	-	✓	X	✓
$h \to bb$	-	-	-	X	X
$h \to \gamma\gamma$	-	-	-	-	X

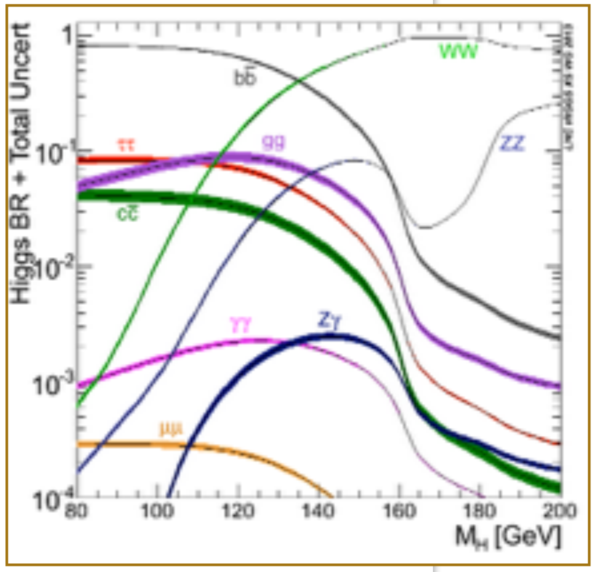

- Cut and count search in several final states classified by:
  N_l, opposite-sign-same-flavor (OSSF) pairs, on/off-Z, N_γ, N_τ, N_b, E_T^{miss}

Final states from hh decays	Search Channels h decays populate
WW^*WW^* $WW^*\tau\tau$ $\tau\tau\tau\tau$ $ZZ^*\tau\tau$ ZZ^*bb	Three or four leptons (upto one τ_h), OSSF pair off-Z or no OSSF pair in bins of E_T^{miss} and b-tag
$\gamma\gamma WW^*$ $\gamma\gamma ZZ^*$ $\gamma\gamma\tau\tau$	2photons ($M_{\gamma\gamma}$ within higgs bin) + 1 or more leptons(upto 2 τ_h),in bins of E_T^{miss}

- Multi-lepton channels contributing the most:
  - Channels **without OSSF**-pair (greatly reduces DY-background)
  - Channels with OSSF-pair but **off-shell Z**
  - Channels with **SSSF-pair**. Has low SM background

Multi-leptons and Photons: Background Estimation

Multi-lepton final states

- **Z+jets**, **W+jets**. Data-driven estimation (of jets misidentified as leptons)
- **$t\bar{t}$ and VV**: MC-based estimation
- **Asymmetric photon conversion**. DY process with one soft lepton and another lepton radiating a photon that converts. Data-driven estimation of photon conversion.

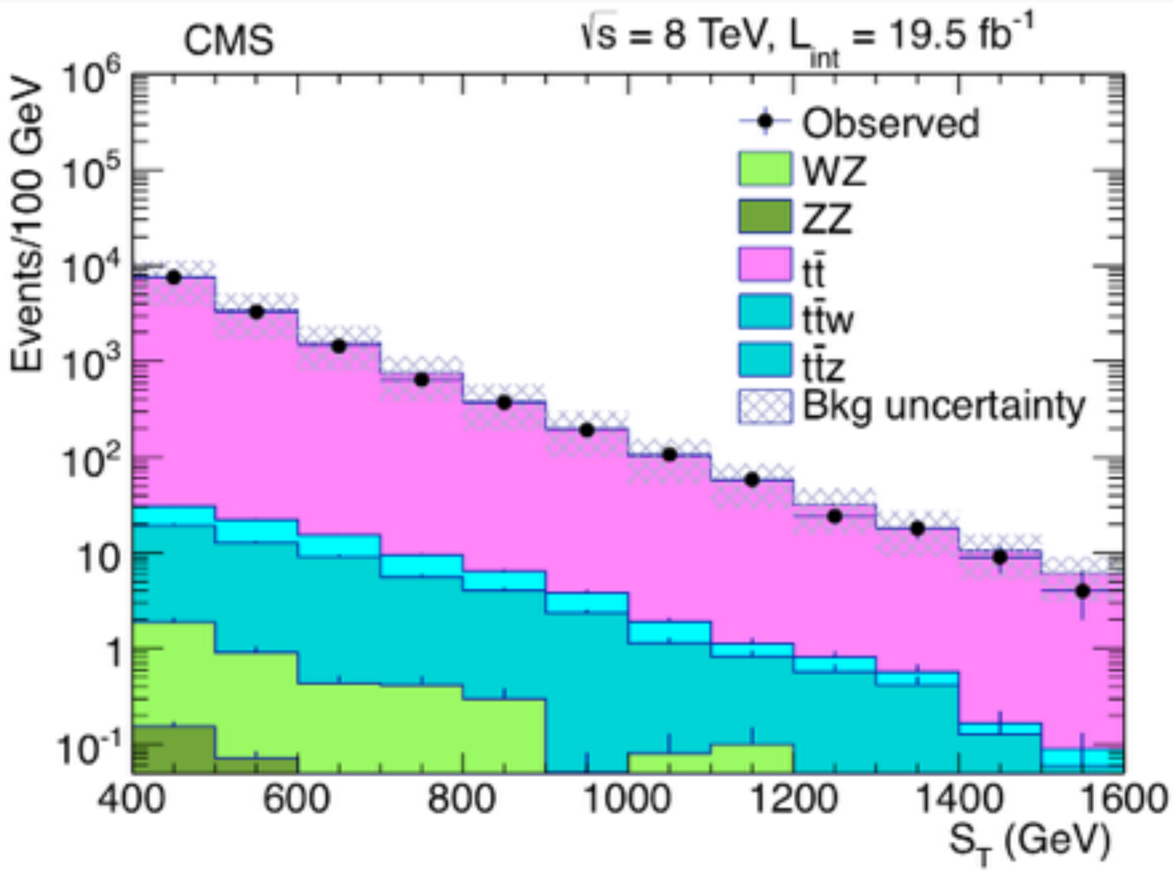

$m_{\gamma\gamma}$

Multi-leptons and Photons: Background Estimation

Multi-lepton final states

- **Z+jets**, **W+jets**. Data-driven estimation (of jets misidentified as leptons)
- **$t\bar{t}$ and VV**: MC-based estimation
- **Asymmetric photon conversion**. DY process with one soft lepton and another lepton radiating a photon that converts. Data-driven estimation of photon conversion.

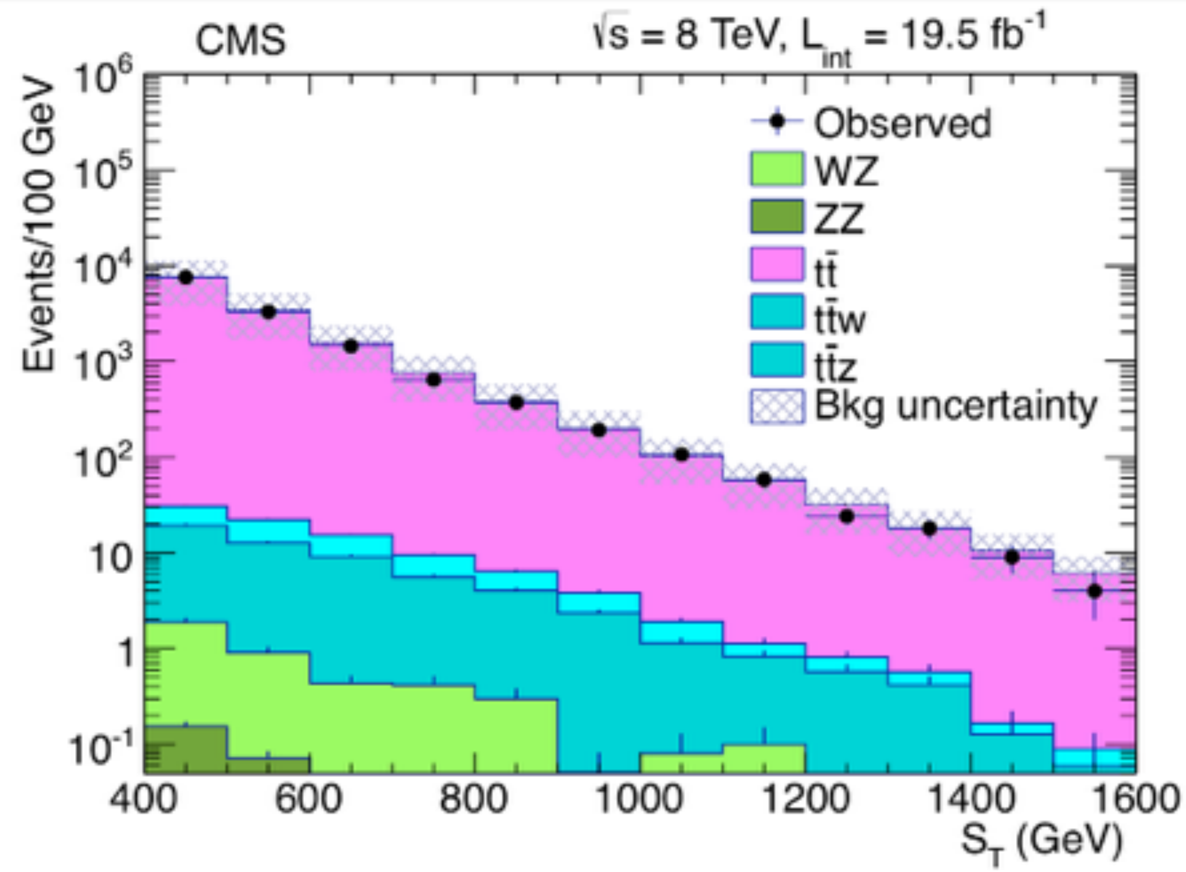

Di-photon final states

- Background estimated from $m_{\gamma\gamma}$ sidebands keeping the range 120 GeV — 130 GeV blinded.
- Fitted to a falling exponential

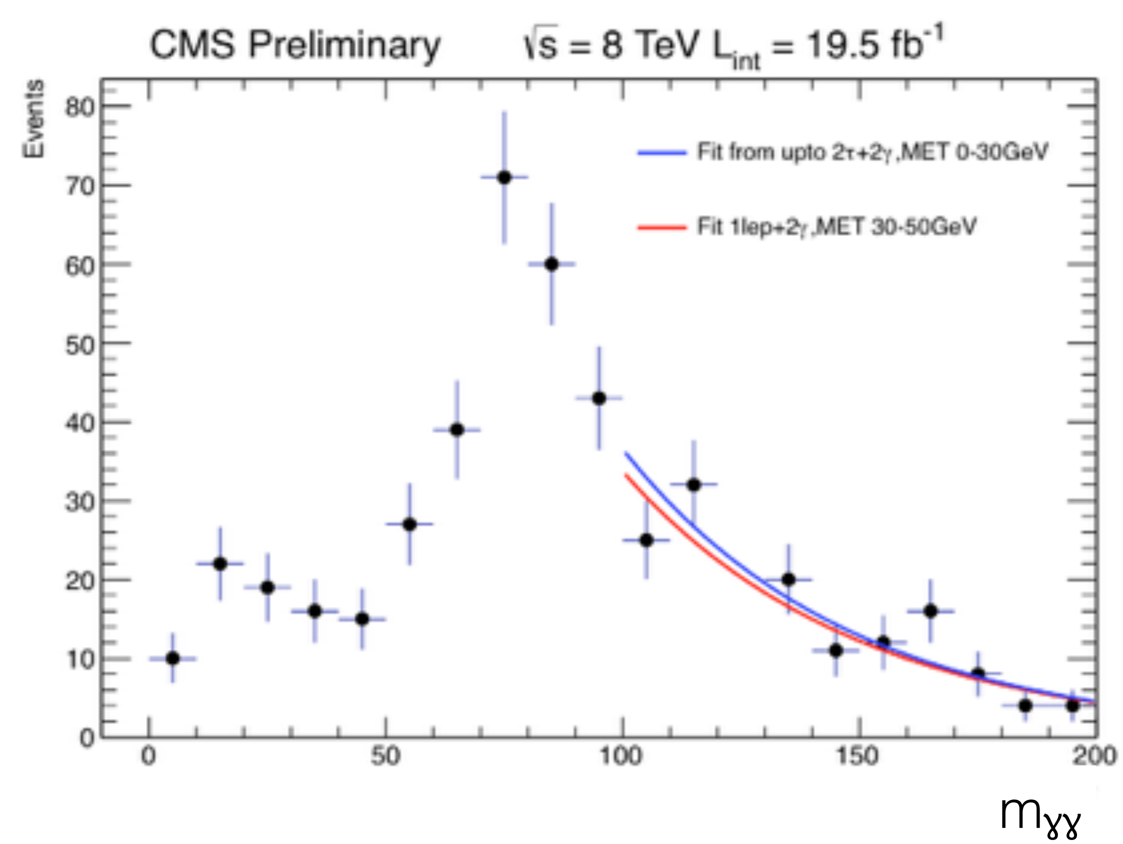

Multi-leptons and Photons: Results

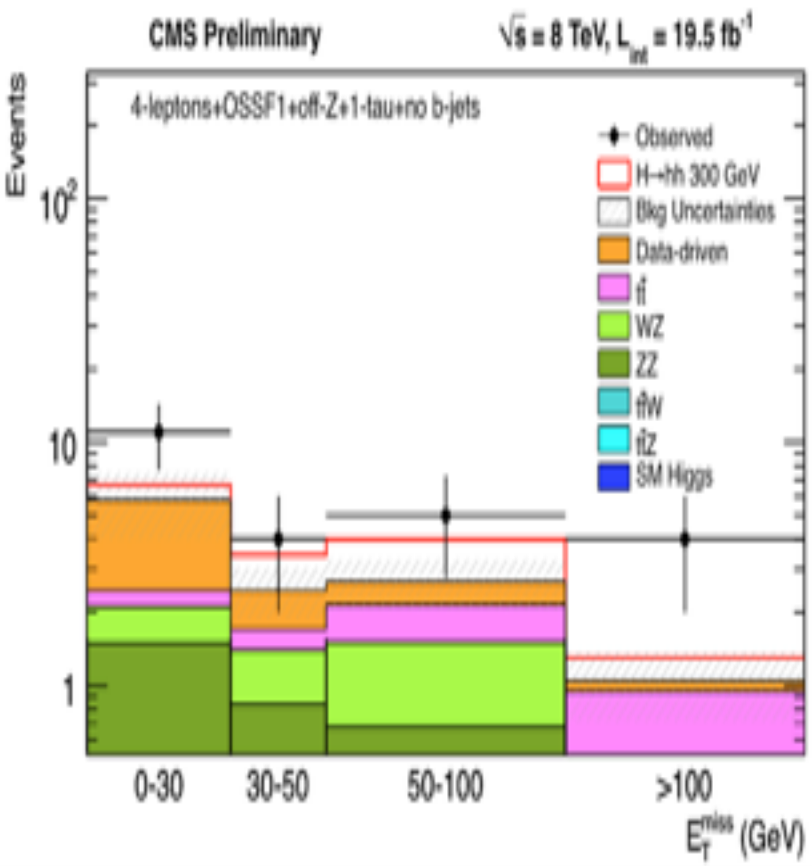

Signal bin with largest excess in 4-leptons, OSSF1, off-Z, 1 τ_{had} and 0 b-jets.

Total excess:
obs (exp) = 20 (10.7 ±1.9)

Local significance ***p* = 1.5%**
40 channels significance: ***p* = 46%**

Multi-leptons and Photons: Results

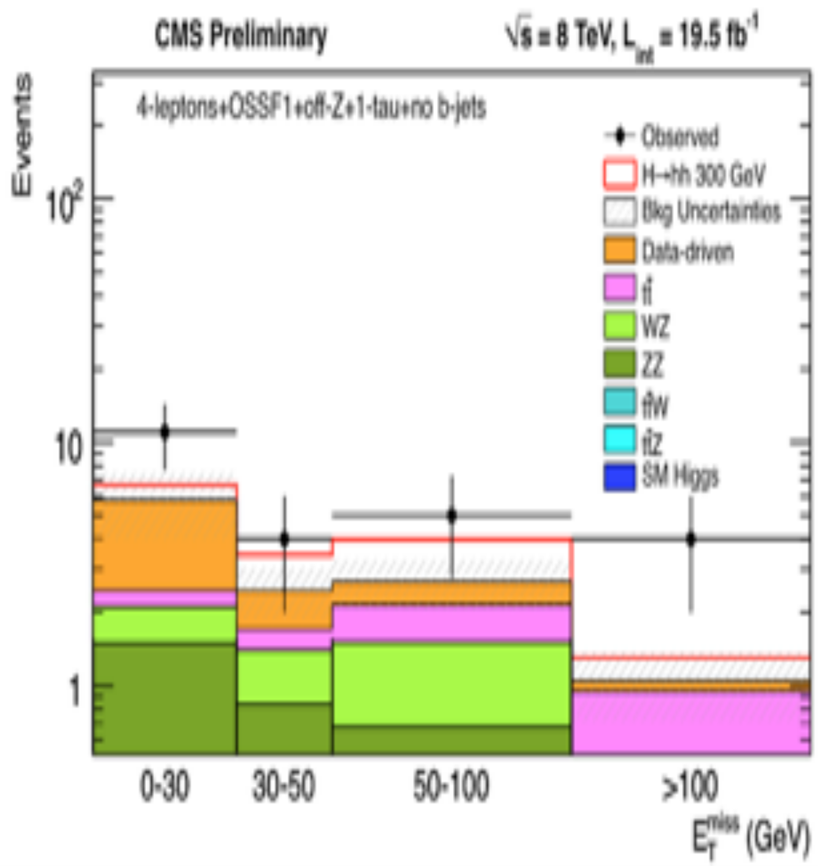

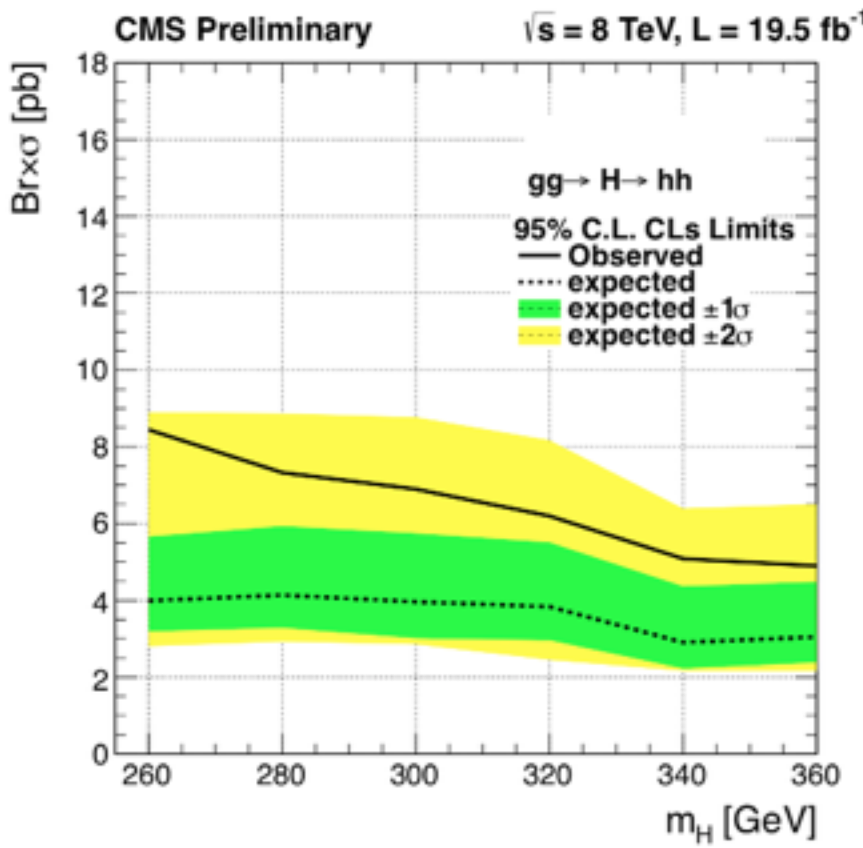

Signal bin with largest excess in 4-leptons, OSSF1, off-Z, 1 τ_{had} and 0 b-jets.

Total excess:
obs (exp) = 20 (10.7 ±1.9)

Local significance ***p* = 1.5%**
40 channels significance: ***p* = 46%**

Observed and expected limits for **σ**(gg→H→hh). Standard Model branching fractions are assumed for the Higgs.

No significant deviation from expectations

Multi-leptons and Photons: Results

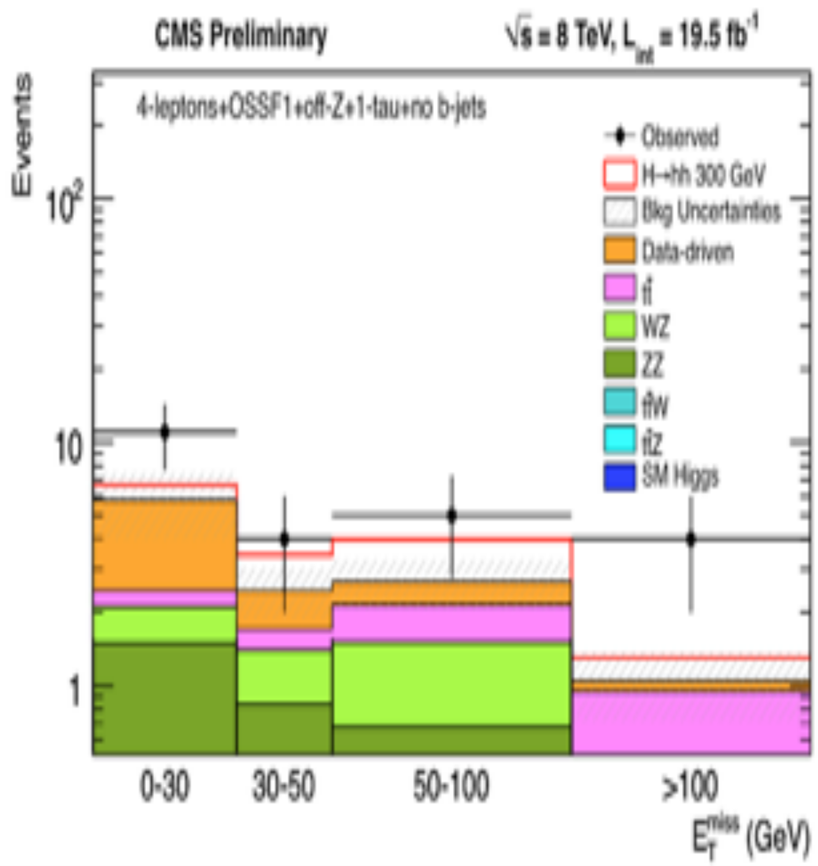

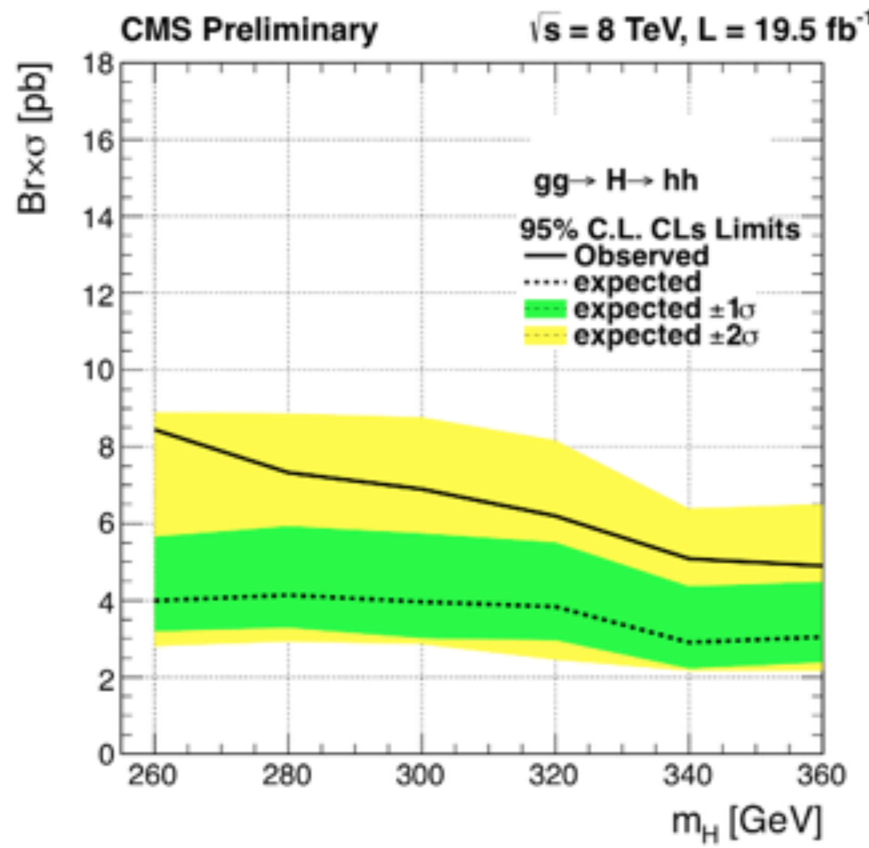

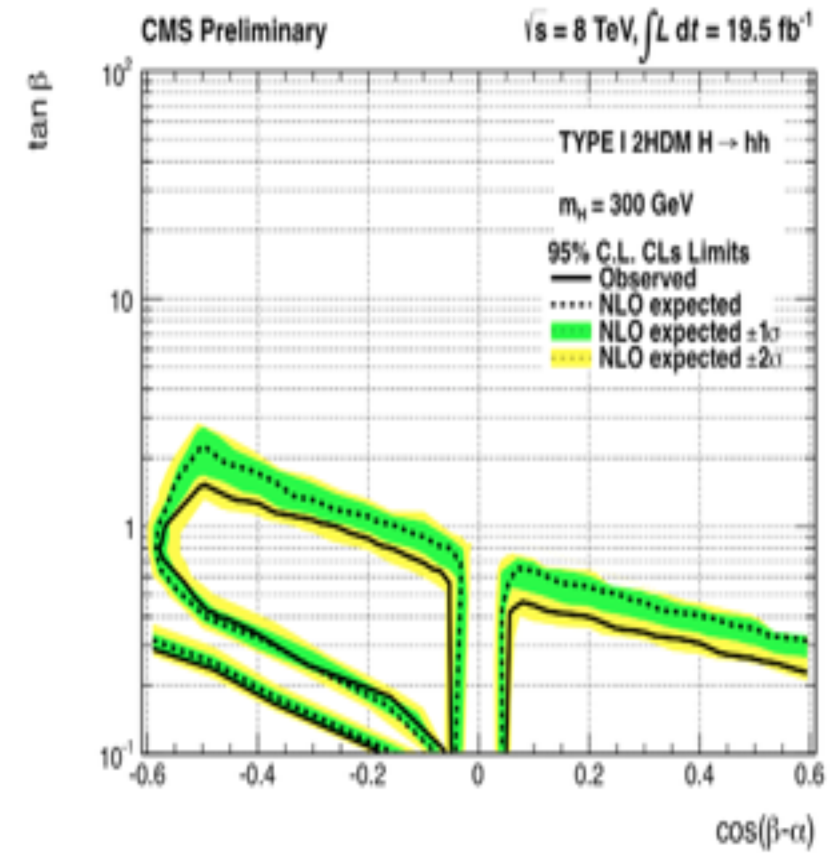

Signal bin with largest excess in 4-leptons, OSSF1, off-Z, 1 τ_{had} and 0 b-jets.

Total excess:
obs (exp) = 20 (10.7 ±1.9)

Local significance ***p* = 1.5%**
40 channels significance: ***p* = 46%**

Observed and expected limits for **σ**(gg→H→hh). Standard Model branching fractions are assumed for the Higgs.

No significant deviation from expectations

Interpret limits on **σ**(gg→H→hh) in Type I 2HDM parameter space

Regions below the curves and within the loops **are excluded**

$H(b\bar{b})H(\gamma\gamma)$: Search Strategy

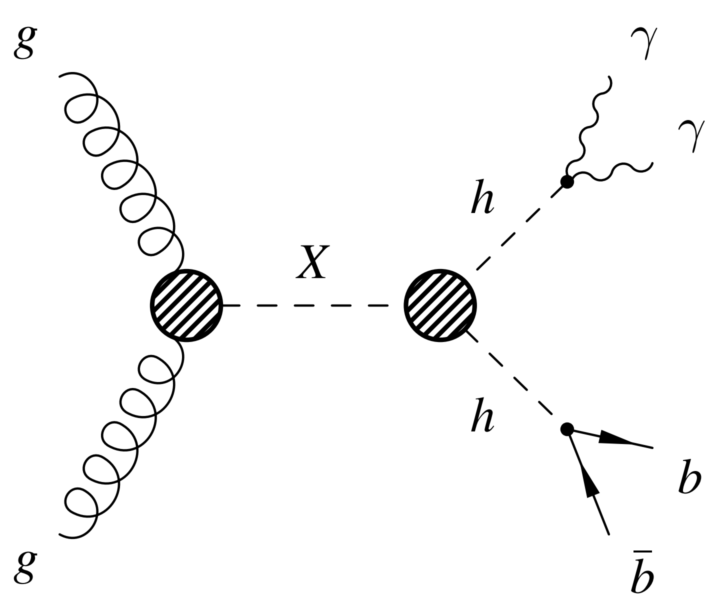

- CMS-HIG-13-032. Gluon-fusion production of massive resonance X that decays to two H(125)H(125) that decays into $(\gamma\gamma)(b\bar{b})$
  - High efficiency to reconstruct photons (>90%)
  - Sharp $H(\gamma\gamma)$ resolution
  - Low QCD multi-jet background
  - Low branching fraction (0.26%)
- $L = 19.7\ \mathrm{fb}^{-1}$. $\sqrt{s} = 8$ TeV
- Two di-photon triggers [used by $H(\gamma\gamma)$ analysis] used to collect data.
- **Two mass regimes** of the analysis:
  - Low Mass Regime: 260 GeV $\leq$ mX $\leq$ 400 GeV
  - High Mass Regime: 400 GeV < mX $\leq$ 1100 GeV
- Each regime analyzed in **two purity categories**:
  - Medium purity: 1 b-tagged jet
  - High purity: 2 b-tagged jets

$H(b\bar{b})H(\gamma\gamma)$: Search Strategy

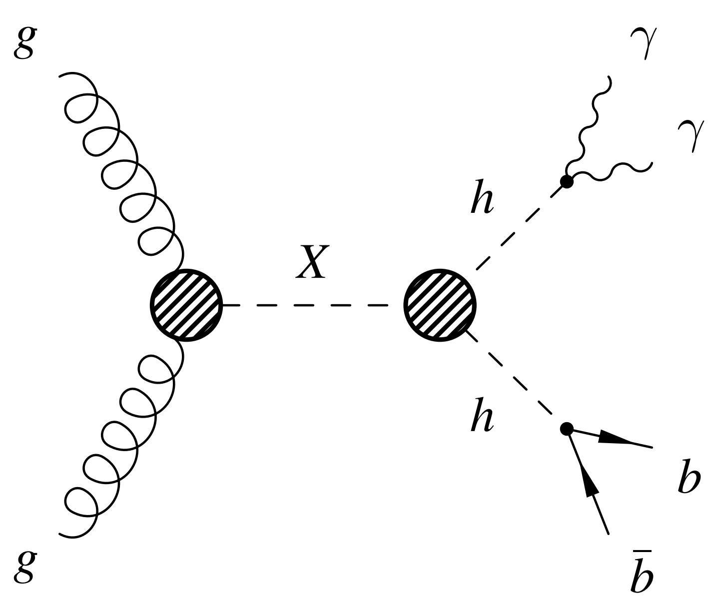

- CMS-HIG-13-032. Gluon-fusion production of massive resonance X that decays to two H(125)H(125) that decays into $(\gamma\gamma)(b\bar{b})$
  - High efficiency to reconstruct photons (>90%)
  - Sharp $H(\gamma\gamma)$ resolution
  - Low QCD multi-jet background
  - Low branching fraction (0.26%)
- $L = 19.7\ fb^{-1}$. $\sqrt{s} = 8$ TeV
- Two di-photon triggers [used by $H(\gamma\gamma)$ analysis] used to collect data.
- **Two mass regimes** of the analysis:
  - Low Mass Regime: 260 GeV $\leq$ mX $\leq$ 400 GeV
  - High Mass Regime: 400 GeV < mX $\leq$ 1100 GeV
- Each regime analyzed in **two purity categories**:
  - Medium purity: 1 b-tagged jet
  - High purity: 2 b-tagged jets

Photon Object Selection

- Tight photon identification
- Sliding pT cuts:
  - $p_{T\gamma 1}/m_{\gamma\gamma} > 1/3$
  - $p_{T\gamma 2}/m_{\gamma\gamma} > 1/4$
- $|\eta_\gamma| < 2.5$
- 100 GeV < $m_{\gamma\gamma}$ < 180 GeV

$H(b\bar{b})H(\gamma\gamma)$: Search Strategy

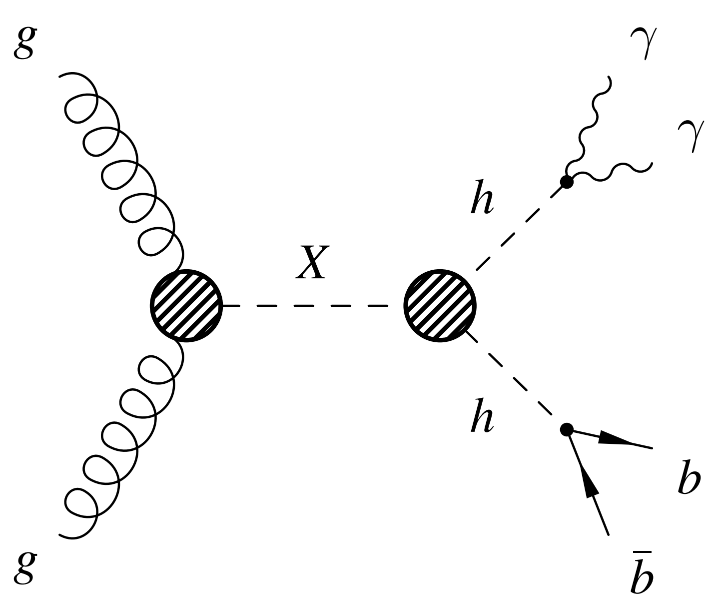

- CMS-HIG-13-032. Gluon-fusion production of massive resonance X that decays to two H(125)H(125) that decays into $(\gamma\gamma)(b\bar{b})$
  - High efficiency to reconstruct photons (>90%)
  - Sharp $H(\gamma\gamma)$ resolution
  - Low QCD multi-jet background
  - Low branching fraction (0.26%)

- $L = 19.7\ fb^{-1}$. $\sqrt{s} = 8$ TeV

- Two di-photon triggers [used by $H(\gamma\gamma)$ analysis] used to collect data.

- **Two mass regimes** of the analysis:
  - Low Mass Regime: 260 GeV $\leq$ mX $\leq$ 400 GeV
  - High Mass Regime: 400 GeV < mX $\leq$ 1100 GeV

- Each regime analyzed in **two purity categories**:
  - Medium purity: 1 b-tagged jet
  - High purity: 2 b-tagged jets

Photon Object Selection

- Tight photon identification
- Sliding pT cuts:
  - $p_{T\gamma 1}/m_{\gamma\gamma} > 1/3$
  - $p_{T\gamma 2}/m_{\gamma\gamma} > 1/4$
- $|\eta_\gamma| < 2.5$
- 100 GeV < $m_{\gamma\gamma}$ < 180 GeV

b-jet Object Selection

- Loose jet identification
- Pileup rejection
- $p_{Tj} > 25$ GeV
- $|\eta_j| < 2.5$
- Combined Secondary Vertex. b-tag eff = 70%, mistag rate = 1-2%

H(b$\bar{b}$)H(ɣɣ): Search Strategy

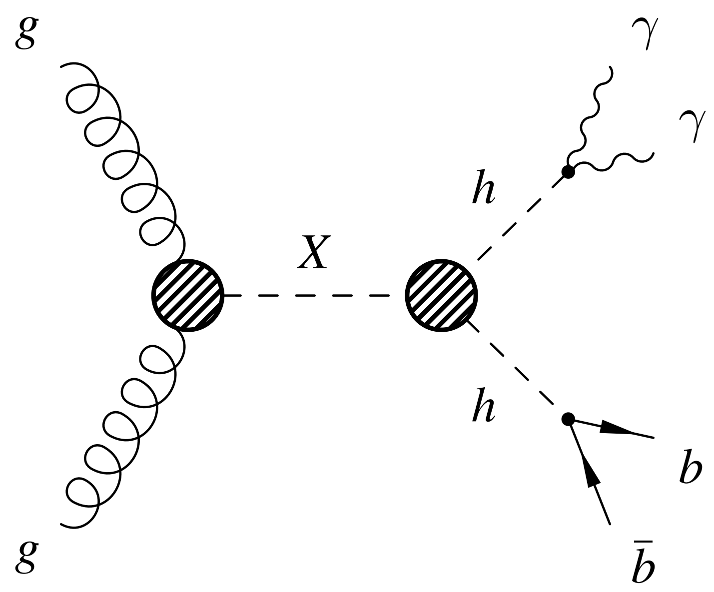

Three invariant mass handles $m_{\gamma\gamma}$, m_{jj}, $m_{\gamma\gamma jj}$

$H(b\bar{b})H(\gamma\gamma)$: Search Strategy

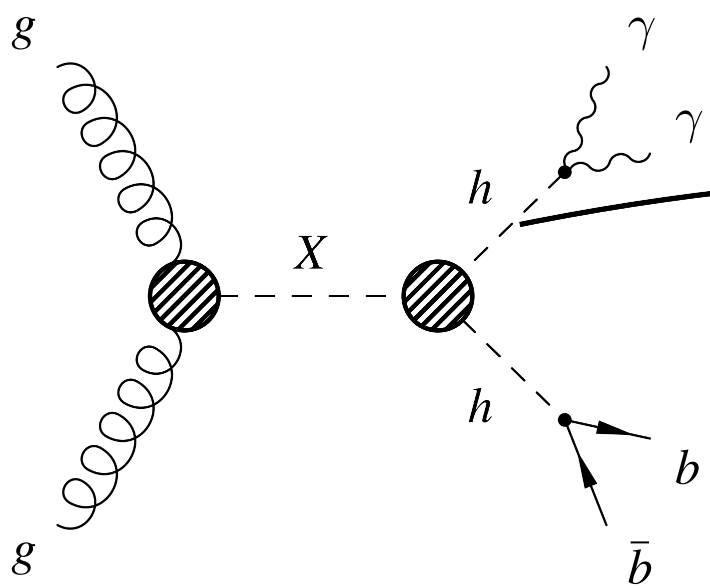

Three invariant mass handles $m_{\gamma\gamma}$, m_{jj}, $m_{\gamma\gamma jj}$

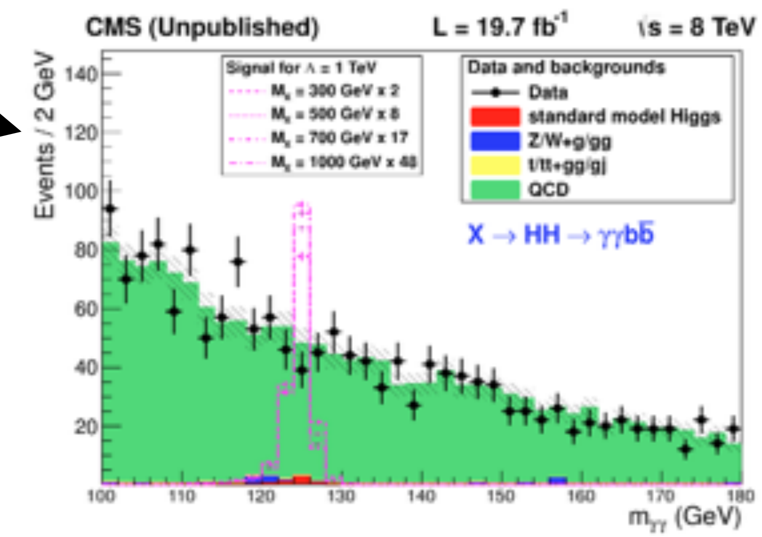

H(b$\bar{b}$)H(ɣɣ): Search Strategy

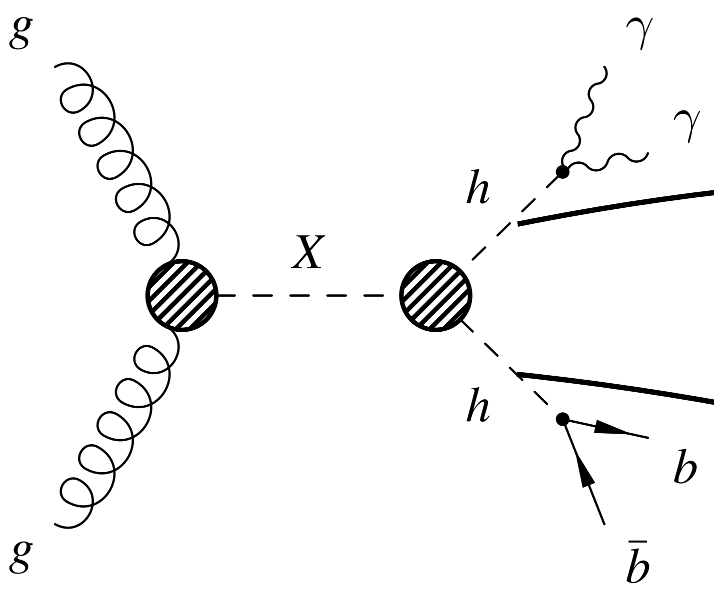

Three invariant mass handles $m_{ɣɣ}$, m_{jj}, $m_{ɣɣjj}$

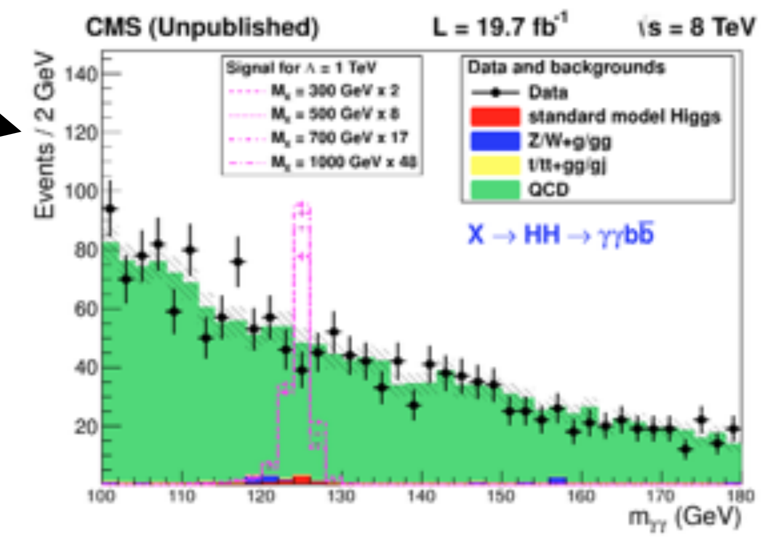

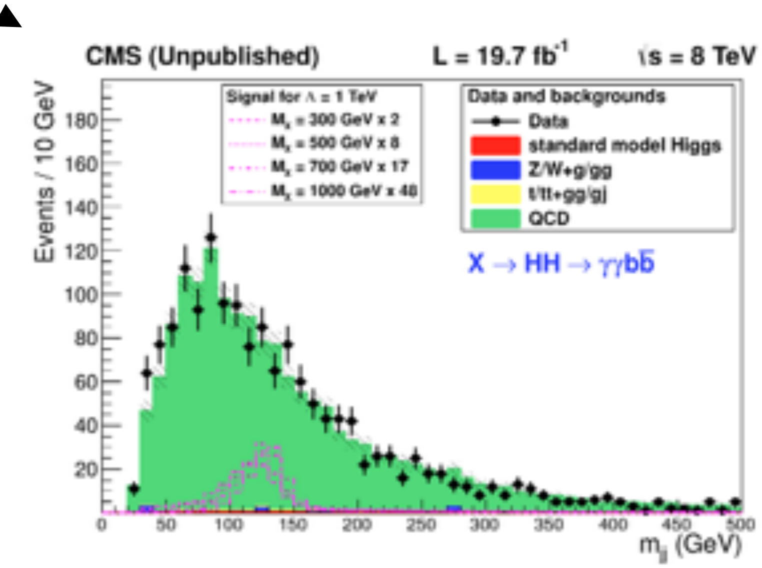

H(b$\bar{b}$)H(γγ): Search Strategy

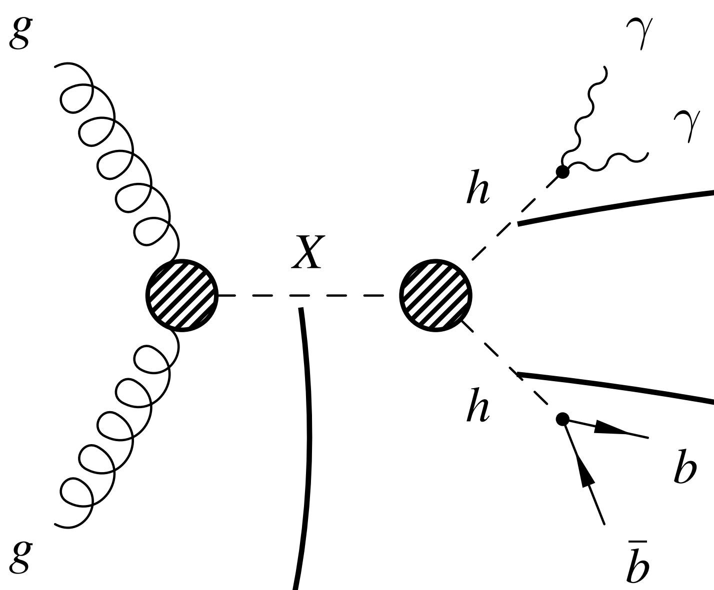

Three invariant mass handles $m_{\gamma\gamma}$, m_{jj}, $m_{\gamma\gamma jj}$

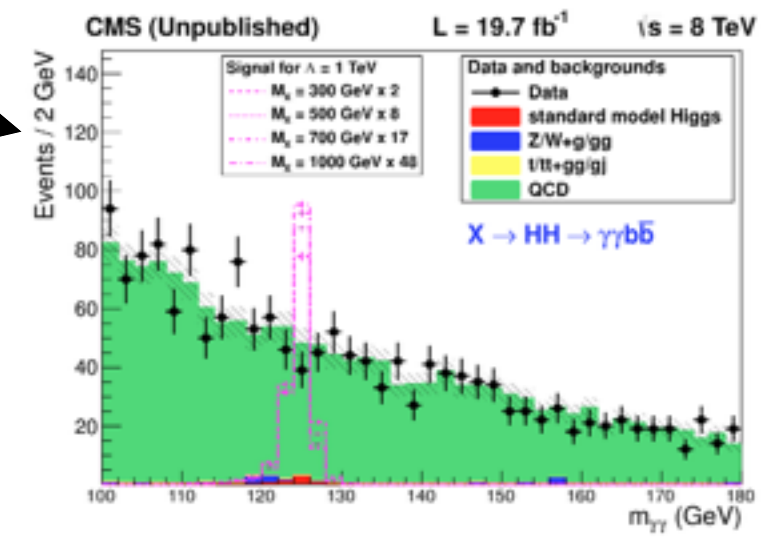

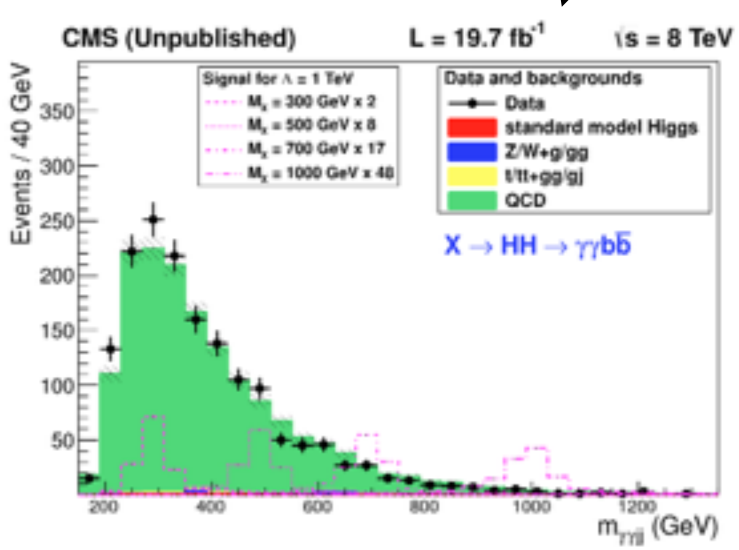

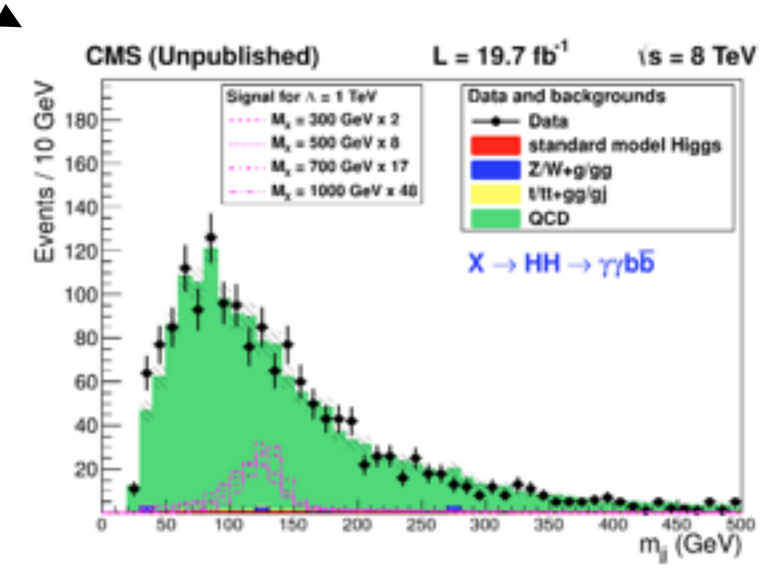

H(b$\bar{b}$)H(γγ): Search Strategy

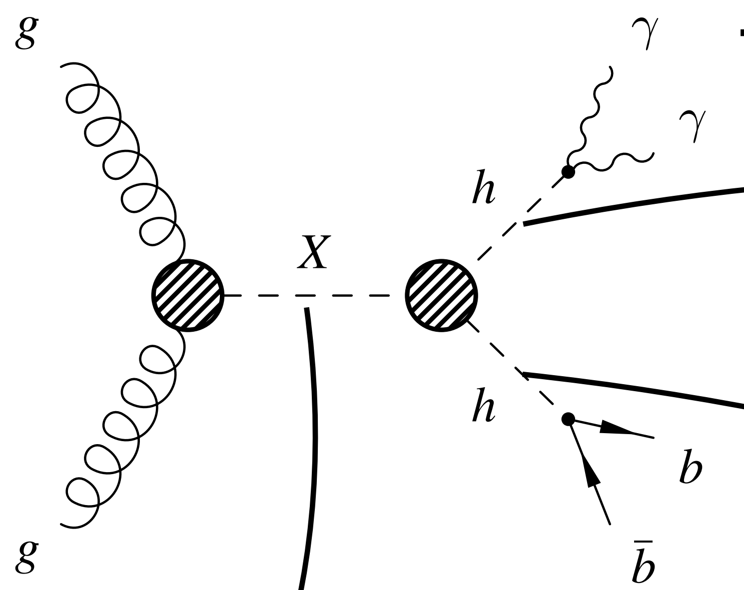

Three invariant mass handles $m_{\gamma\gamma}$, m_{jj}, $m_{\gamma\gamma jj}$

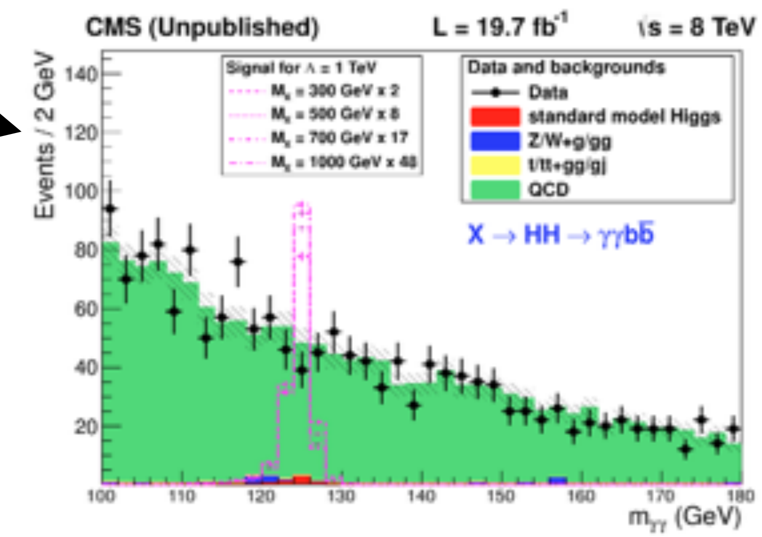

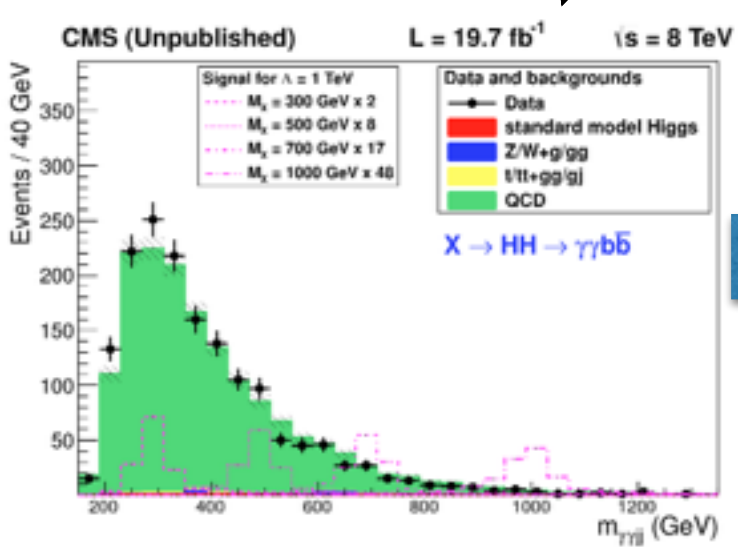

Kinematic Fit

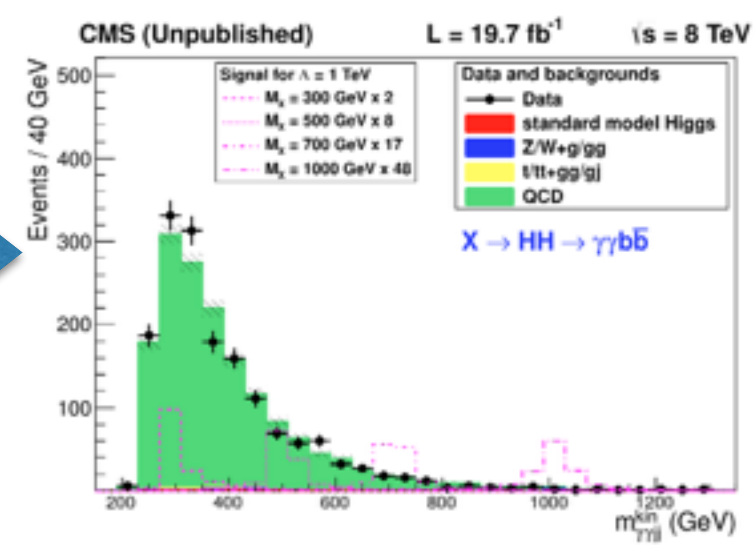

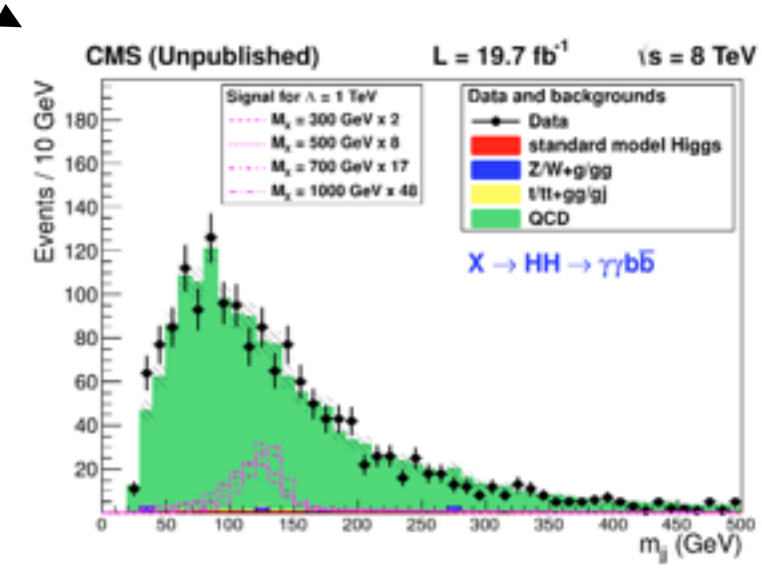

$H(b\bar{b})H(\gamma\gamma)$: Search Strategy

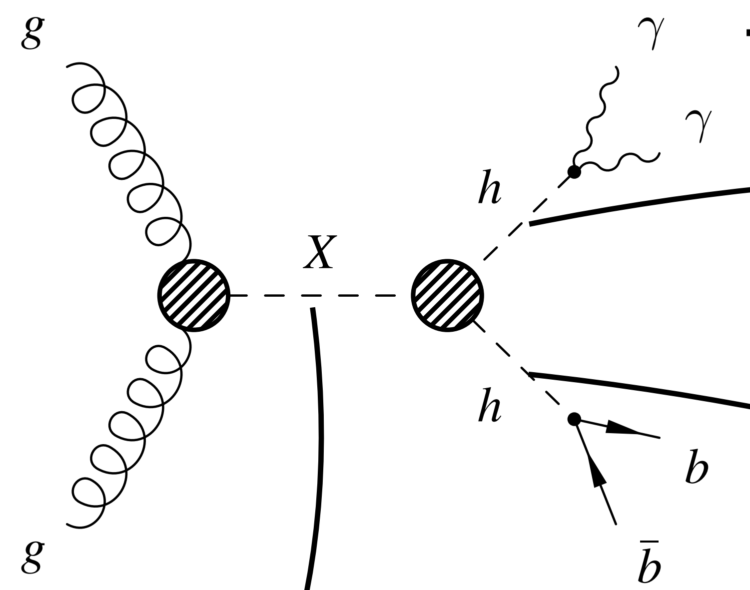

Three invariant mass handles $m_{\gamma\gamma}$, m_{jj}, $m_{\gamma\gamma jj}$

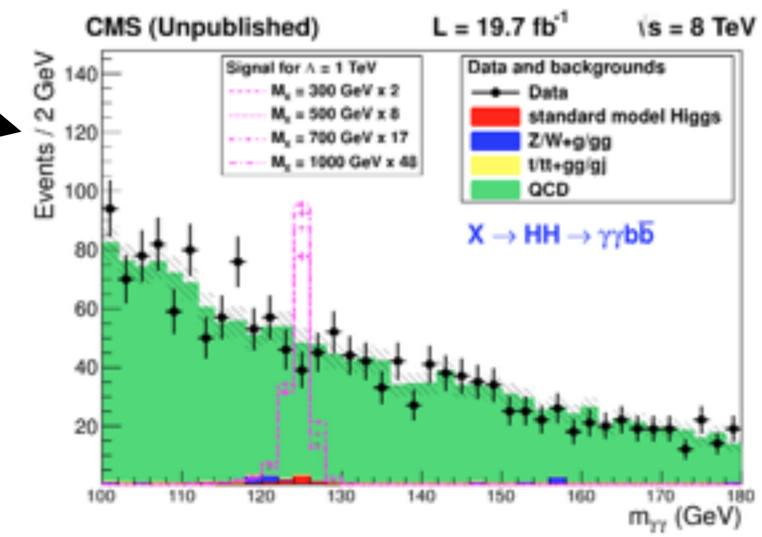

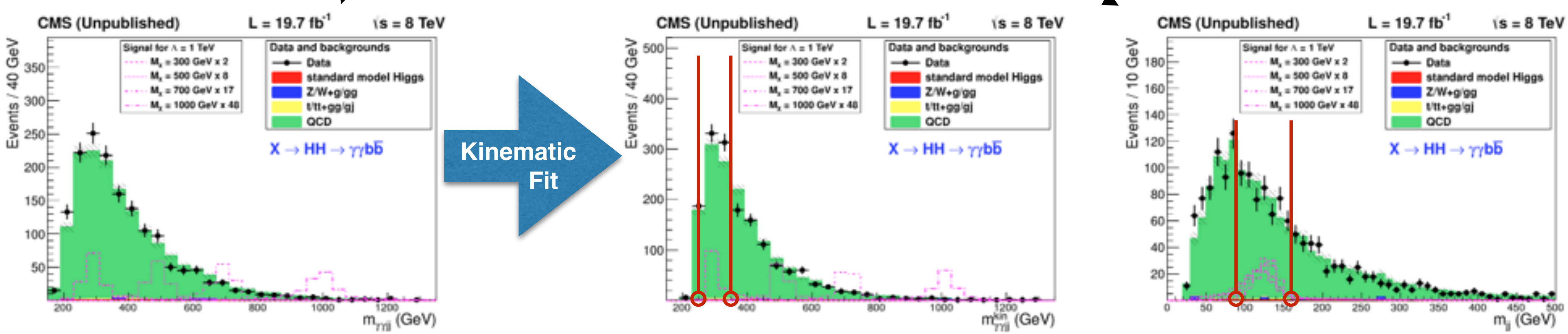

Low Mass Regime.

- Cut on $m_{\gamma\gamma jj}$ AND m_{jj}.
- Fit $m_{\gamma\gamma}$

H(b$\bar{b}$)H(ɣɣ): Search Strategy

Three invariant mass handles $m_{\gamma\gamma}$, m_{jj}, $m_{\gamma\gamma jj}$

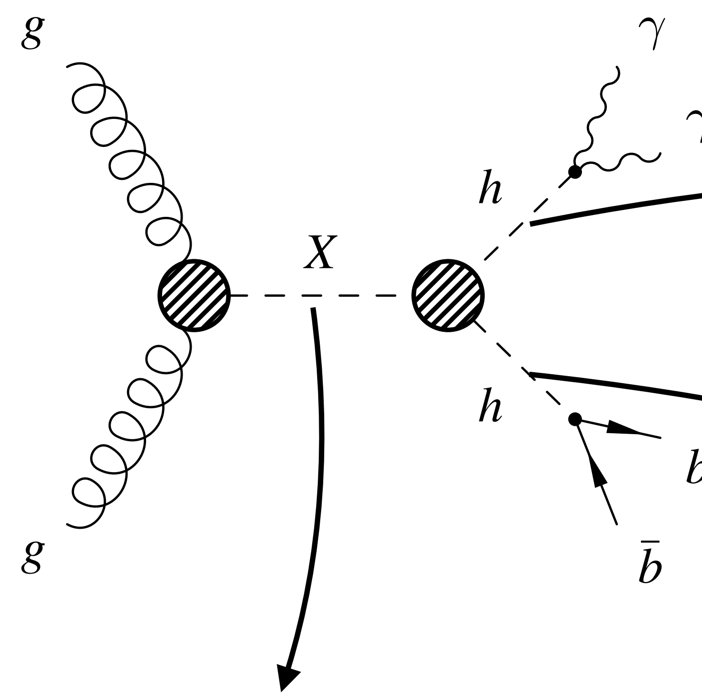

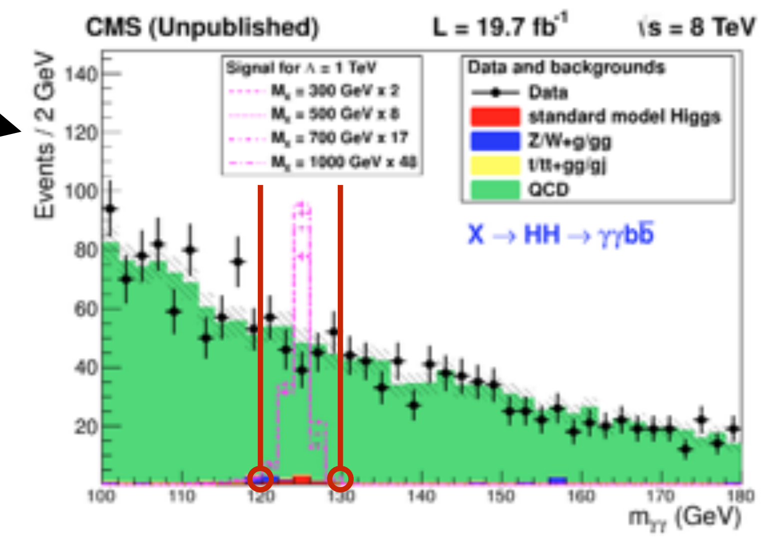

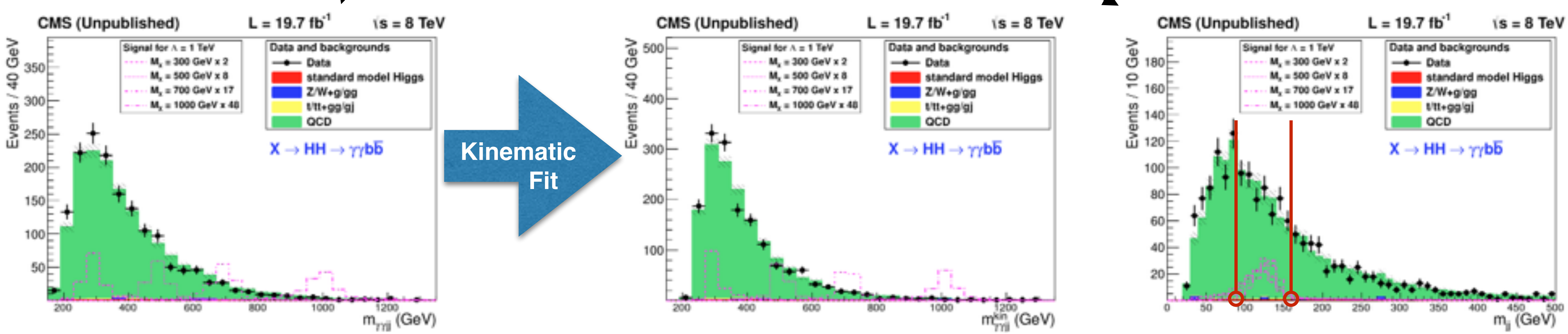

Low Mass Regime.

- Cut on $m_{\gamma\gamma jj}$ AND m_{jj}.
- Fit $m_{\gamma\gamma}$

High Mass Regime

- Cut on $m_{\gamma\gamma}$ AND m_{jj}.
- Kinematically constrain $m_{\gamma\gamma}$ and m_{jj} to 125 GeV within energy resolutions
- Fit $m_{\gamma\gamma jj}$

H(b$\bar{b}$)H(ɣɣ): Signal and Background Modeling

Low Mass Regime

Simulated signal shape in $m_{\gamma\gamma}$ for the medium purity category

Events in $m_{\gamma\gamma}$ spectrum in medium purity for signal hypothesis of 300 GeV (sliding photon p_T cuts) Fitted to power-law

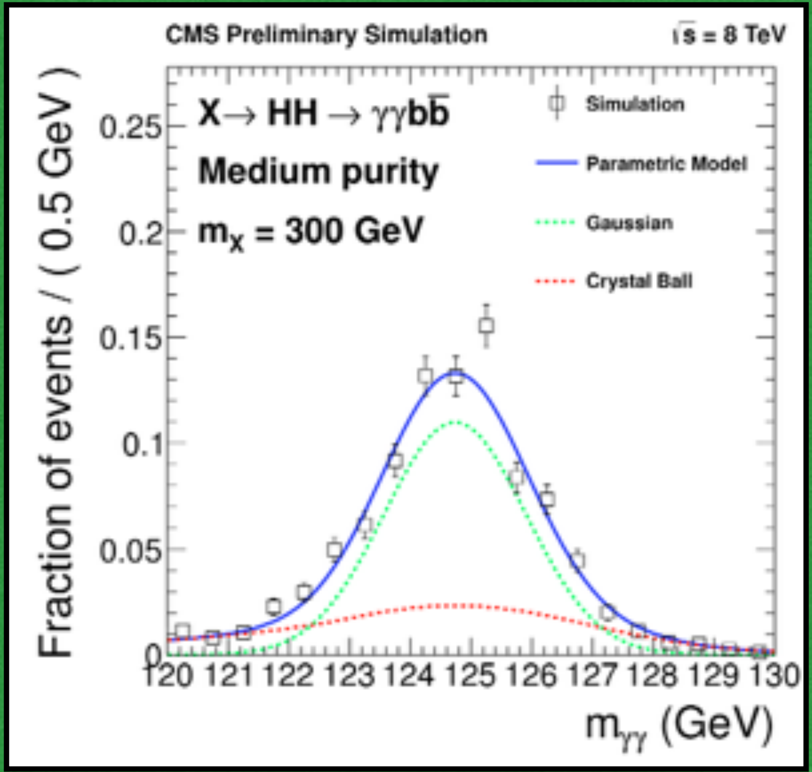

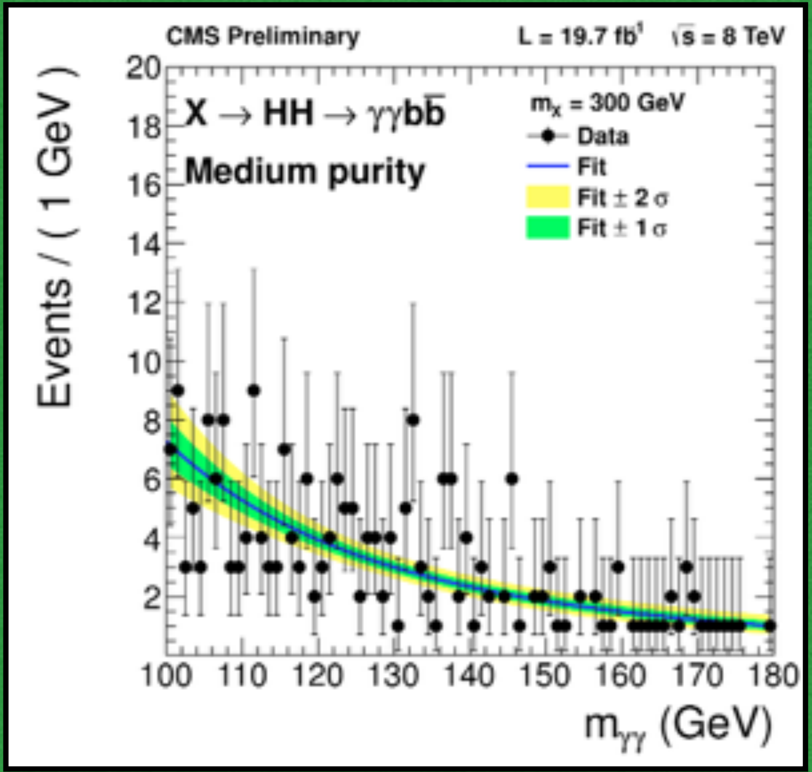

H($b\bar{b}$)H($\gamma\gamma$): Signal and Background Modeling

Low Mass Regime

Simulated signal shape in $m_{\gamma\gamma}$ for the medium purity category

Events in $m_{\gamma\gamma}$ spectrum in medium purity for signal hypothesis of 300 GeV (sliding photon p_T cuts)
Fitted to power-law

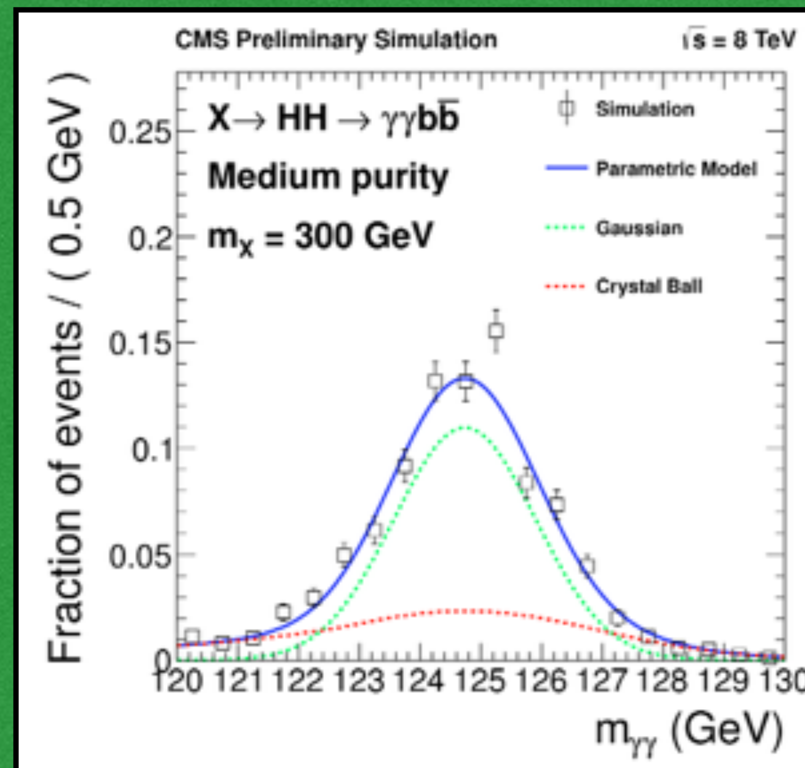

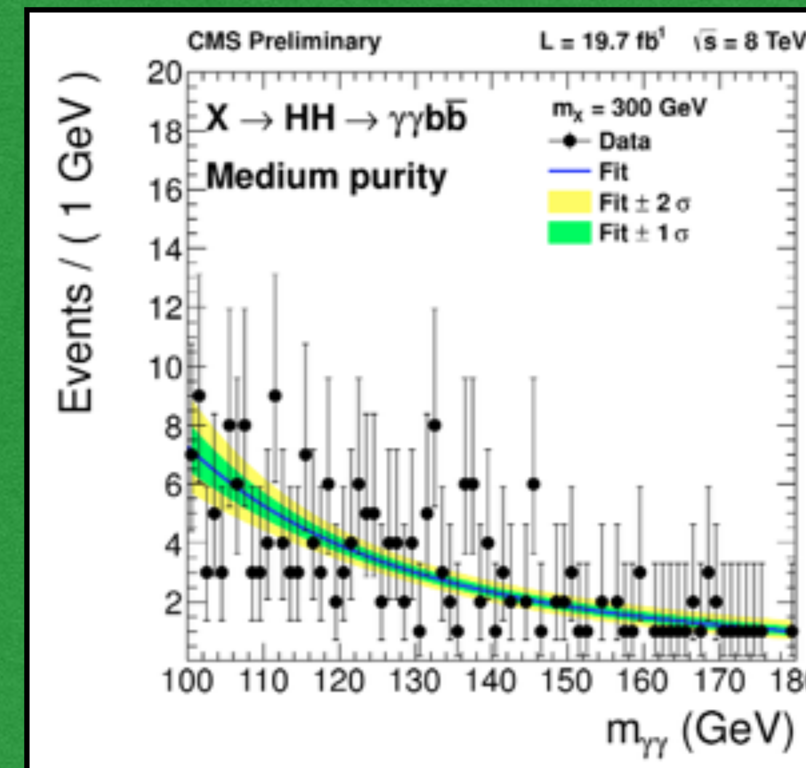

High Mass Regime

Simulated signal shape in $m_{\gamma\gamma jj}^{kinFit}$ for the medium purity category

Events in $m_{\gamma\gamma jj}^{\mathrm{kinFit}}$ spectrum for signal hypothesis of 500 GeV

Bias Study

Several “true” background shapes tried. **Negligible bias** on signal strength.

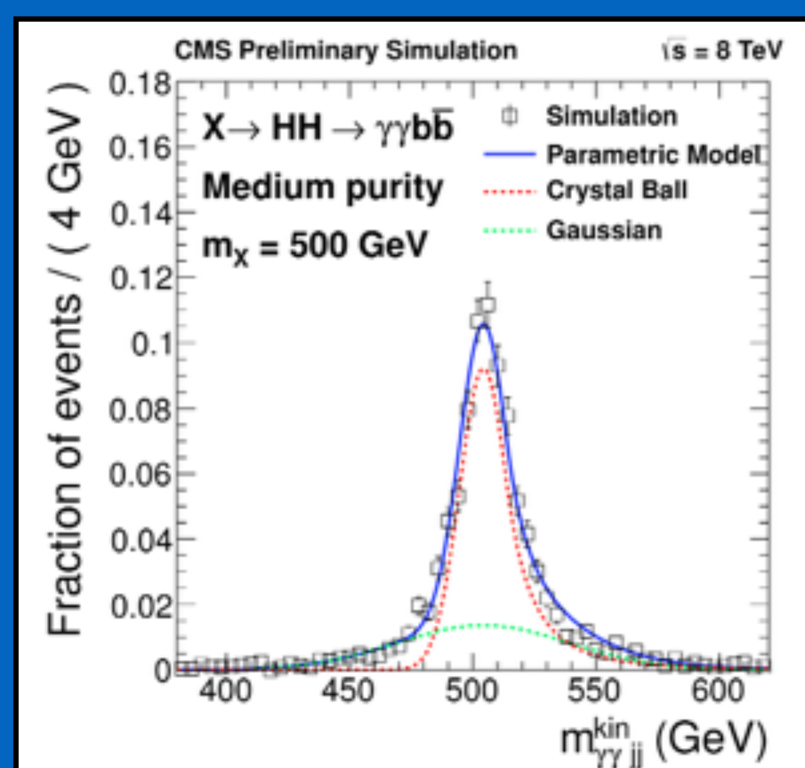

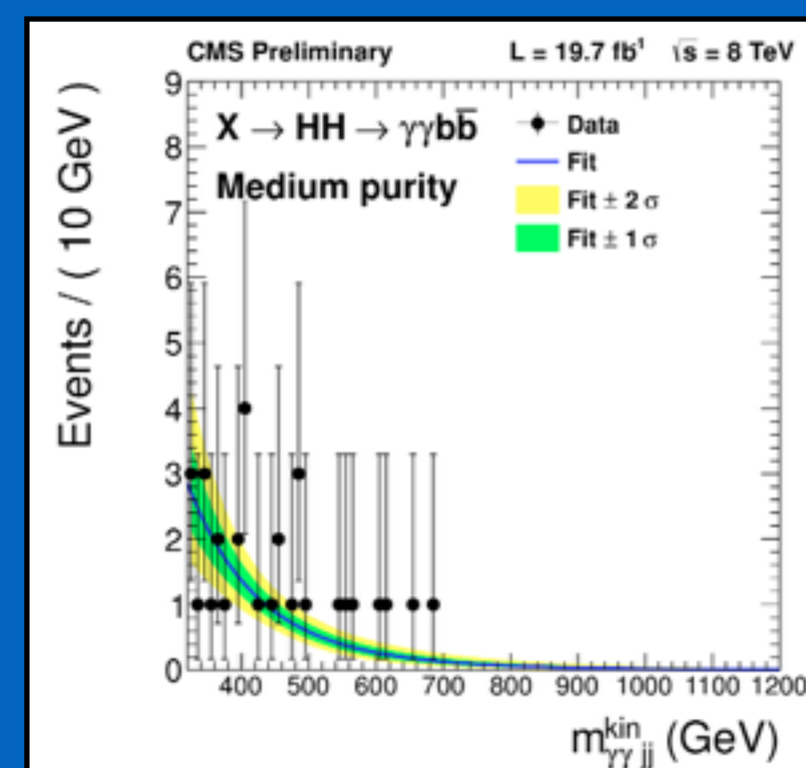

H(b$\bar{b}$)H(γγ): Results

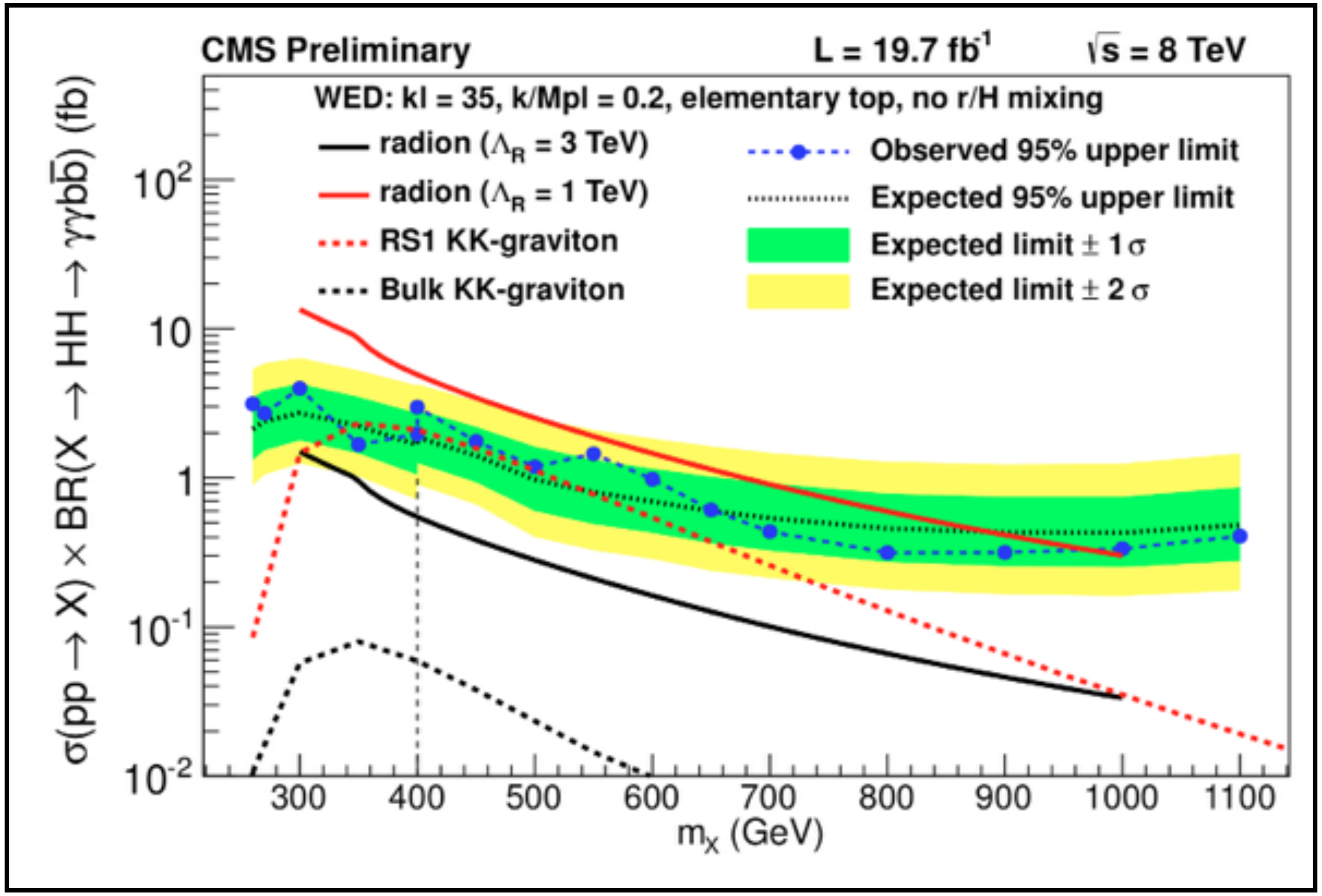

No significant deviation from expectations

- Analysis is **statistics-limited**
- Systematic uncertainties worsen expected limits by 1.7% at most

- Cross sections of the radion assume *k*-factor for top-loop in gluon-fusion production of R to be identical to that of Higgs production. Also, Br(R→HH) = 0.25

H($b\bar{b}$)H($b\bar{b}$): Search Strategy

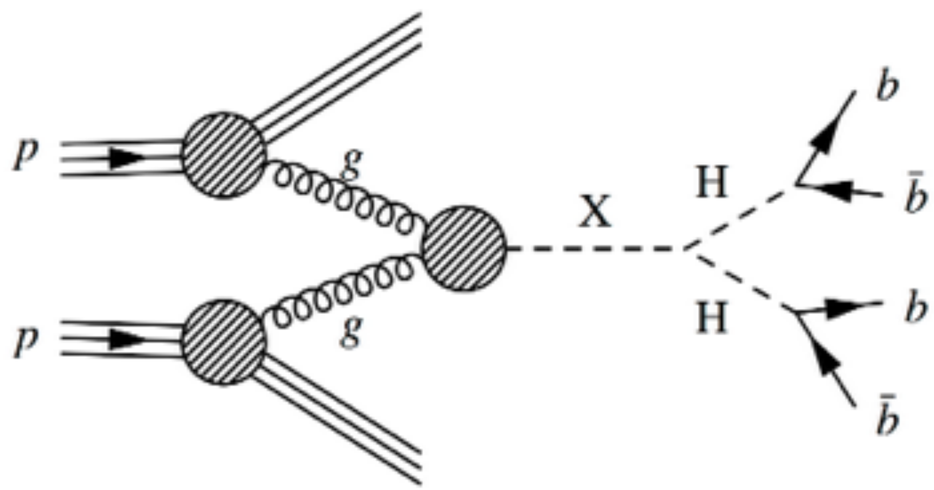

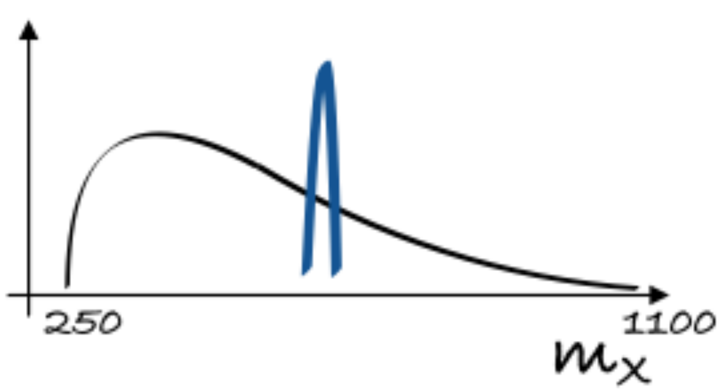

- CMS-HIG-14-013. Highest Higgs branching fraction to $b\bar{b}$. Unearth signal from under **copious 4-jet QCD multi-jet background**. We rely on:
  - The **CMVA b-tagging** algorithm. 2x better fake rejection than CSV at 70% efficiency
  - **Data-validated model** of the QCD multi-jet background
  - Good $\boldsymbol{m_{b\bar{b}}}$ **resolution**
- L = 17.93 fb^{-1}. $\sqrt{s}$ = 8 TeV
- Trigger: 2 b-tags with **online-CSV** algorithm
- **Two mass regimes:**
  - Low Mass Regime: 270 GeV ≤ mX ≤ 450 GeV
  - High Mass Regime: 450 GeV < mX ≤ 1100 GeV
- **Kinematic constraint** on jet energies to the Higgs mass
- Parametric form for **signal modeled from MC**
- Background decomposed into two components
  - **$t\bar{t}$ component**. Parametric form from MC
  - **QCD multi-jet component**. Form modeled from data sidebands, validated in several Control Regions

$H(b\bar{b})H(b\bar{b})$: QCD Background Modeling

All-hadronic final state **dominated by multi-jet QCD**. Cannot rely on MC. **Functional form** from studying data.

Signal Region (SR) defined in (m_{H1}, m_{H2}) plane
$\Delta m^2_{H1} + \Delta m^2_{H1} < (17.5\ \text{GeV})^2$ where $\Delta m_{H1,2} = m_{H1,2} - 125$ GeV
We cannot look in here. Blind Analysis.

Sideband Region (SB) defined as
$(35\ \text{GeV})^2 < \Delta m^2_{H1} + \Delta m^2_{H1} < (17.5\ \text{GeV})^2$
and $\Delta m_{H1} \Delta m_{H2} < 0$

Validation Region (VR) and Validation Region Sideband (VB) centered around (90 GeV, 90 GeV)

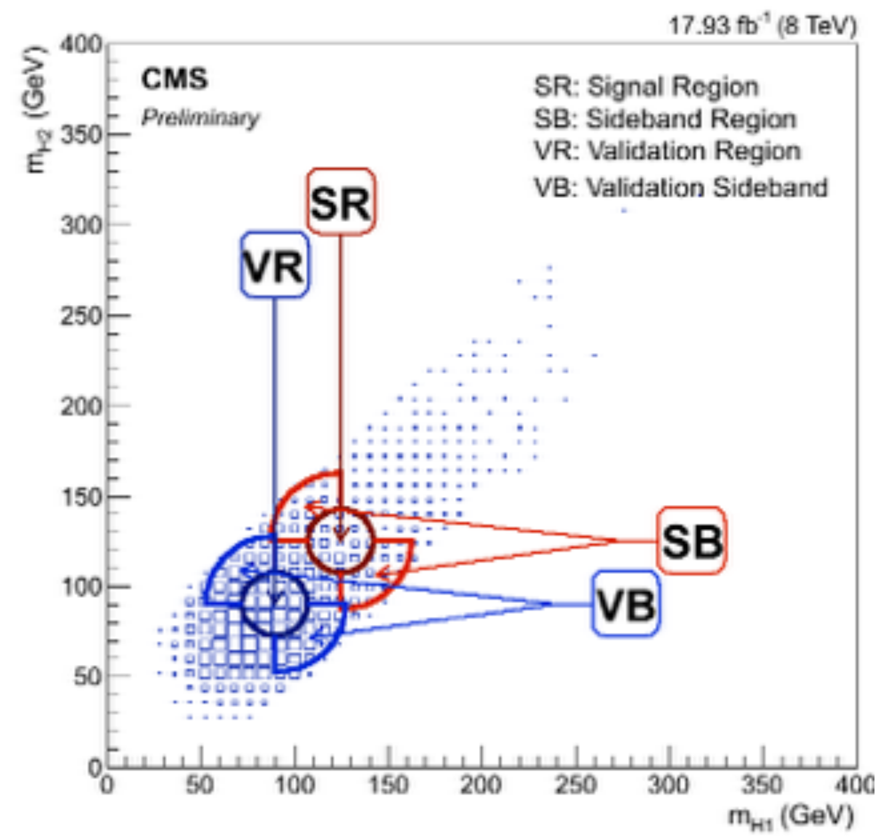

$H(b\bar{b})H(b\bar{b})$: QCD Background Modeling

All-hadronic final state **dominated by multi-jet QCD**. Cannot rely on MC. **Functional form** from studying data.

Signal Region (SR) defined in (m_{H1}, m_{H2}) plane

$\Delta m^2_{H1} + \Delta m^2_{H1} < (17.5\ \mathrm{GeV})^2$ where $\Delta m_{H1,2} = m_{H1,2} - 125$ GeV

We cannot look in here. Blind Analysis.

Sideband Region (SB) defined as

$(35\ \mathrm{GeV})^2 < \Delta m^2_{H1} + \Delta m^2_{H1} < (17.5\ \mathrm{GeV})^2$

and $\Delta m_{H1} \Delta m_{H2} < 0$

Validation Region (VR) and Validation Region Sideband (VB) centered around (90 GeV, 90 GeV)

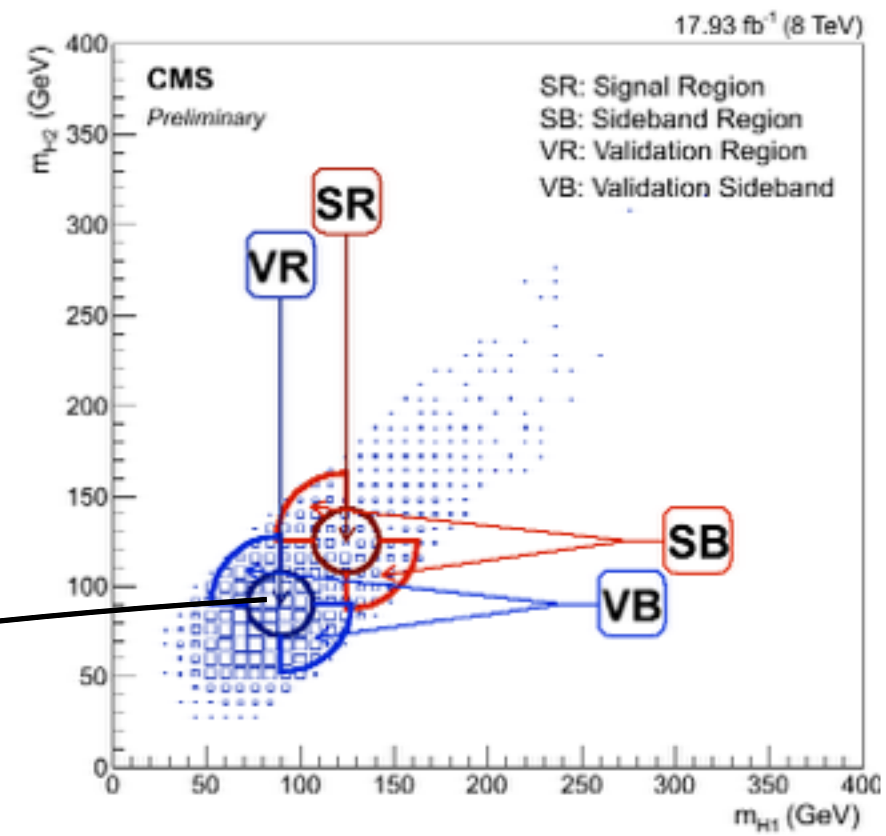

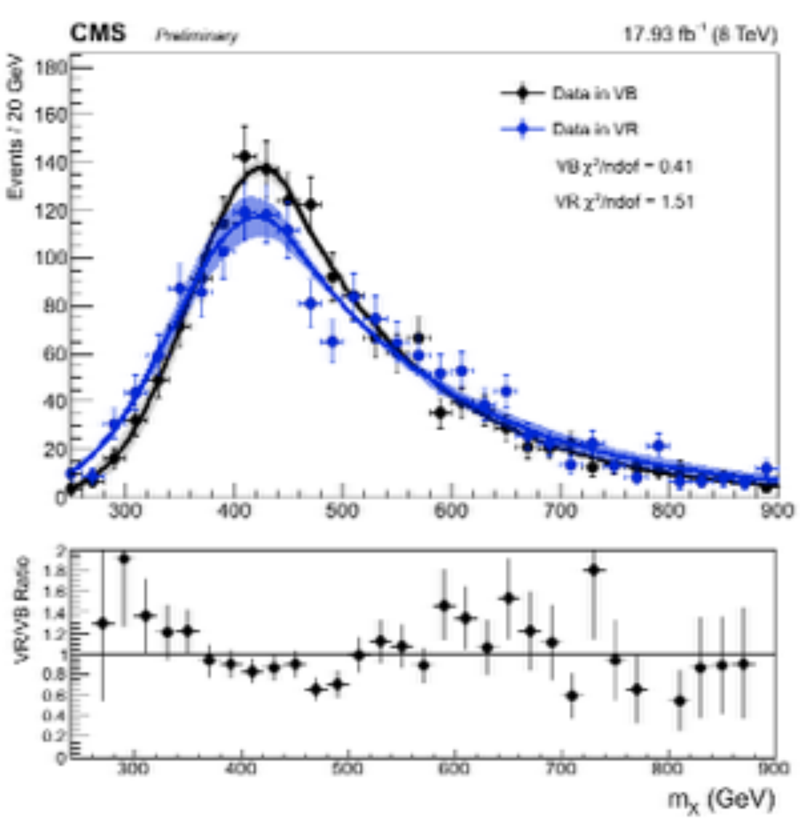

$H(b\bar{b})H(b\bar{b})$: QCD Background Modeling

All-hadronic final state **dominated by multi-jet QCD**. Cannot rely on MC. **Functional form** from studying data.

Signal Region (SR) defined in (m_{H1}, m_{H2}) plane
$\Delta m^2_{H1} + \Delta m^2_{H1} < (17.5\ \text{GeV})^2$ where $\Delta m_{H1,2} = m_{H1,2} - 125$ GeV
We cannot look in here. Blind Analysis.

Sideband Region (SB) defined as
$(35\ \text{GeV})^2 < \Delta m^2_{H1} + \Delta m^2_{H1} < (17.5\ \text{GeV})^2$
and $\Delta m_{H1} \Delta m_{H2} < 0$

Validation Region (VR) and Validation Region Sideband (VB) centered around (90 GeV, 90 GeV)

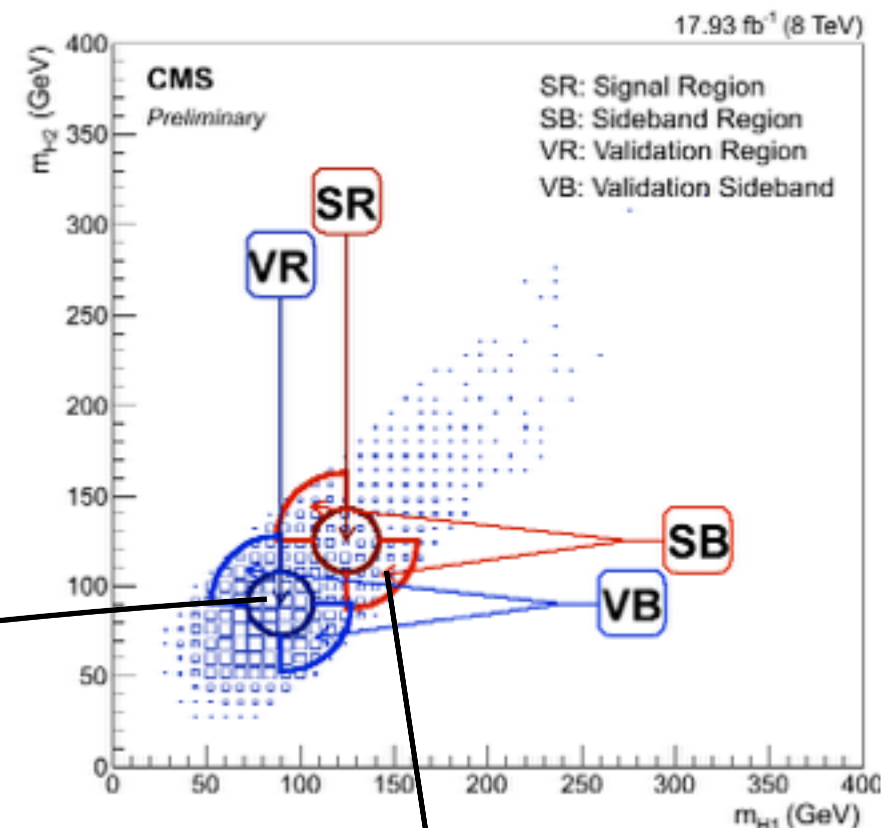

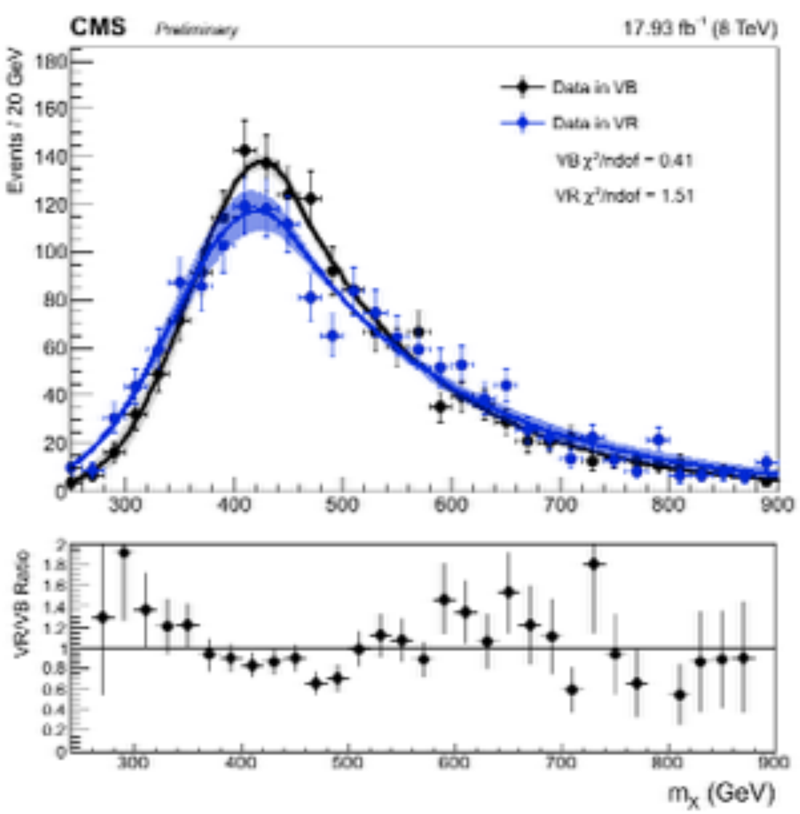

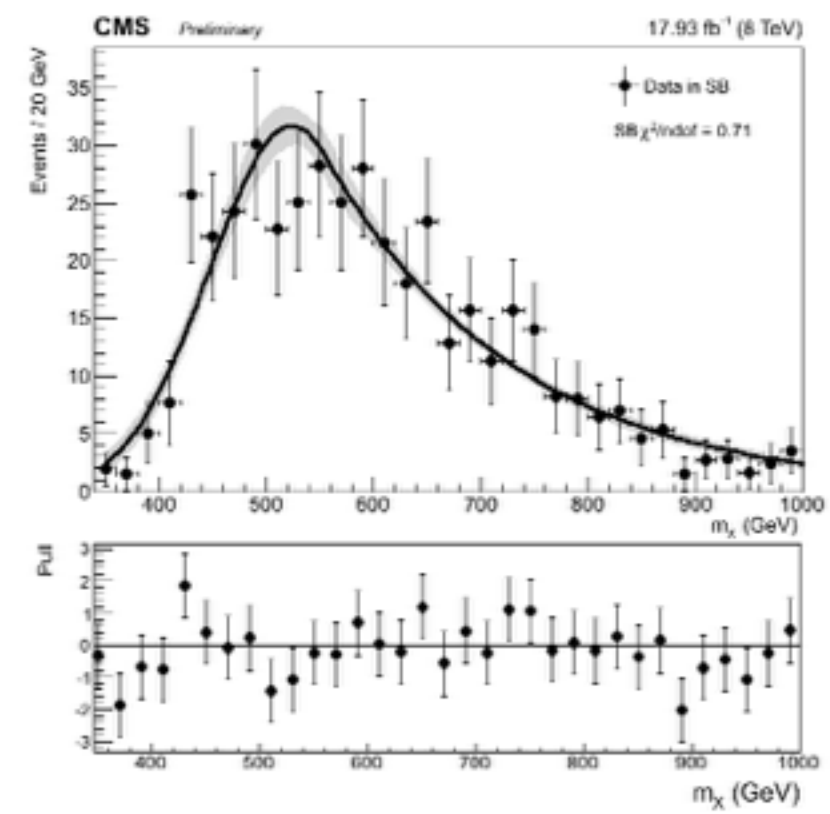

$H(b\bar{b})H(b\bar{b})$: QCD Background Modeling

All-hadronic final state **dominated by multi-jet QCD**. Cannot rely on MC. **Functional form** from studying data.

Signal Region (SR) defined in (m_{H1}, m_{H2}) plane
$\Delta m^2_{H1} + \Delta m^2_{H1} < (17.5\ \text{GeV})^2$ where $\Delta m_{H1,2} = m_{H1,2} - 125$ GeV
We cannot look in here. Blind Analysis.

Sideband Region (SB) defined as
$(35\ \text{GeV})^2 < \Delta m^2_{H1} + \Delta m^2_{H1} < (17.5\ \text{GeV})^2$
and $\Delta m_{H1} \Delta m_{H2} < 0$

Validation Region (VR) and Validation Region Sideband (VB) centered around (90 GeV, 90 GeV)

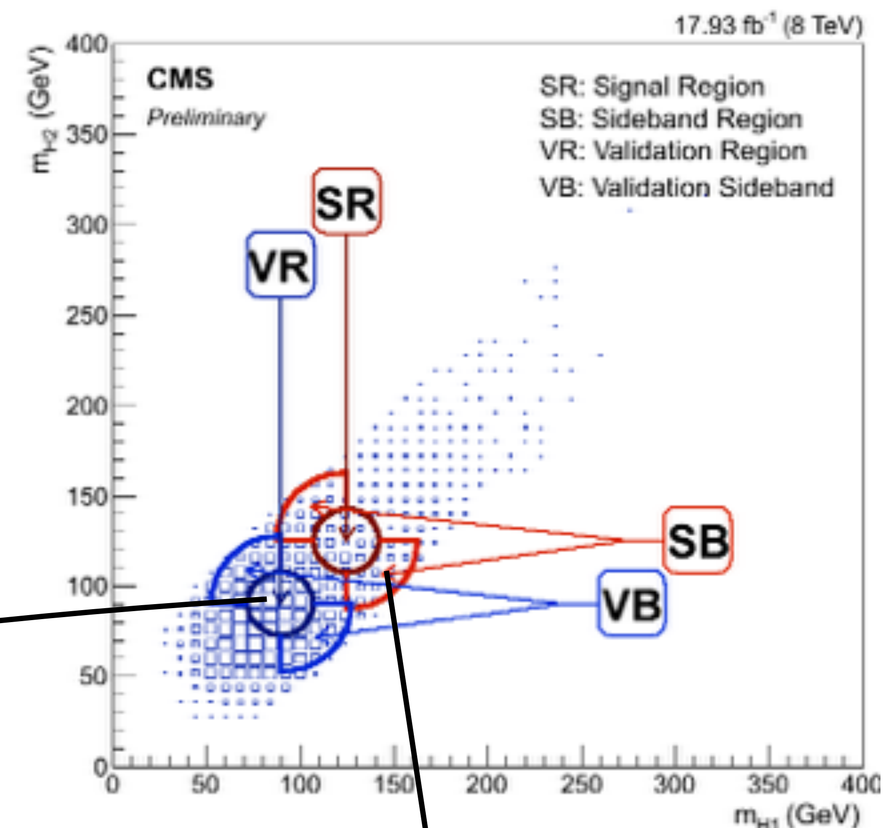

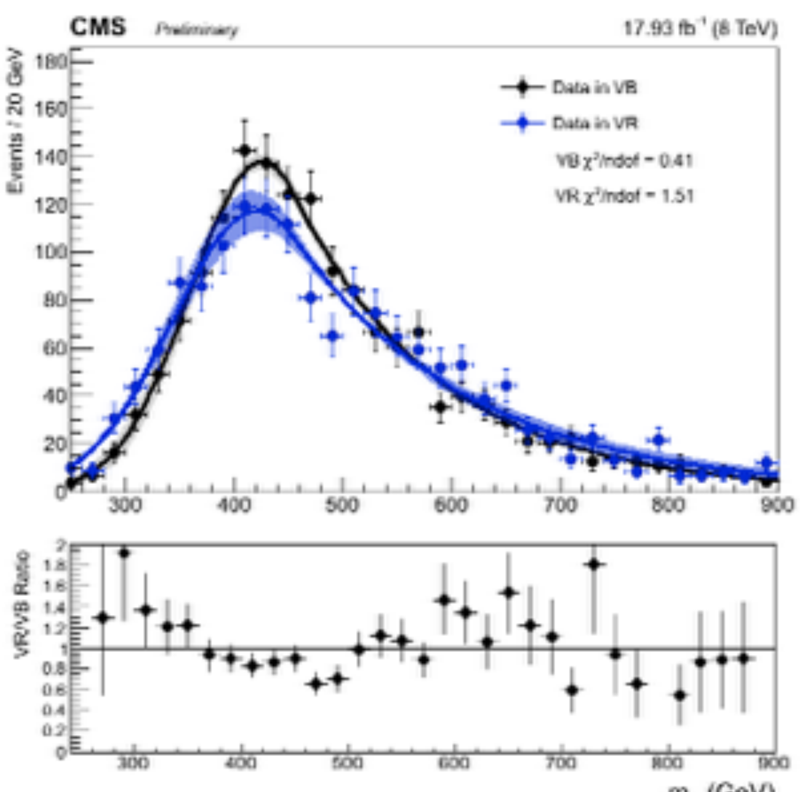

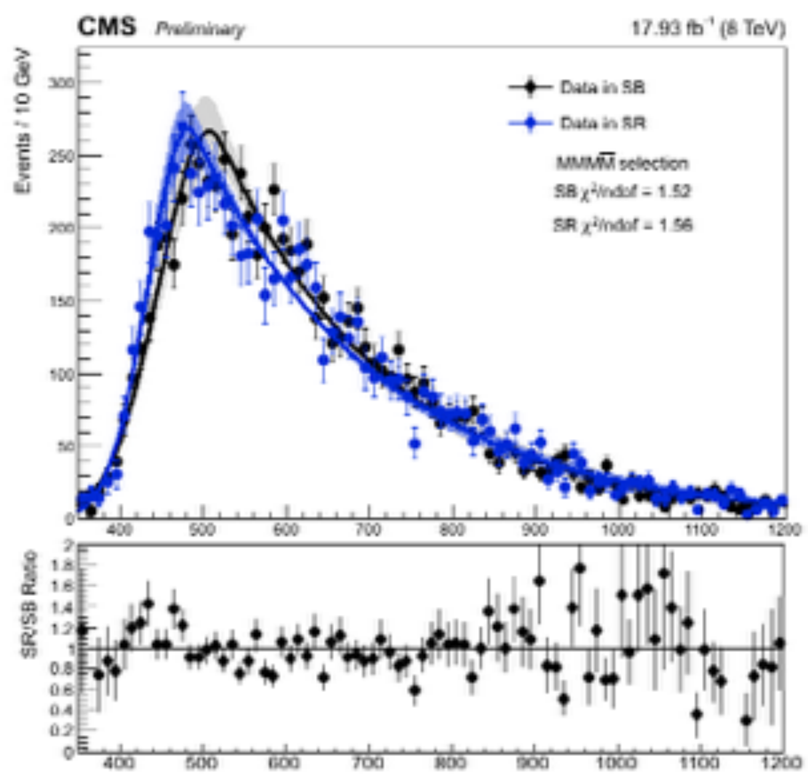

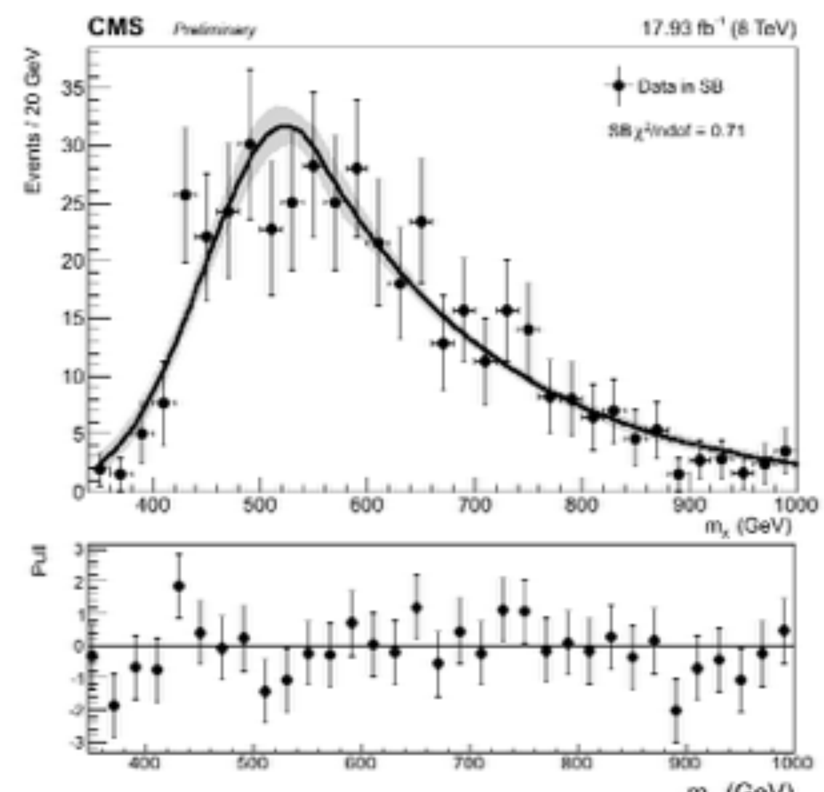

$H(b\bar{b})H(b\bar{b})$: Signal and $t\bar{t}$ Background

Event Selection Criteria

- Event contains at least 4 jets with $p_T > 40$ GeV, $|\eta| < 2.5$, CMVA $\epsilon = 70\%$
- **Low Mass Regime**:
  - HH candidates from the selected jets such that $|m_H - 125 \text{ GeV}| < 35$ GeV
  - At least 2 of these jets with $p_T > 90$ GeV
- **High Mass Regime**:
  - HH candidates from the selected jets such that jets associated with an H have $\Delta R < 1.5$
  - If $m_X > 740$ GeV, H $p_T > 300$ GeV
- In case of multiple HH candidates, we choose the combination that minimizes $|m_{H1} - m_{H2}|$
- m_{HH} must fall within SR

Signal Modeling

- Signal shape from simulation of **RS1 radion** decaying to $b\bar{b}b\bar{b}$ via HH.
- **Negligible natural width** 1 GeV
- Samples
  m_X = 270 GeV to 1100 GeV

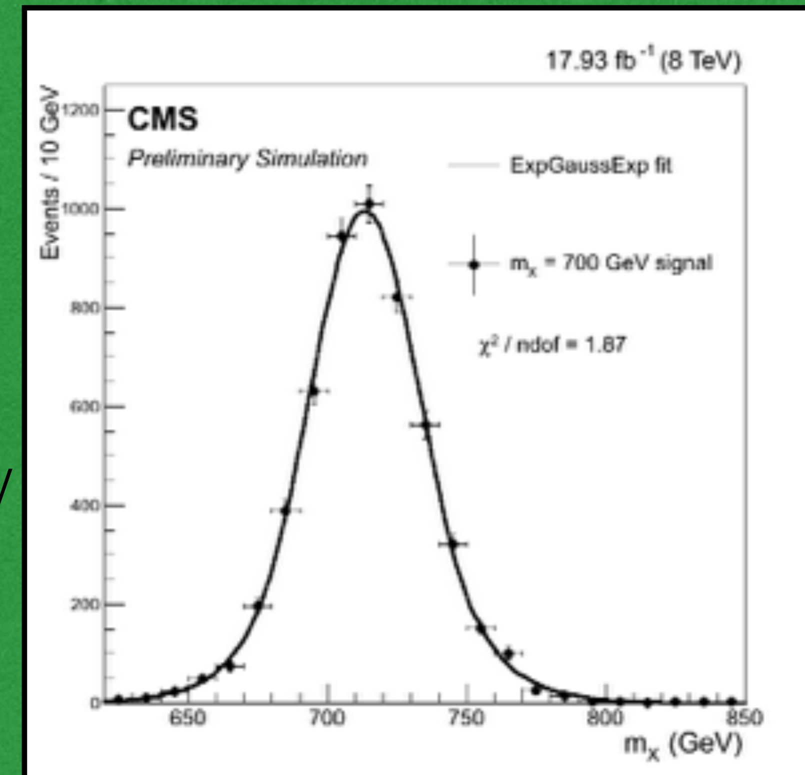

H($b\bar{b}$)H($b\bar{b}$): Signal and $t\bar{t}$ Background

Event Selection Criteria

- Event contains at least 4 jets with p_T > 40 GeV, $|\eta|$ < 2.5, CMVA ϵ = 70%
- **Low Mass Regime**:
  - HH candidates from the selected jets such that $|m_H - 125\text{ GeV}| < 35$ GeV
  - At least 2 of these jets with p_T > 90 GeV
- **High Mass Regime**:
  - HH candidates from the selected jets such that jets associated with an H have ΔR < 1.5
  - If m_X > 740 GeV, H p_T > 300 GeV
- In case of multiple HH candidates, we choose the combination that minimizes $|m_{H1} - m_{H2}|$
- m_{HH} must fall within SR

Signal Modeling

- Signal shape from simulation of **RS1 radion** decaying to $b\bar{b}b\bar{b}$ via HH.
- **Negligible natural width** 1 GeV
- Samples m_X = 270 GeV to 1100 GeV

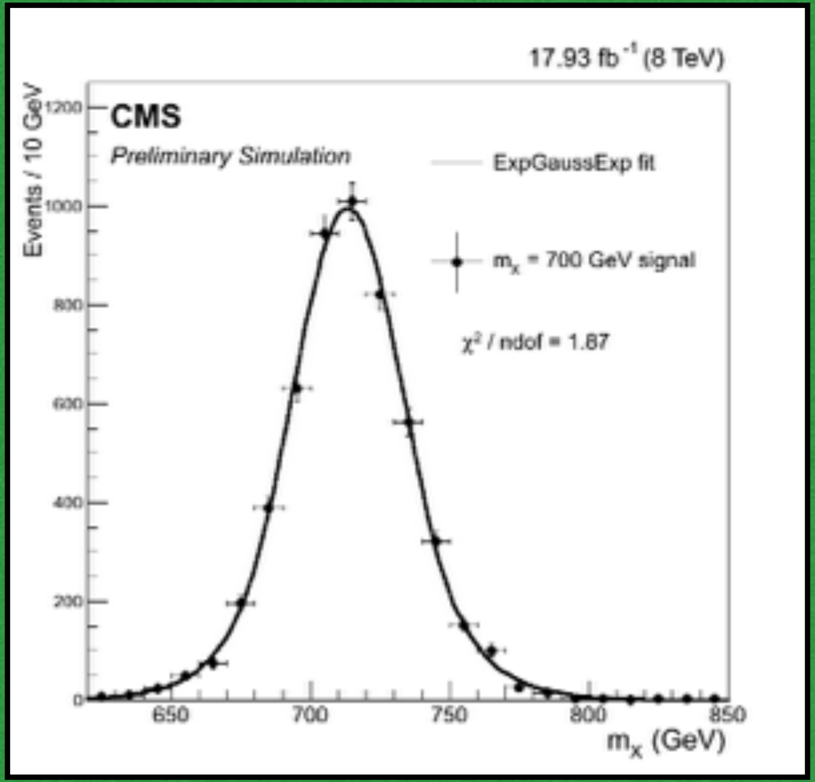

$t\bar{t}$ Modeling

- $t\bar{t}$ contributes **22% (27%)** of background in Low (High) mass regimes
- Modeled from MC.

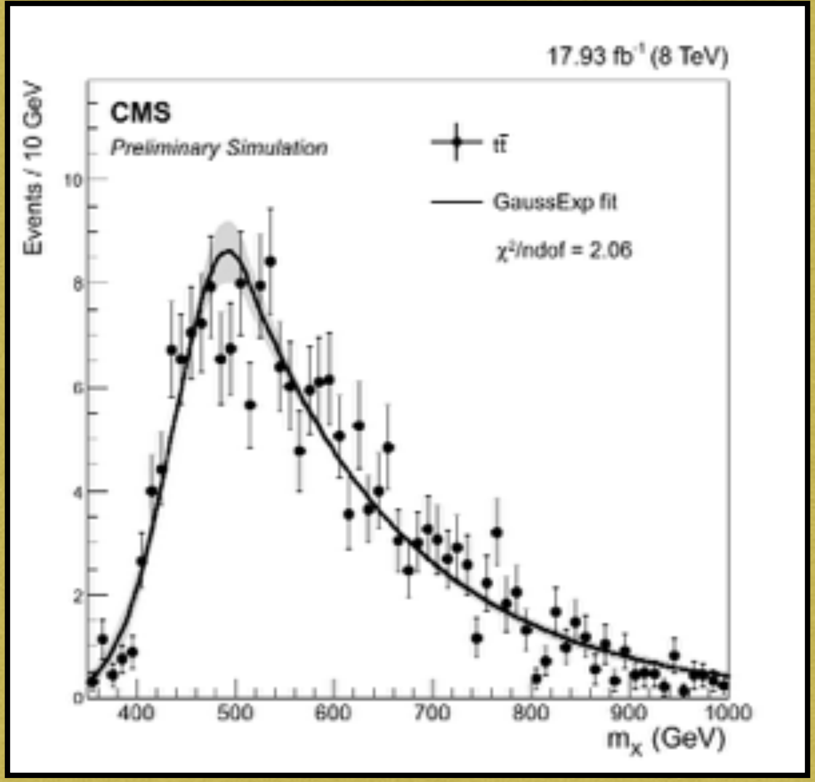

$H(b\bar{b})H(b\bar{b})$: Results

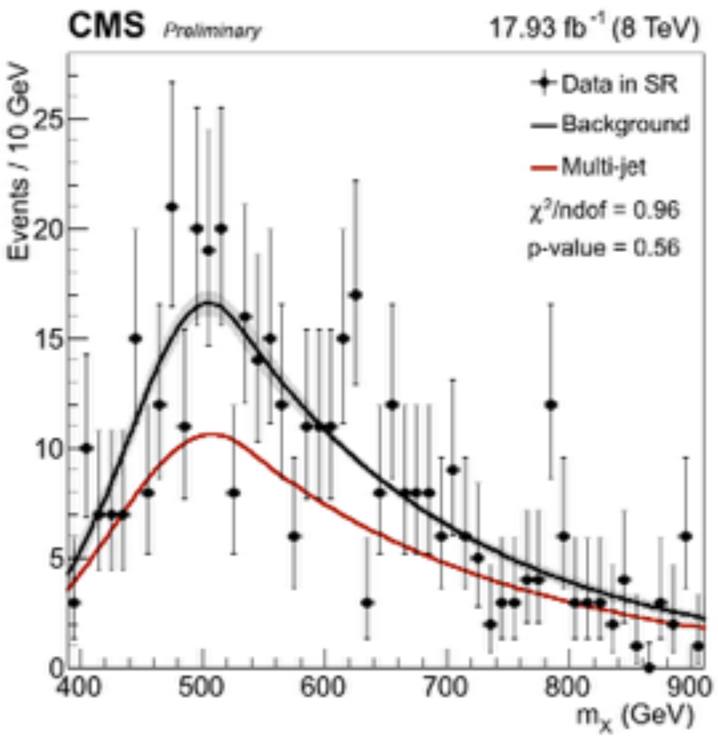

- Background-only fit shown to data between 400 GeV and 900 GeV.
- Shaded region corresponds to 1σ variation of parameterized fit.
- **No clear deviation from background-only hypothesis.** Compute upper limits.

$H(b\bar{b})H(b\bar{b})$: Results

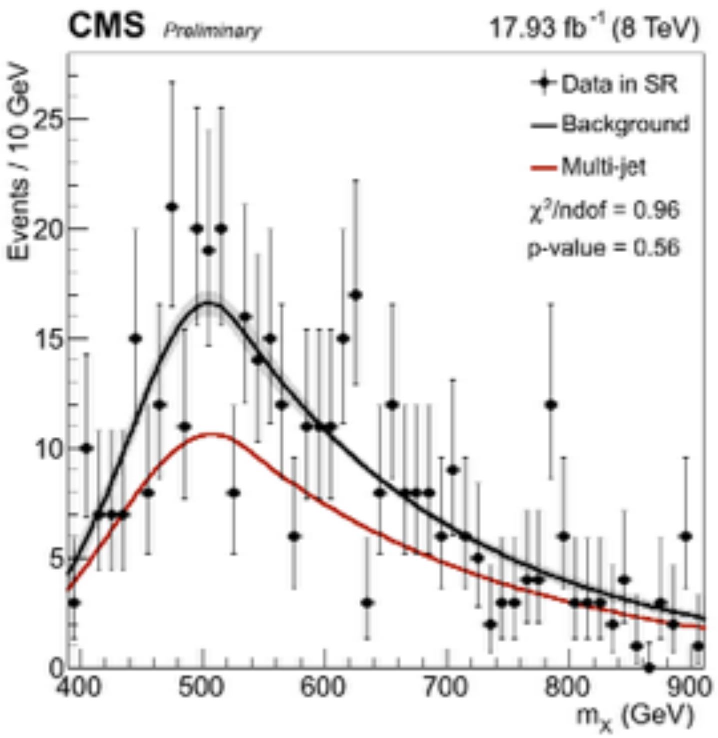

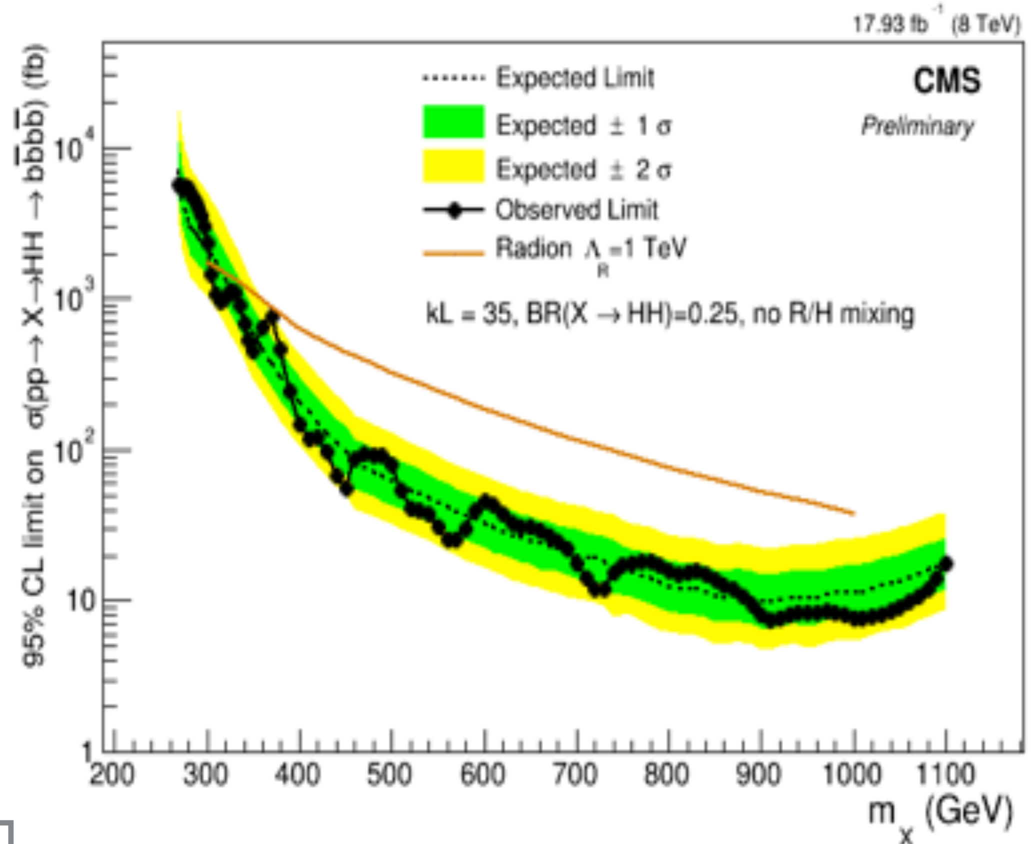

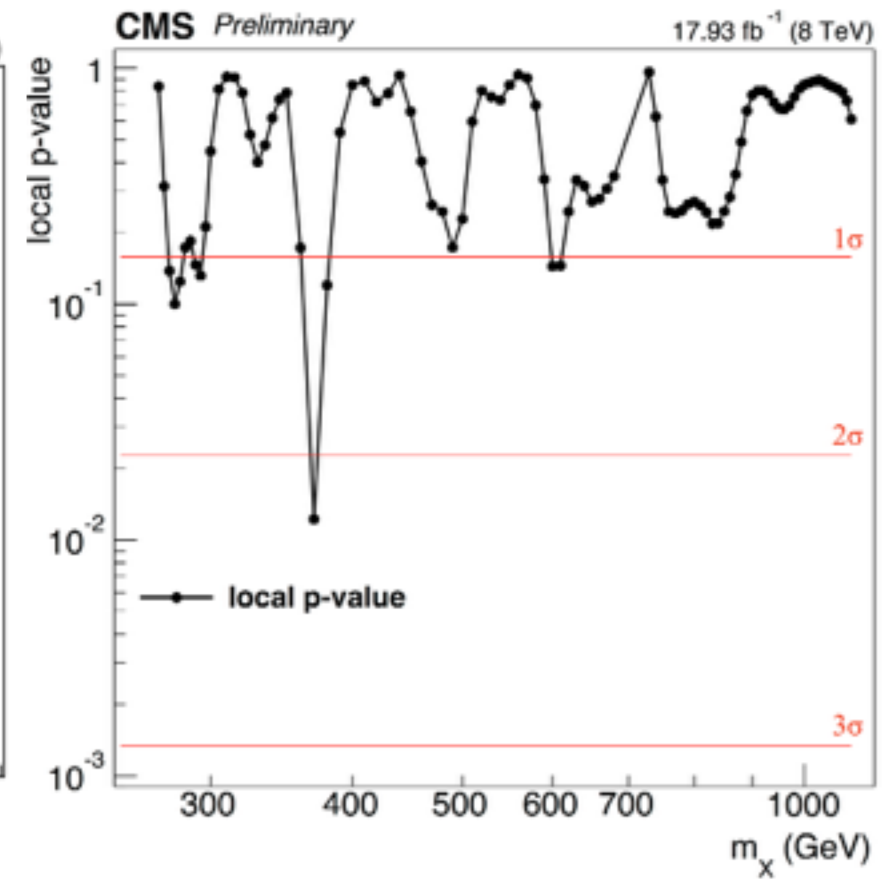

- Background-only fit shown to data between 400 GeV and 900 GeV.
- Shaded region corresponds to 1σ variation of parameterized fit.
- **No clear deviation from background-only hypothesis.** Compute upper limits.

- Maximum excess has local p-value of 2.1σ, global p-value of 1σ. **No significant excess** and no significant deviation from expected limits.
- The RS1 radion in WED scenario kL = 35, right handed top on EWK brane, no radion-Higgs mixing with Λ_R = 1 TeV is excluded between 300 GeV and 1 TeV

(Cross sections of the radion assume *k*-factor for top-loop in gluon-fusion production of R to be identical to that of Higgs production. Br(R→HH) = 0.25)

Combined two-Higgs Results and Conclusions

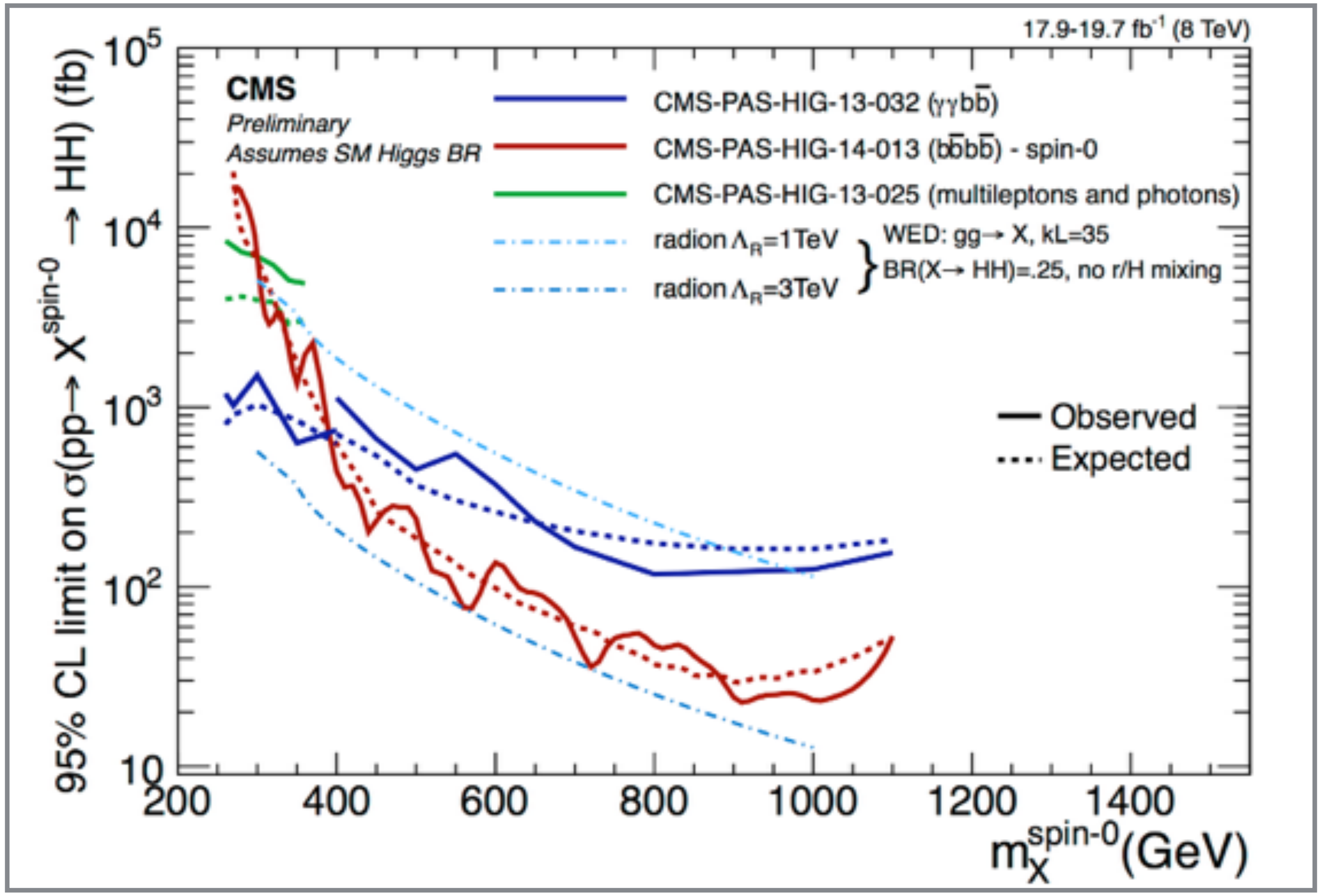

- CMS has **produced results** from searches for double Higgs production at 8 TeV.
- H(γγ)H($b\bar{b}$) and H($b\bar{b}$)H($b\bar{b}$) sensitivities cross. **Complementary searches**.
- **No statistically significant signal** has been observed. Upper limits set at 95% confidence through diverse decay channels of the Higgs
- Resonant searches **constrain Beyond the Standard Model Physics**: 2HDM and WED (RS1)

Analyses gearing up for Run II data

BACKUP

Multi-lepton and Photons: Systematics

Source of Uncertainty	Uncertainty
Luminosity	2.6%
PDF	10%
$E_{\mathrm{T}}^{\mathrm{miss}}$ Resolution/Smearing: 0-50 GeV, 50-100 GeV, $>$ 100 GeV	(-3%, +4%, +4%)
Jet Energy Scale	0.5%
B-Tag scale factor	0.1% (WZ), 6% ($t\bar{t}$)
Muon ID/Isolation at 30 GeV	0.2%
Electron ID/Isolation at 30 GeV	0.6%
Trigger Efficiency	5%
$t\bar{t}$ xsec	10%
$t\bar{t}$ fake rate contribution	50%
WZ cross-section	15%
ZZ cross-section	15%

Table 6: The systematic uncertainties associated with this analysis. The $E_{\mathrm{T}}^{\mathrm{miss}}$ resolution systematic is given for WZ background on Z for different cuts on $E_{\mathrm{T}}^{\mathrm{miss}}$ and for different cuts on M_T given a cut of $E_{\mathrm{T}}^{\mathrm{miss}} > 50$ GeV.

Multi-lepton and Photons: Event Counts

4 Lepton Results										
Selection	on- or off-Z	E_T^{miss}	N_τ=0, N_{b-Jet}=0		N_τ=1, N_{b-Jet}=0		N_τ=0, $N_{b-Jet}\geq 1$		N_τ=1, $N_{b-Jet}\geq 1$	
			obs	expect	obs	expect	obs	expect	obs	expect
OSSF0	NA	(100,∞)	0	0.07 ± 0.07	0	0.18 ± 0.09	0	0.05 ± 0.05	0	0.16 ± 0.1
OSSF0	NA	(50,100)	0	0.07 ± 0.06	2	0.8 ± 0.35	0	0 ± 0.03	0	0.43 ± 0.22
OSSF0	NA	(30,50)	0	0.001 ± 0.02	0	0.47 ± 0.24	0	0 ± 0.02	0	0.11 ± 0.09
OSSF0	NA	(0,30)	0	0.007 ± 0.02	1	0.4 ± 0.16	0	0.001 ± 0.02	0	0.02 ± 0.04
OSSF1	off-Z	(100,∞)	0	0.07 ± 0.04	4	1 ± 0.33	0	0.14 ± 0.09	0	0.46 ± 0.2
OSSF1	on-Z	(100,∞)	2	0.6 ± 0.2	2	3.4 ± 0.8	1	0.8 ± 0.41	0	0.6 ± 0.26
OSSF1	off-Z	(50,100)	0	0.21 ± 0.09	5	2.6 ± 0.6	0	0.21 ± 0.11	1	0.7 ± 0.32
OSSF1	on-Z	(50,100)	2	1.3 ± 0.39	10	12 ± 2.5	2	0.6 ± 0.33	1	0.8 ± 0.3
OSSF1	off-Z	(30,50)	1	0.16 ± 0.07	4	2.4 ± 0.5	0	0.06 ± 0.06	0	0.47 ± 0.21
OSSF1	on-Z	(30,50)	3	1.2 ± 0.35	11	14 ± 3.1	0	0.22 ± 0.12	0	0.8 ± 0.31
OSSF1	off-Z	(0,30)	1	0.38 ± 0.18	11	5.7 ± 1.7	0	0.05 ± 0.04	0	0.5 ± 0.26
OSSF1	on-Z	(0,30)	1	2 ± 0.5	32	30 ± 9.2	1	0.19 ± 0.11	3	1.3 ± 0.42
OSSF2	TwoZ	(100,∞)	0	0.02 ± 0.15	–	–	0	0.21 ± 0.13	–	–
OSSF2	OneZ	(100,∞)	1	0.43 ± 0.15	–	–	0	0.5 ± 0.29	–	–
OSSF2	off-Z	(100,∞)	0	0.06 ± 0.03	–	–	0	0.09 ± 0.07	–	–
OSSF2	TwoZ	(50,100)	3	2.8 ± 2.1	–	–	0	0.33 ± 0.11	–	–
OSSF2	OneZ	(50,100)	1	2 ± 0.7	–	–	1	0.5 ± 0.28	–	–
OSSF2	off-Z	(50,100)	2	0.2 ± 0.14	–	–	0	0.12 ± 0.1	–	–
OSSF2	TwoZ	(30,50)	19	22 ± 9	–	–	2	0.7 ± 0.24	–	–
OSSF2	OneZ	(30,50)	6	6.5 ± 2.4	–	–	0	0.32 ± 0.12	–	–
OSSF2	off-Z	(30,50)	3	1.4 ± 0.6	–	–	1	0.15 ± 0.08	–	–
OSSF2	TwoZ	(0,30)	118	109 ± 28	–	–	3	2 ± 0.5	–	–
OSSF2	OneZ	(0,30)	24	29 ± 7.6	–	–	1	0.6 ± 0.17	–	–
OSSF2	off-Z	(0,30)	5	7.8 ± 2.3	–	–	0	0.18 ± 0.06	–	–

Table 7: Observed yields for four lepton events from 19.5 fb^{-1} data recorded in 2012. The channels are broken down by the number of and mass of any opposite-sign, same-flavor pairs (whether on or off Z), whether there are any b-jets present and the E_T^{miss}. Expected yields are the sum of simulation and data-driven estimates of backgrounds in each channel. The channels are exclusive.

3 Lepton Results										
Selection		E_T^{miss}	N(τ)=0, NbJet=0		N(τ)=1, NbJet=0		N(τ)=0, NbJet≥1		N(τ)=1, NbJet≥1	
			obs	expect	obs	expect	obs	expect	obs	expect
OSSF0(SS)		(200,∞)	1	1.3 ± 0.6	2	1.4 ± 0.5	0	0.7 ± 0.36	0	0.7 ± 0.5
OSSF0(SS)		(150,200)	2	2.1 ± 0.9	0	3 ± 1.1	1	2.1 ± 1	0	1.5 ± 0.6
OSSF0(SS)		(100,150)	9	10 ± 4.9	4	9.9 ± 3	12	12 ± 5.9	4	6.3 ± 2.8
OSSF0(SS)		(50,100)	34	37 ± 15	54	66 ± 14	32	32 ± 15	24	22 ± 10
OSSF0(SS)		(0,50)	47	46 ± 11	196	221 ± 51	28	24 ± 11	21	31 ± 9.6
OSSF0		(200,∞)	–	–	5	4.8 ± 2.4	–	–	6	5.9 ± 3.1
OSSF0		(150,200)	–	–	12	18 ± 9.1	–	–	21	20 ± 10
OSSF0		(100,150)	–	–	94	96 ± 47	–	–	91	121 ± 61
OSSF0		(50,100)	–	–	351	329 ± 173	–	–	300	322 ± 163
OSSF0		(0to50)	–	–	682	767 ± 207	–	–	230	232 ± 118
OSSF1	below-Z	(200,∞)	2	2.5 ± 0.9	4	2.1 ± 1	1	1.9 ± 0.7	2	2.4 ± 1.2
OSSF1	on-Z	(200,∞)	17	19 ± 6.3	4	5.6 ± 1.9	1	2.4 ± 0.8	3	2.1 ± 0.9
OSSF1	below-Z	(150,200)	7	4.4 ± 1.7	11	9.3 ± 4.6	3	4.7 ± 2.1	7	11 ± 5.9
OSSF1	on-Z	(150,200)	38	32 ± 8.5	10	11 ± 3.6	4	5.4 ± 1.7	2	5.7 ± 2.7
OSSF1	below-Z	(100,150)	21	26 ± 9.9	45	56 ± 27	20	23 ± 11	56	66 ± 33
OSSF1	on-Z	(100,150)	134	129 ± 29	43	51 ± 16	20	18 ± 6	24	28 ± 14
OSSF1	below-Z	(50,100)	157	129 ± 30	383	380 ± 104	58	60 ± 28	166	173 ± 87
OSSF1	on-Z	(50,100)	862	732 ± 141	1363	1227 ± 323	80	62 ± 17	117	101 ± 48
OSSF1	below-Z	(0,50)	543	559 ± 93	10186	9171 ± 2714	40	52 ± 14	257	256 ± 79
OSSF1	on-Z	(0,50)	4041	4061 ± 691	51361	51369 ± 15340	181	181 ± 28	1003	1012 ± 286

Table 8: Observed yields for three lepton events from 19.5 fb^{-1} data recorded in 2012. The channels are broken down by the number of and mass of any opposite-sign, same-flavor pairs (whether on or off Z), whether there are any b-jets present and the E_T^{miss}. Expected yields are the sum of simulation and data-driven estimates of backgrounds in each channel. The channels are exclusive.

2 Lepton and 2 Photon Results				
Selection		E_T^{miss}	obs	expect
OSSF1	off-Z	(50,∞)	0	0.19±0.25
OSSF1	on-Z	(50,∞)	0	0.1±0.17
OSSF1	off-Z	(30,50)	1	0.17±0.25
OSSF1	on-Z	(30,50)	1	0.33±0.28
OSSF1	off-Z	(0,30)	1	1.2±0.74
OSSF1	on-Z	(0,30)	0	1.01±0.55
OSSF0	NA	(0,∞)	0	0±0.17

Table 9: Observed yields for two lepton and two photon events from 19.5 fb^{-1} data recorded in 2012. The channels are broken down the number of and mass of any opposite-sign, same-flavor pairs (whether on or off Z), and the E_T^{miss}. Only channels where invariant mass of photons lies in the higgs mass window (120-130 GeV) are considered. Expected yields are data-driven estimates of backgrounds in each channel. The channels are exclusive.

1 Lepton and 2 Photon Results		
E_T^{miss}	obs	expect
(50,∞)	9	14.3±7.15
(30,50)	31	22.1±11.05
(0,30)	74	79.1±39.55

Table 10: Observed yields for one lepton and diphoton events from 19.5 fb^{-1} data recorded in 2012. The channels are broken down in bins of E_T^{miss}. There are no hadronic taus in these channels. Only channels where the invariant mass of photons lies in the higgs mass window (120-130 GeV) are considered. Expected yields are data-driven estimates of backgrounds in each channel. The channels are exclusive.

Multi-lepton and Photons: Results

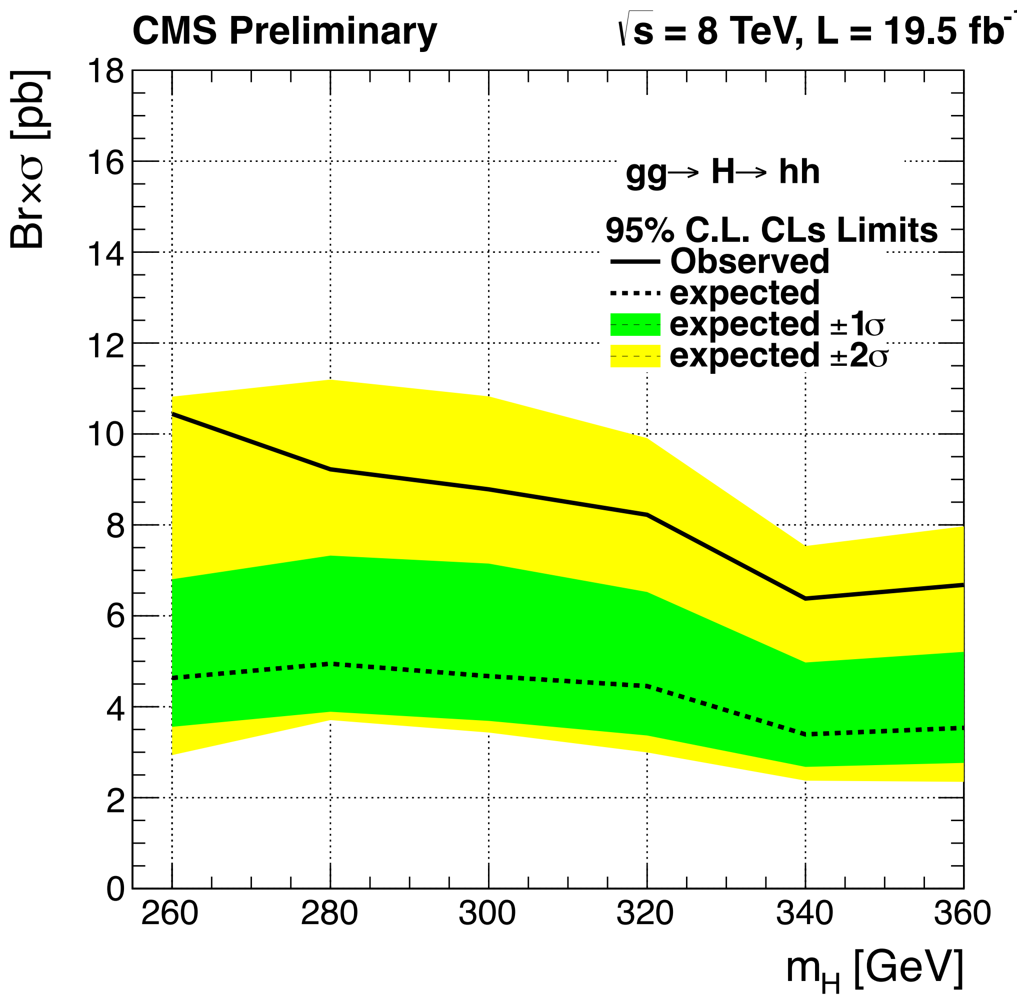

Figure 6: Observed and expected limits with 1- and 2-σ bands for $H \rightarrow hh$ in terms of σ * Br. These limits are based only on multilepton channels. Brs for h are assumed to have SM values. No contribution from gg→A→Zh is considered in this limit.

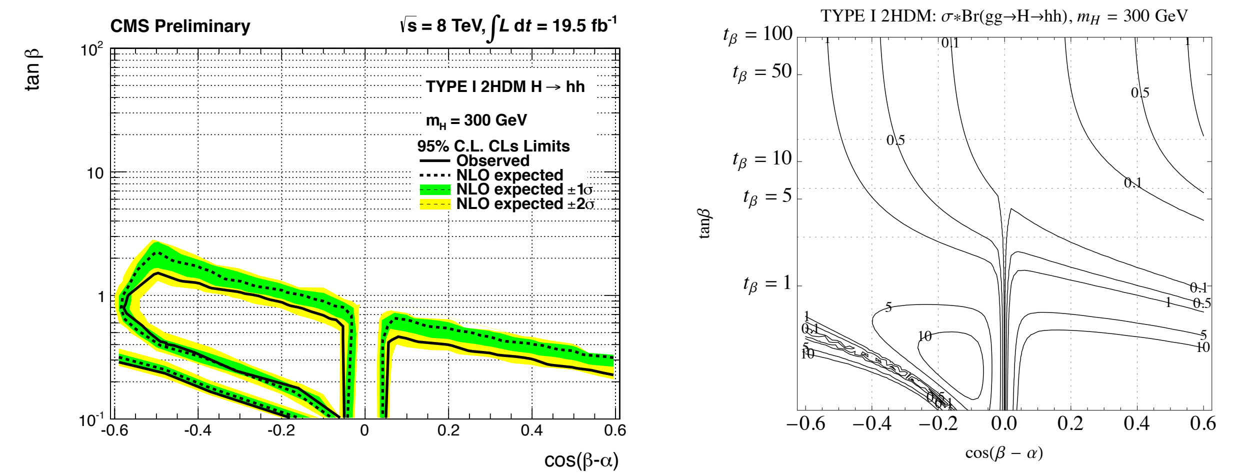

Figure 11: Left: Observed and expected limits on Heavy higgs of mass 300 GeV in Type I 2HDM. The parameters α and β determine the cross section for H production, the Br$(H \rightarrow hh)$ and the Br$(h \rightarrow WW, ZZ, \tau\tau, \gamma\gamma)$. Right: The σ * Br(H→hh) contours for TYPE I 2HDM. This figure is similar to one from theory paper by Nathaniel Craig et al. [4], the only difference is plotting of $\tan\beta$, instead of β, on the vertical axis. The regions below the observed limit lines and within the loop by marked by observed limit are excluded.

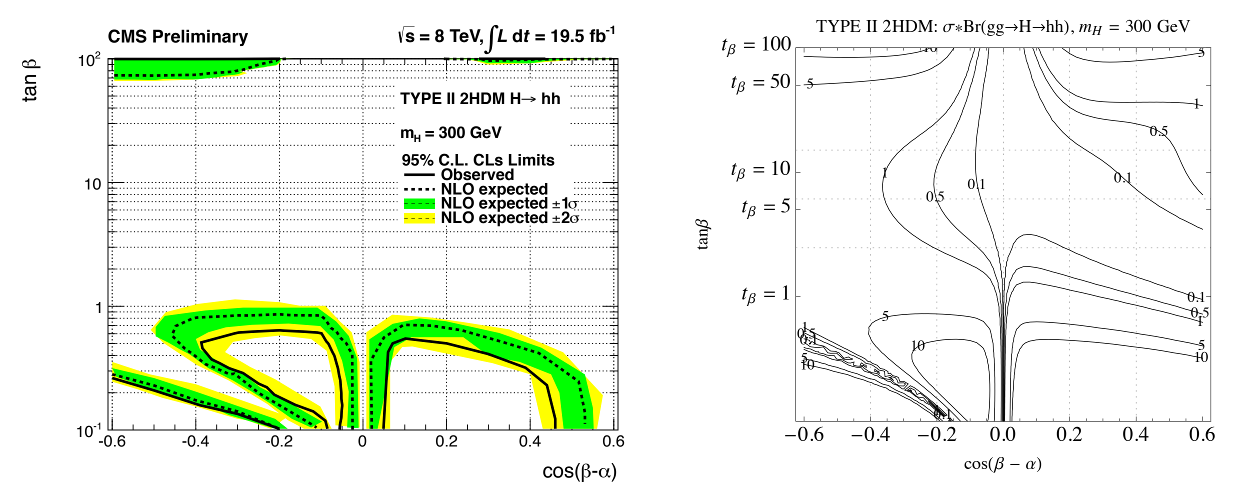

Figure 12: Left: Observed and expected limits on Heavy higgs of mass 300 GeV in Type II 2HDMs. The parameters α and β determine the cross section for H production, the Br$(H \rightarrow hh)$ and the Br$(h \rightarrow WW, ZZ, \tau\tau, \gamma\gamma)$. Right: The σ * Br(H→hh) contours for TYPE II 2HDM. This figure is similar to one from theory paper by Nathaniel Craig et al. [4], the only difference is plotting of $\tan\beta$, instead of β, on the vertical axis. The regions below the observed limit lines and within the loop by marked by observed limit are excluded.

- Type 1, in which $y_1^{u,d,e} = 0$; all fermions couple to one doublet.
- Type 2, in which $y_1^u = y_2^d = y_2^e = 0$; the up-type quarks couple to one doublet and the down-type quarks and leptons couple to the other.
- Type 3, in which $y_1^u = y_1^d = y_2^e = 0$; quarks couple to one doublet and leptons to the other.
- Type 4, in which $y_1^u = y_1^e = y_2^d = 0$; up-type quarks and leptons couple to one doublet and down-type quarks couple to the other.

Multi-lepton and Photons: Results

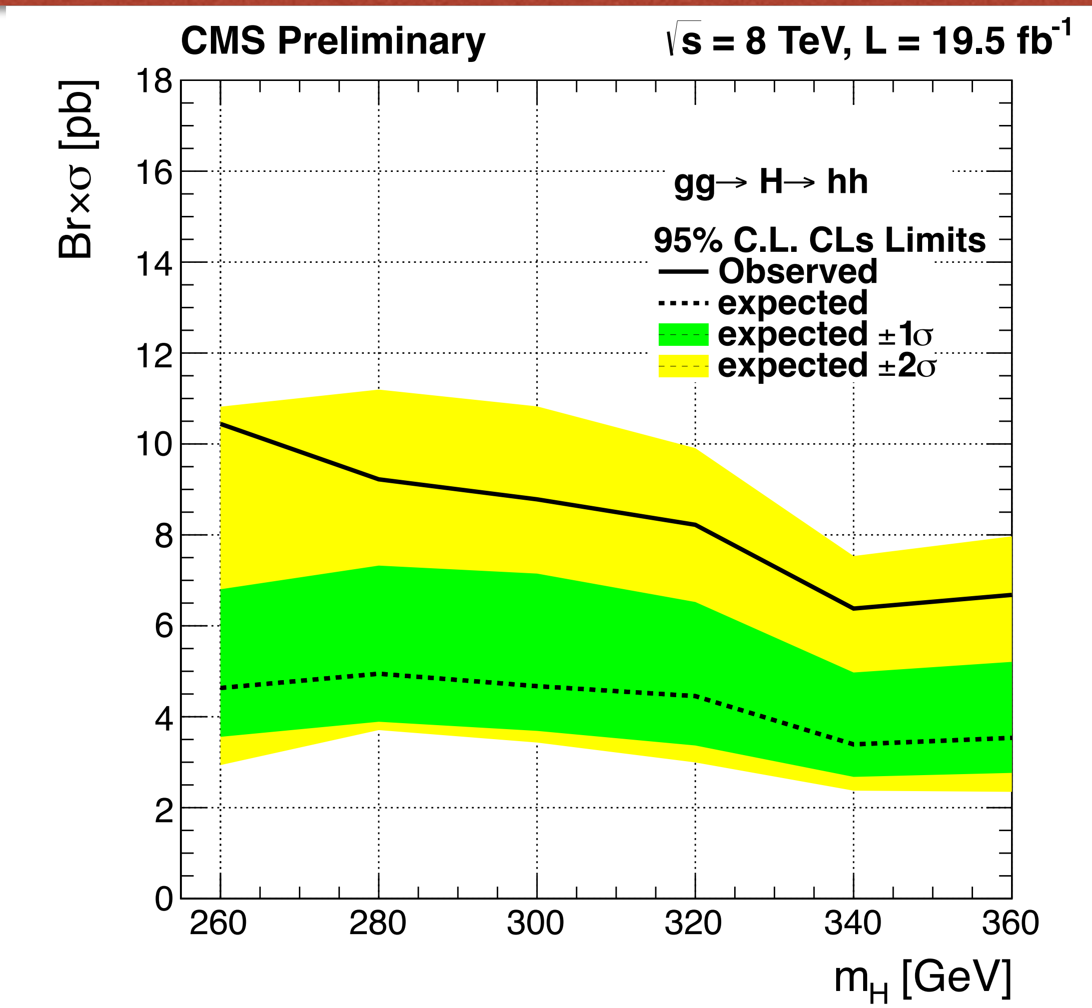

Figure 6: Observed and expected limits with 1- and 2-σ bands for $H \to hh$ in terms of σ * Br. These limits are based only on multilepton channels. Brs for h are assumed to have SM values. No contribution from gg→A→Zh is considered in this limit.

$$\Delta L = -\sum_{i=1,2} \left(y_i^u Q \tilde{\Phi}_i \bar{u} + y_i^d Q \Phi_i \bar{d} + y_i^e L \Phi_i \bar{e} + h.c. \right)$$

- Type 1, in which $y_1^{u,d,e} = 0$; all fermions couple to one doublet.
- Type 2, in which $y_1^u = y_2^d = y_2^e = 0$; the up-type quarks couple to one doublet and the down-type quarks and leptons couple to the other.
- Type 3, in which $y_1^u = y_1^d = y_2^e = 0$; quarks couple to one doublet and leptons to the other.
- Type 4, in which $y_1^u = y_1^e = y_2^d = 0$; up-type quarks and leptons couple to one doublet and down-type quarks couple to the other.

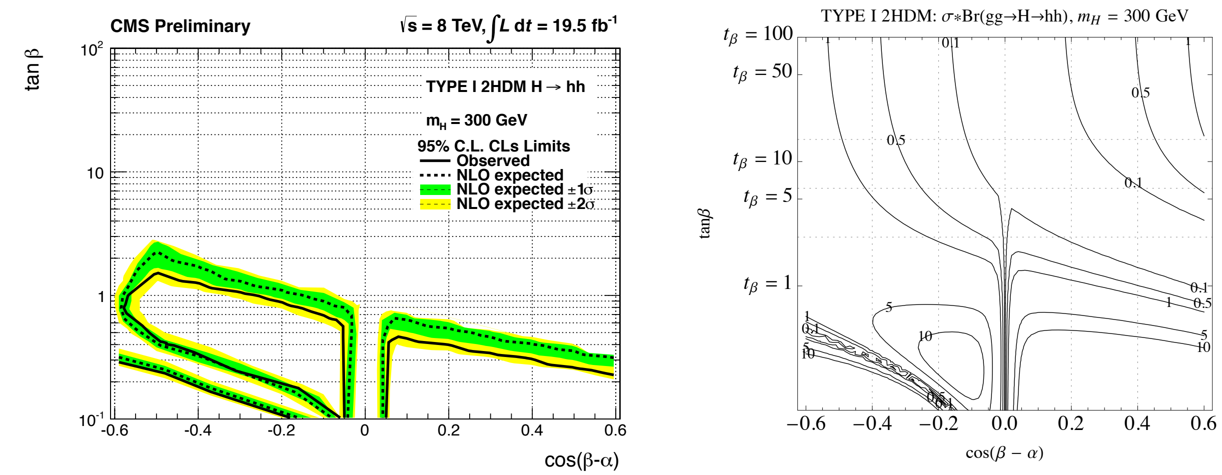

Figure 11: Left: Observed and expected limits on Heavy higgs of mass 300 GeV in Type I 2HDM. The parameters α and β determine the cross section for H production, the $\mathrm{Br}(H \to hh)$ and the $\mathrm{Br}(h \to WW, ZZ, \tau\tau, \gamma\gamma)$. Right: The σ * Br(H→hh) contours for TYPE I 2HDM. This figure is similar to one from theory paper by Nathaniel Craig et al. [4], the only difference is plotting of $\tan\beta$, instead of β, on the vertical axis. The regions below the observed limit lines and within the loop by marked by observed limit are excluded.

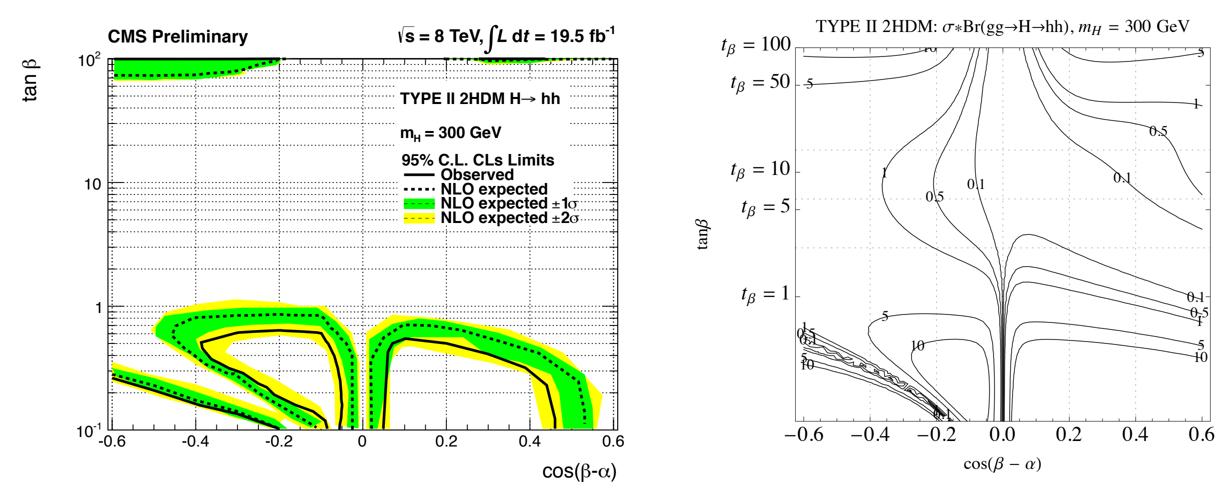

Figure 12: Left: Observed and expected limits on Heavy higgs of mass 300 GeV in Type II 2HDMs. The parameters α and β determine the cross section for H production, the $\mathrm{Br}(H \to hh)$ and the $\mathrm{Br}(h \to WW, ZZ, \tau\tau, \gamma\gamma)$. Right: The σ * Br(H→hh) contours for TYPE II 2HDM. This figure is similar to one from theory paper by Nathaniel Craig et al. [4], the only difference is plotting of $\tan\beta$, instead of β, on the vertical axis. The regions below the observed limit lines and within the loop by marked by observed limit are excluded.

H(b$\bar{b}$)H(γγ): Signal Spectra

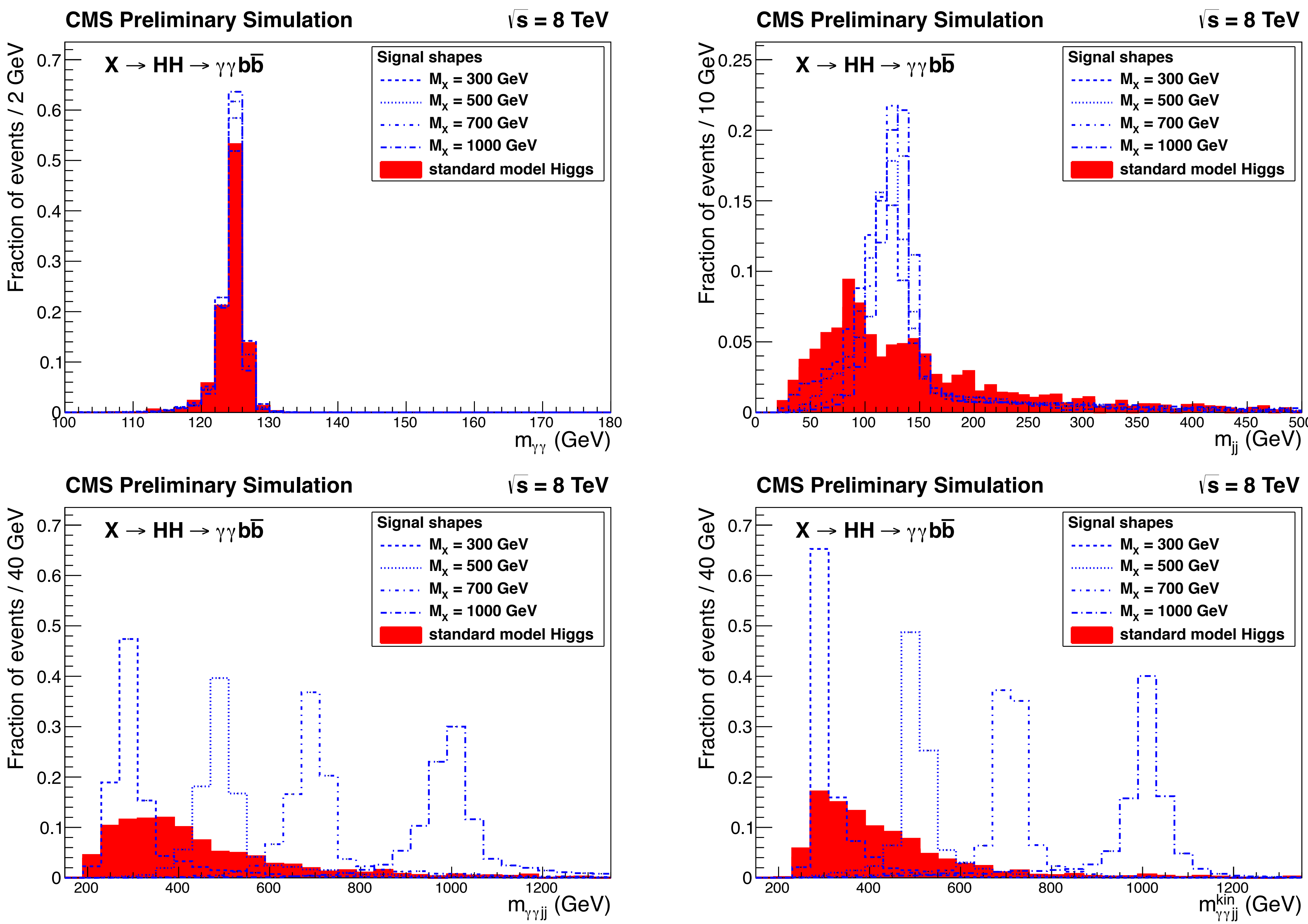

Figure 1: Simulated mass spectra for the signal and the sum of all production mechanisms of the standard model Higgs boson, after basic selections on photons and requesting at least one loose b–tagged jet. The two top plots show the $m_{\gamma\gamma}$ (left) and m_{jj} (right) spectra, while the bottom plots show the $m_{\gamma\gamma\mathrm{jj}}$ spectrum before the kinematic fit (left) and after the kinematic fit (right). All spectra are normalized to unity.

H(b$\bar{b}$)H(γγ): Background Fits

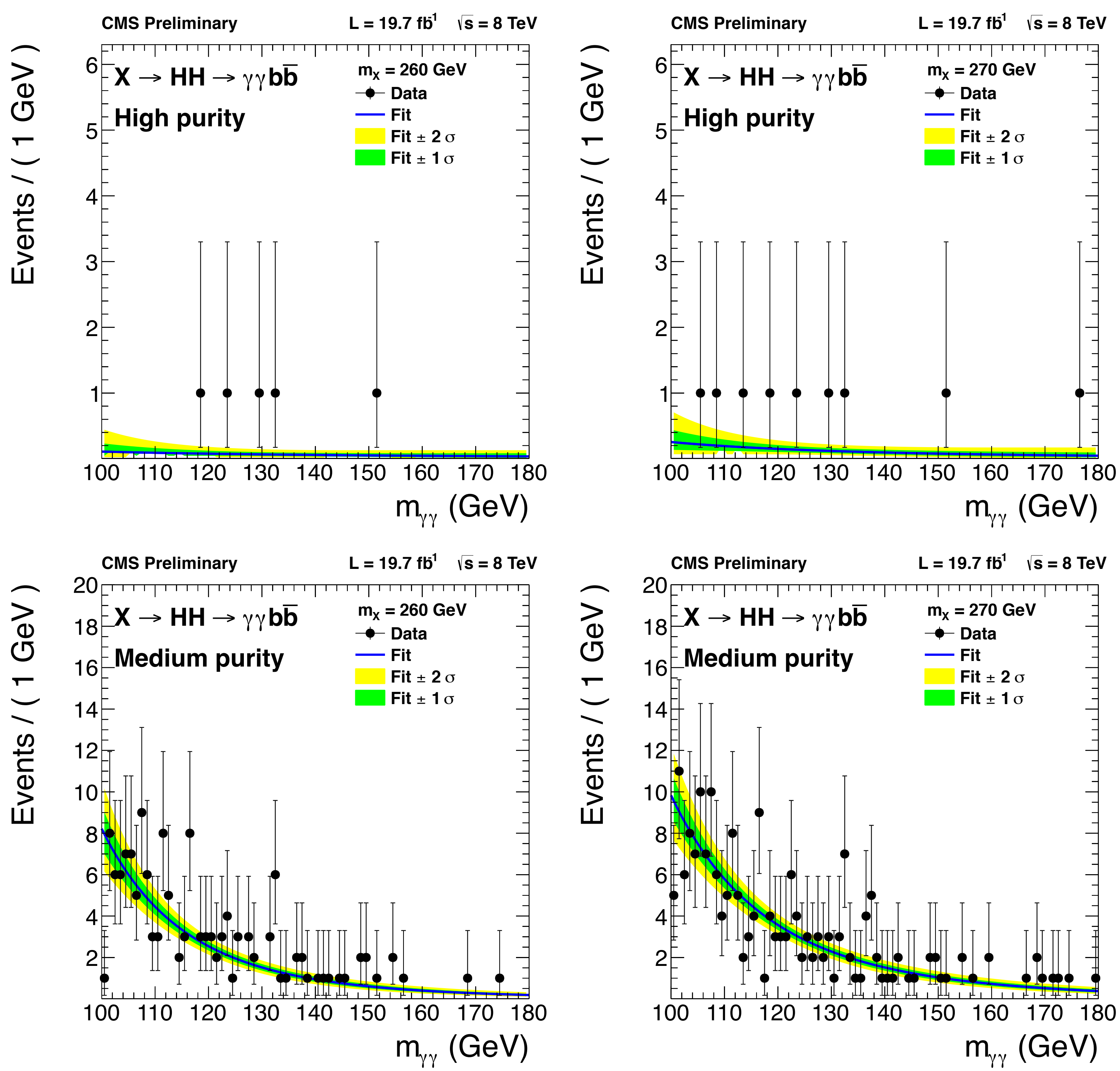

Figure 3: Non-resonant background fits in $m_{\gamma\gamma}$ for the high-purity (top) and medium-purity (bottom) categories for two heavy resonance mass hypotheses - 260 GeV (left) and 270 GeV (right).

H($b\bar{b}$)H($\gamma\gamma$): Background Fits

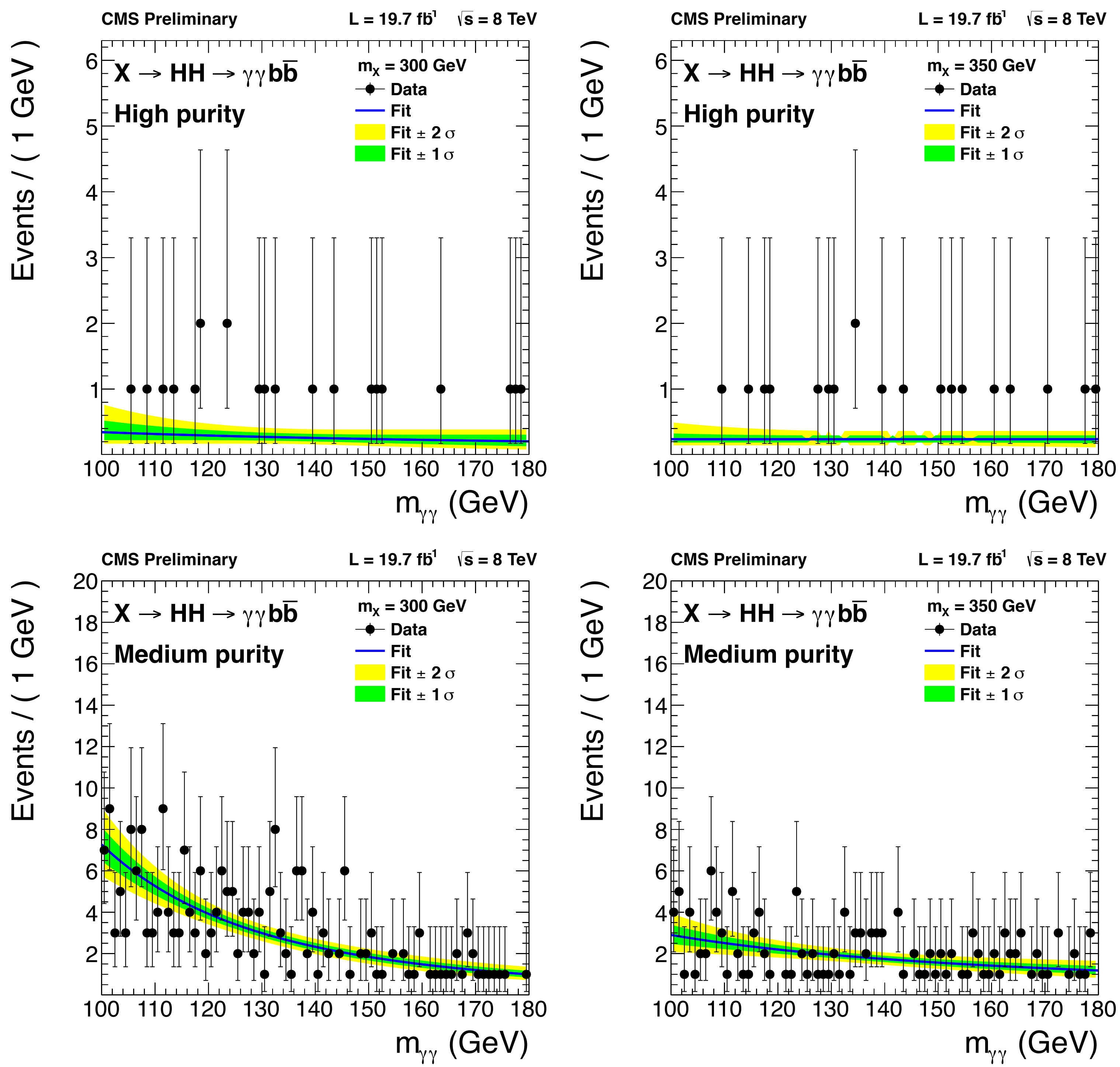

Figure 4: Events in $m_{\gamma\gamma}$ spectrum in high-purity (top) and medium-purity (bottom) categories for two heavy resonance mass hypotheses - 300 GeV (left) and 350 GeV (right). The non-resonant component of the background is shown (black line) with 1 and 2σ bands on the background estimation.

H($b\bar{b}$)H($\gamma\gamma$): Background Fits

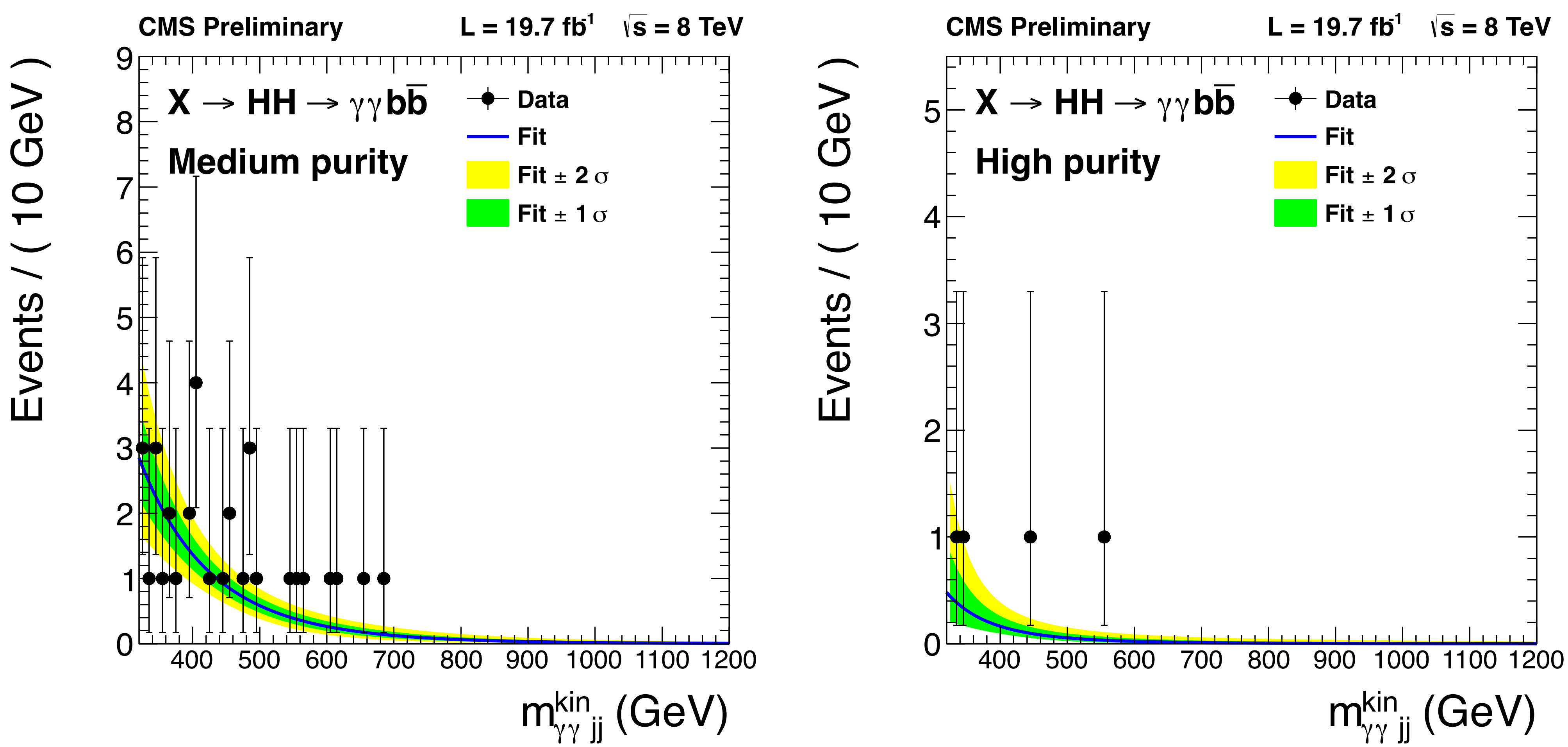

Figure 6: Events in $m_{\gamma\gamma jj}$ spectrum in medium-purity (left) and high-purity (right) categories. The non-resonant component of the background is shown (black line) with 1 and 2σ bands on the background estimation.

$H(b\bar{b})H(\gamma\gamma)$: Systematics

Common normalization uncertainties	
Luminosity	2.6%
Diphoton trigger acceptance	1.0%
Low mass analysis: fit to $m_{\gamma\gamma}$	
Normalization uncertainties	
Photons selection acceptance	1.0%
"b-tag" eff. uncertainty 2 btag cat	4.6%
"b-tag" eff. uncertainty 1 btag cat	-1.2%
m_{jj} and $p_{T,j}$ cut acceptance (JES & JER)	1.5%
$m_{\gamma\gamma jj}$ cut acceptance (PES $\oplus$ JES & PER $\oplus$ JER)	2%
Shape uncertainties	
Parametric scale shift (PES$\oplus$M(H) uncertainty)	$\frac{\Delta m_{\gamma\gamma}}{m_{\gamma\gamma}} = 0.45 \oplus 0.35\%$
Parametric resolution shift (RES)	$\frac{\Delta \sigma}{m_{\gamma\gamma}} = 0.25\%$
	$\frac{\Delta \sigma}{\sigma_{\gamma\gamma}} = 22\%$
High mass analysis: fit to $m^{kin}_{\gamma\gamma jj}$	
Normalization uncertainties	
Photons selection acceptance	1.0%
"b-tag" eff. uncertainty 2 btag cat	5.3%
"b-tag" eff. uncertainty 1 btag cat	-1.8%
m_{jj} and $p_{T,j}$ cut acceptance (JES & JER)	1.5%
$m_{\gamma\gamma}$ cut acceptance (PES & PER)	0.5%
Extra High pt norm. uncertainty	5.0%
Shape uncertainties	
Parametric abs. shift (PES $\oplus$ JES)	$\frac{\Delta m_{\gamma\gamma jj}}{m_{\gamma\gamma jj}} = 0.45 \oplus (0.8 \oplus 1.0) = 1.4\%$
Parametric shift (PER $\oplus$ JER)	$\frac{\Delta \sigma}{\sigma_{\gamma\gamma jj}} = 10\%$

Table 4: Systematic uncertainties by fit strategy.

$H(b\bar{b})H(\gamma\gamma)$: Results

m_X	Observed limit (fb)	Expected limit (fb)	Observed limit (fb)	Expected limit (fb)
			High-purity category only	
260	3.14	2.12	3.54	2.41
270	2.70	2.40	3.07	2.74
300	3.98	2.73	3.64	3.14
350	1.67	2.23	2.17	2.66
400	1.97	1.66	3.40	2.01

m_X	Observed limit (fb)	Expected limit (fb)
400	2.98	1.87
450	1.76	1.42
500	1.19	0.97
550	1.45	0.80
600	0.98	0.69
650	0.61	0.60
700	0.44	0.54
800	0.31	0.46
900	0.32	0.43
1000	0.33	0.43
1100	0.41	0.48

H($b\bar{b}$)H($b\bar{b}$): Combined MVA tagger

The CMVA tagger combines features from different b-taggers:

- Jet Probability for IP
- CSV for combining SV information
- Soft leptons information when available
- Inclusive Vertex Finder to determine Secondary Vertices

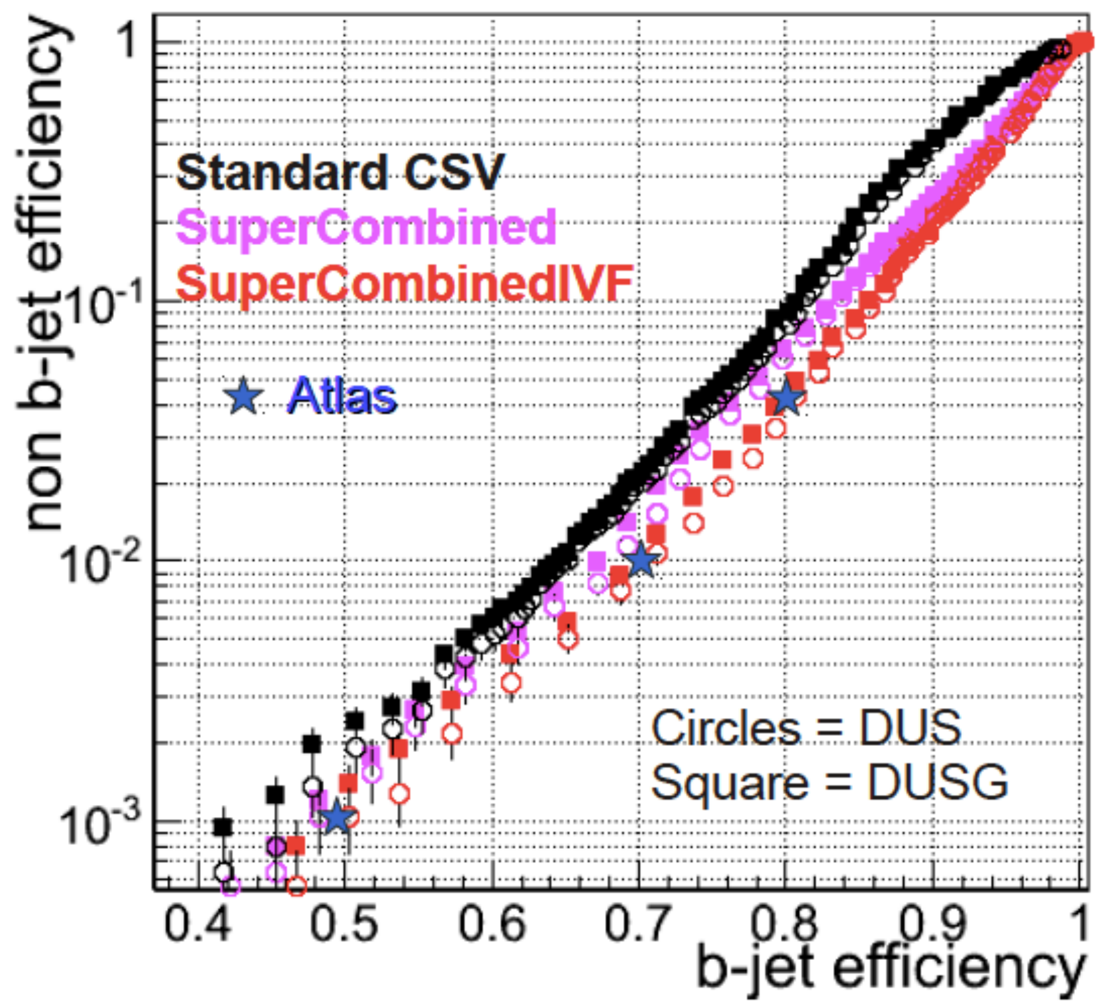

- **2x better fake rejection at 70% efficiency**

- CMVA SF for MC computed as a correction to CSV SF, determined in a $t\bar{t}$ enriched region of data

- ±1σ variations of this scale factors propagates to a 12.7% systematic uncertainty on the signal efficiency

$H(b\bar{b})H(b\bar{b})$: Signal Modeling and Efficiencies

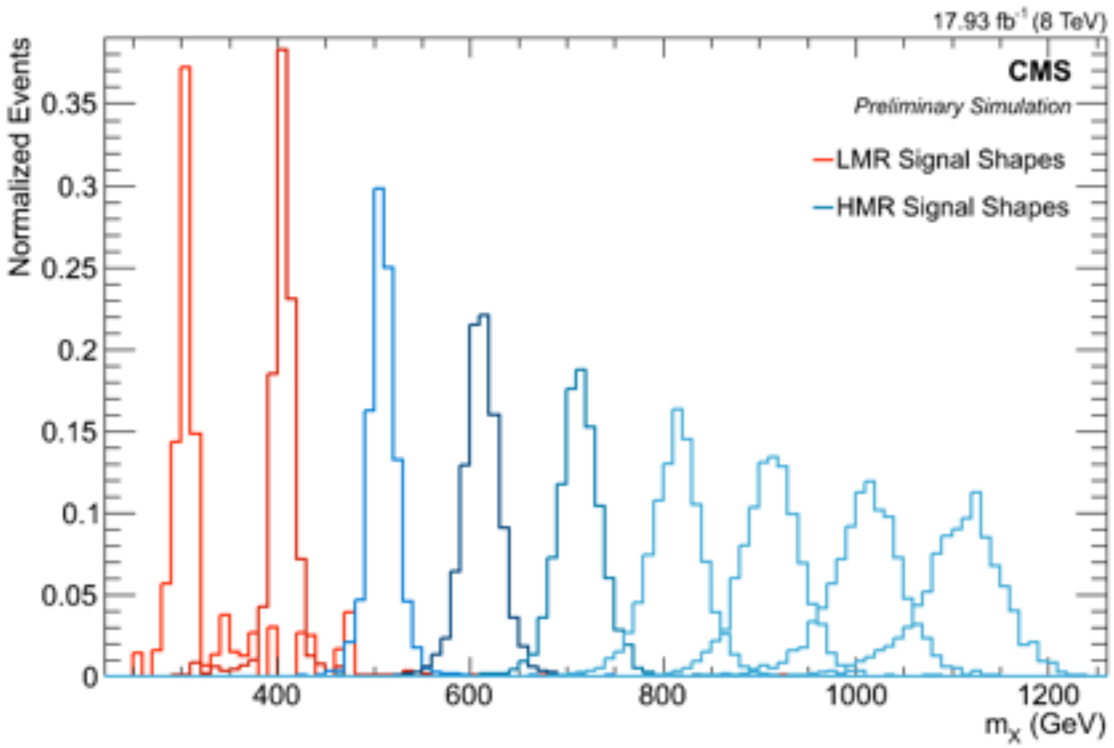

The m_X distribution of signal events after the event selection criteria for each of mass hypothesis. Momenta of b-jets have been corrected by the kinematic constraint to m_H

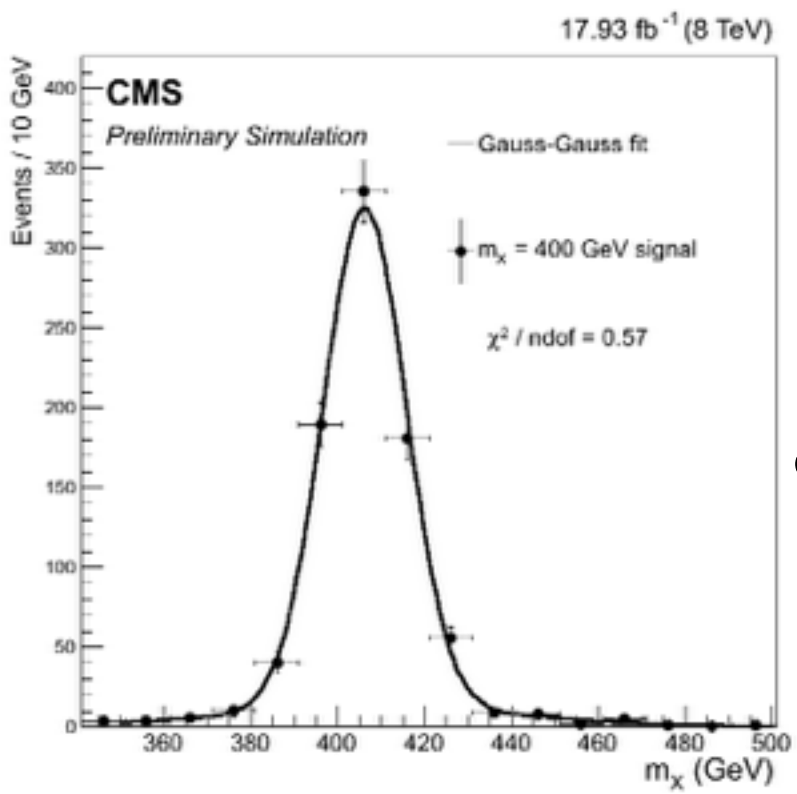

The sum of two Gaussians fitted to the mX= 400 GeV distribution of simulated signal events after the event selection criteria for the Low Mass Regime.

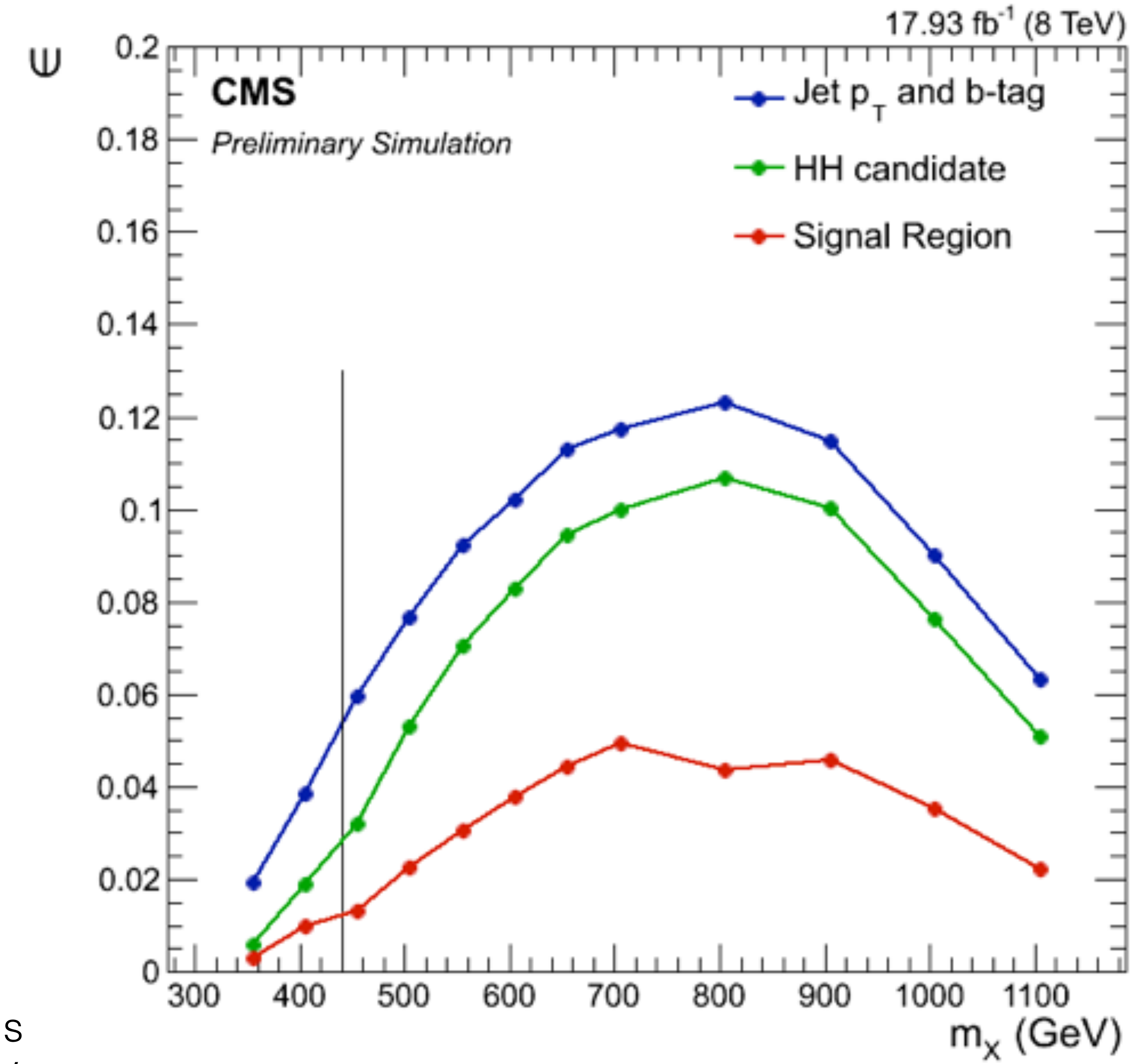

The selection efficiency for X to $H(b\bar{b})H(b\bar{b})$ signal events at different stages of the event selection for each mass hypothesis. The vertical lines represents the transition from the Low Mass Regime and the High Mass Regime as evaluated to optimize the expected significance.

$H(b\bar{b})H(b\bar{b})$: Background Composition

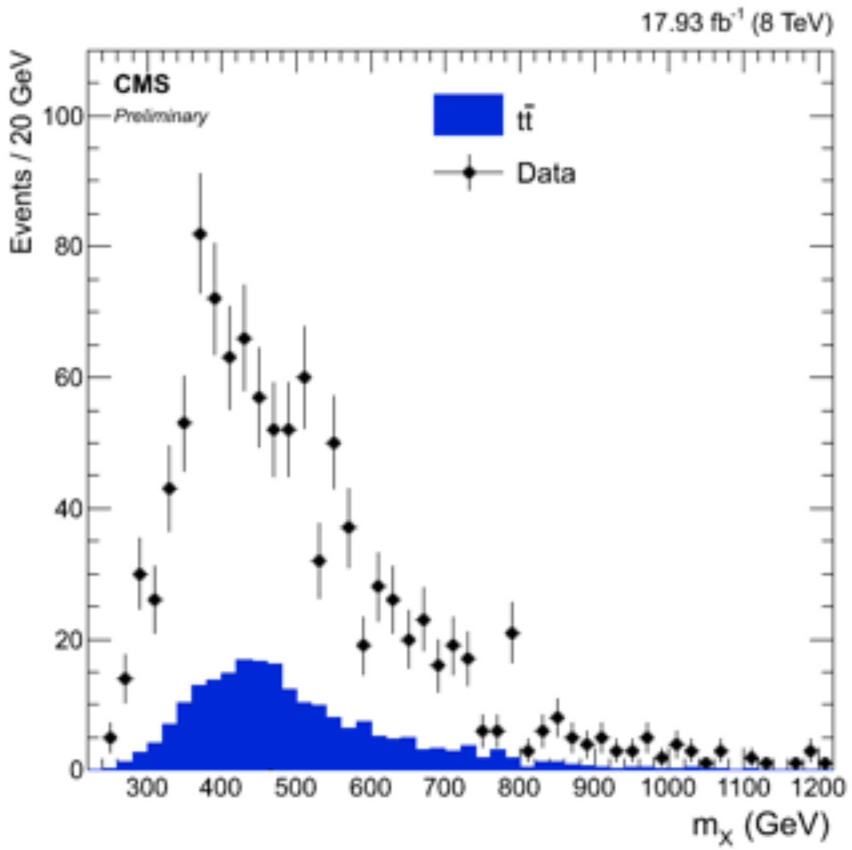

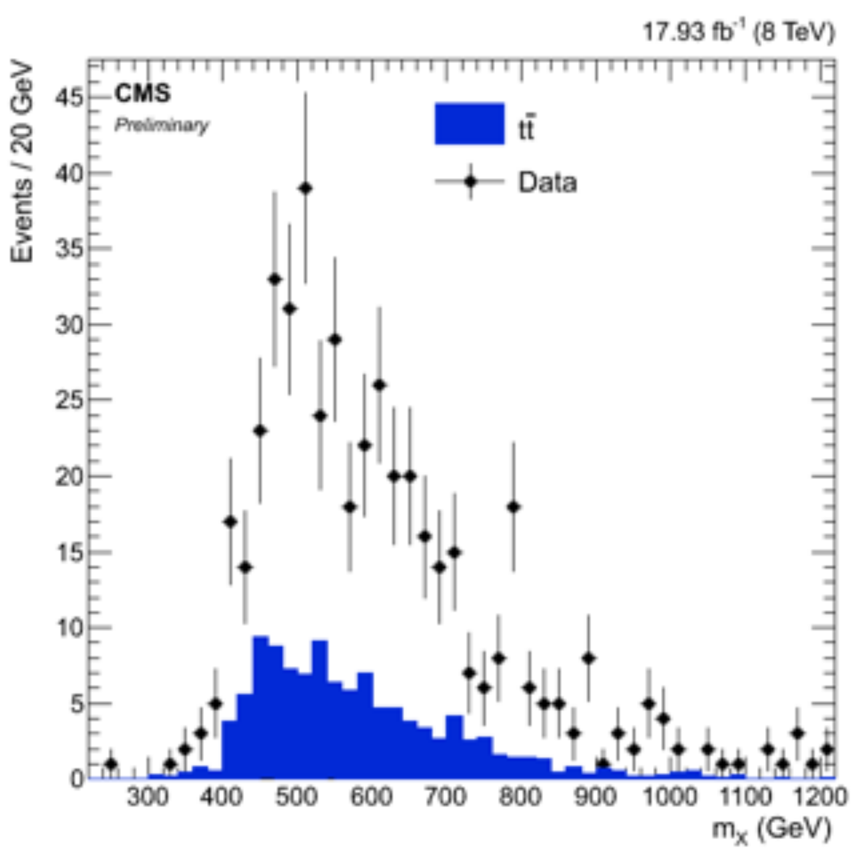

	LMR (%)	MMR & HMR (%)
Z + jets	< 0.1	< 0.04
ZZ	0.003	0.003
ZH	< 0.001	< 0.004
$t\bar{t}$	22	27

The contribution of Z+jets, ZZ, ZH and $t\bar{t}$ to the background after all selection criteria. The remainder of the background comes from QCD multi-jet events

The $t\bar{t}$ composition of the data events in the SR region for the Low Mass Region (top) and the High Mass Region (bottom) as estimated in simulation. All event weights to correct for data/MC differences in pile-up, trigger and b-tagging efficiencies have been applied. Momenta of b-jets have been corrected by the kinematic constraint to m_H.

H($b\bar{b}$)H($b\bar{b}$): $t\bar{t}$ Modeling

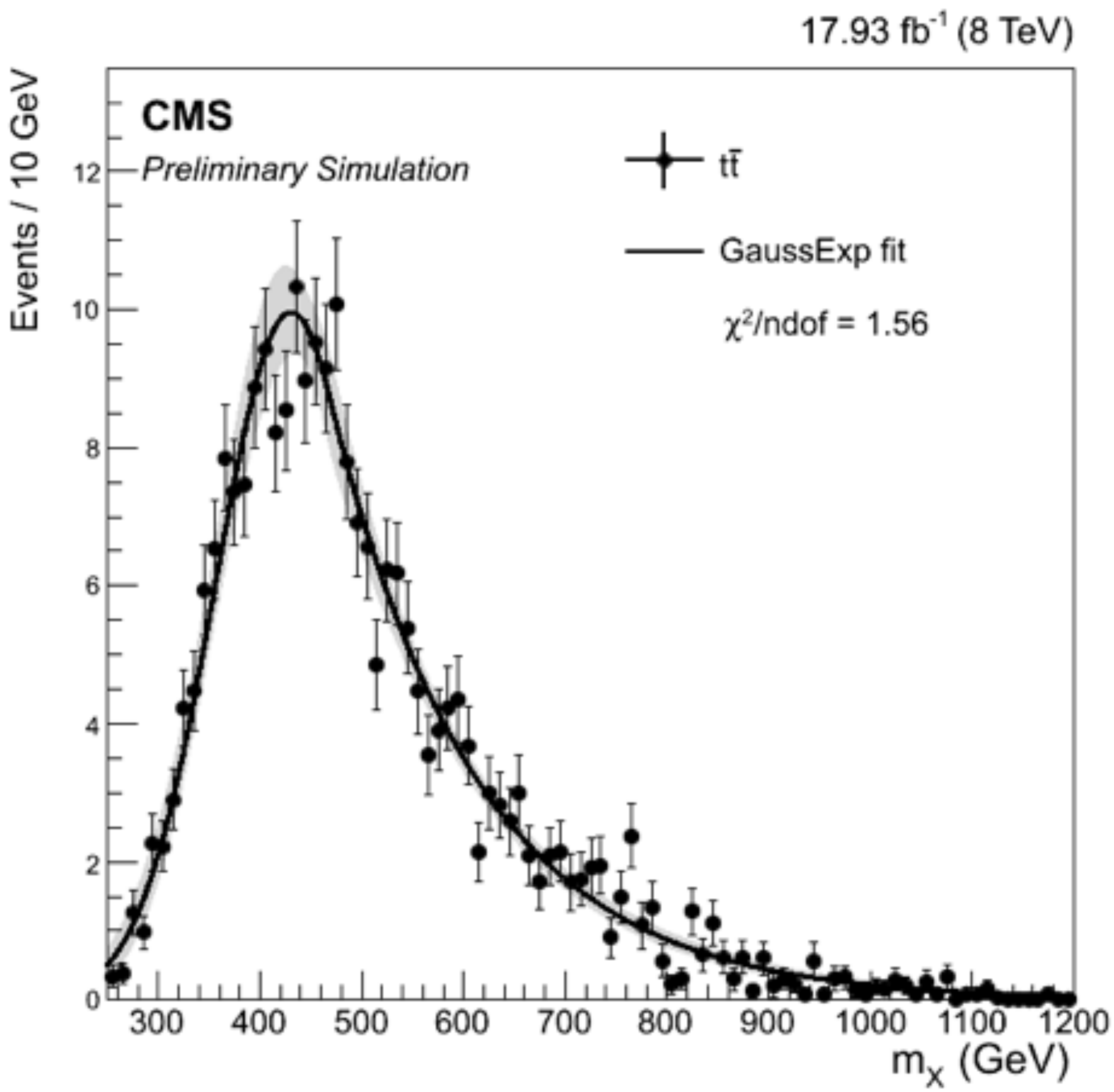

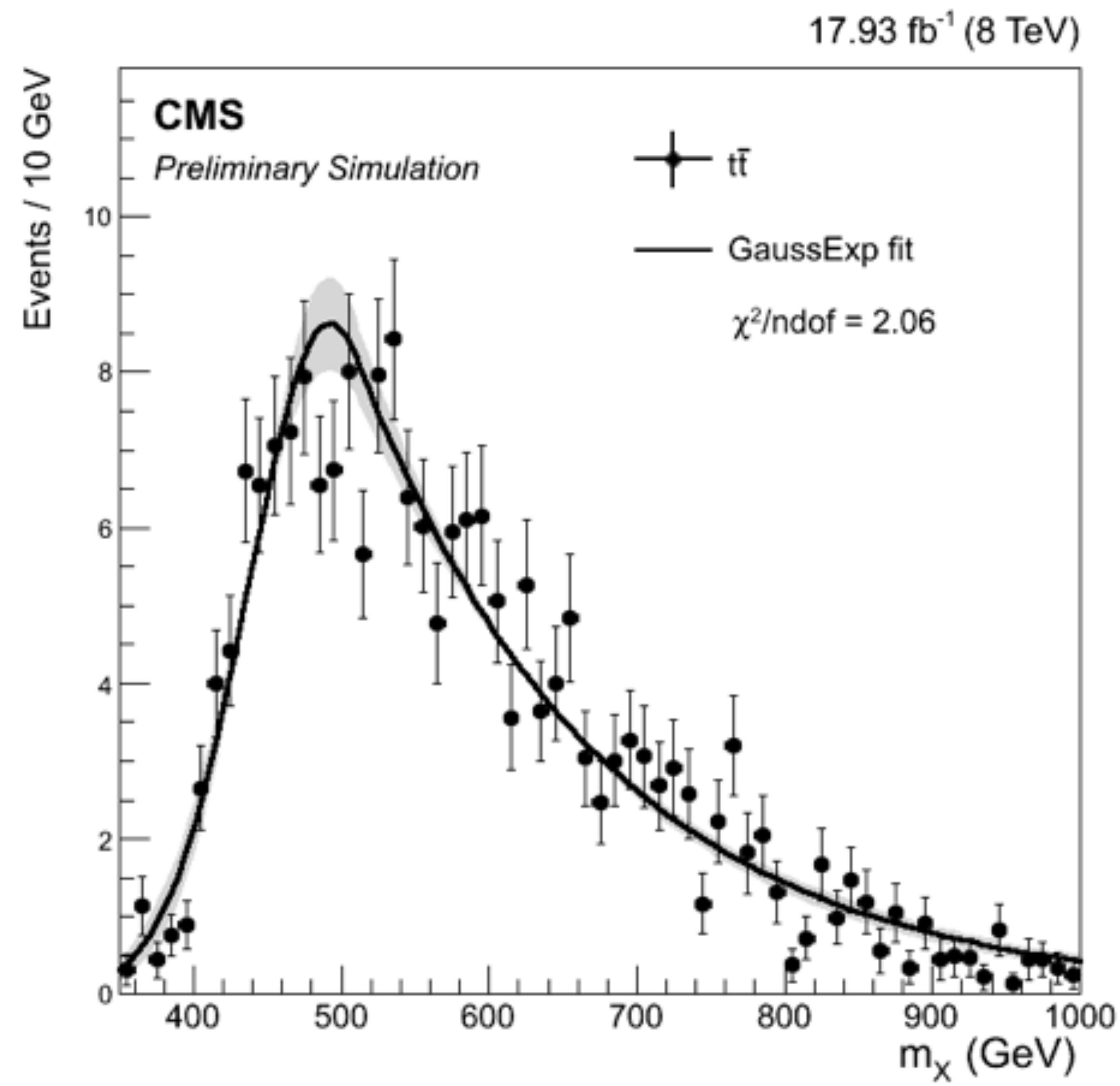

The m_X of simulated ttbar events after the event selection criteria for the Low Mass Region (left) and High Mass Region (right). The distributions are fitted to the GaussExp function

$H(b\bar{b})H(b\bar{b})$: QCD Multi-jet Modeling

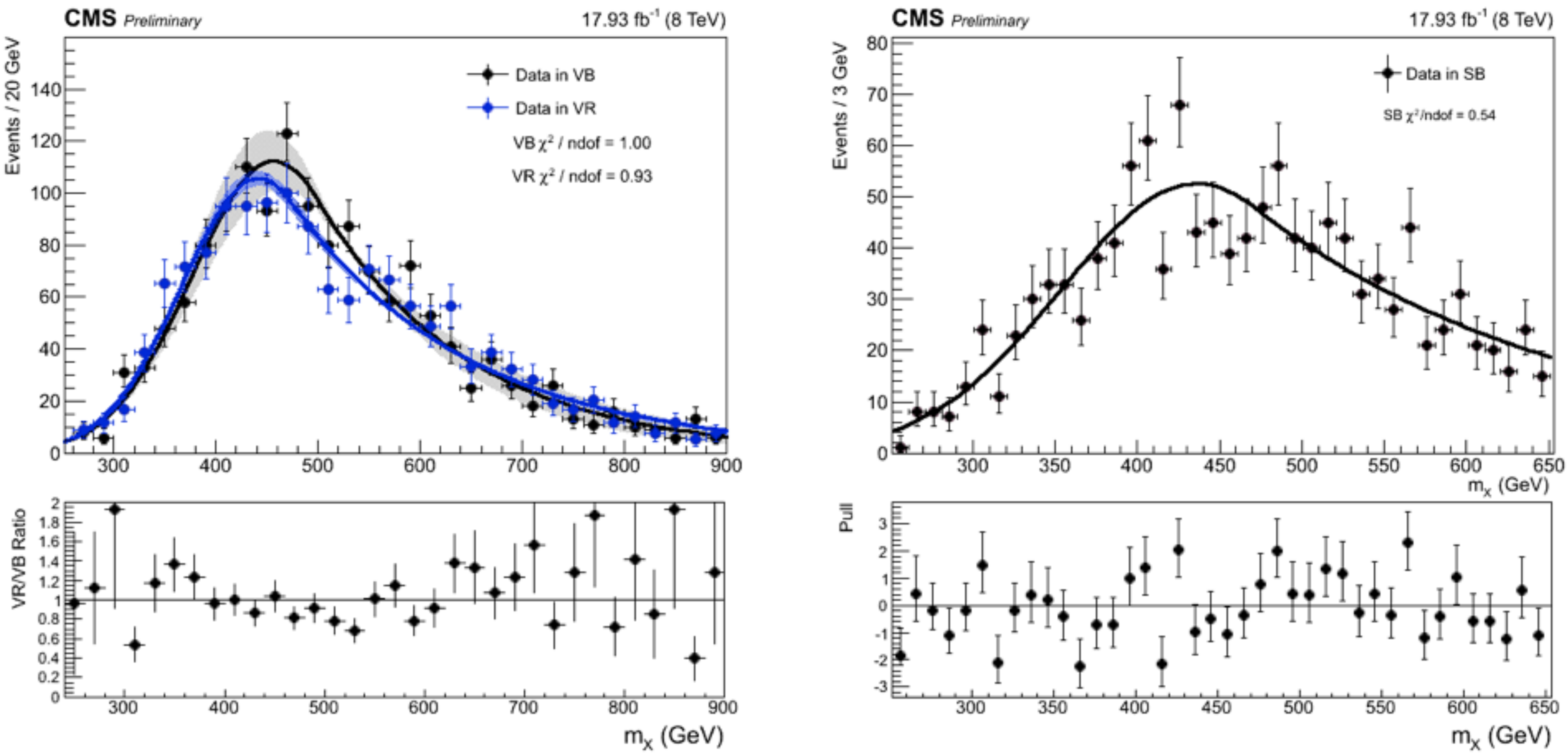

Low Mass Region: The m_X distributions of the QCD multi-jet component of the background in the Validation Region & Sideband (VR & VB) on the left and the Signal Region Sideband (SB) of LMR. The distributions are fitted to the GaussExp function.

$H(b\bar{b})H(b\bar{b})$: QCD Multi-jet Modeling

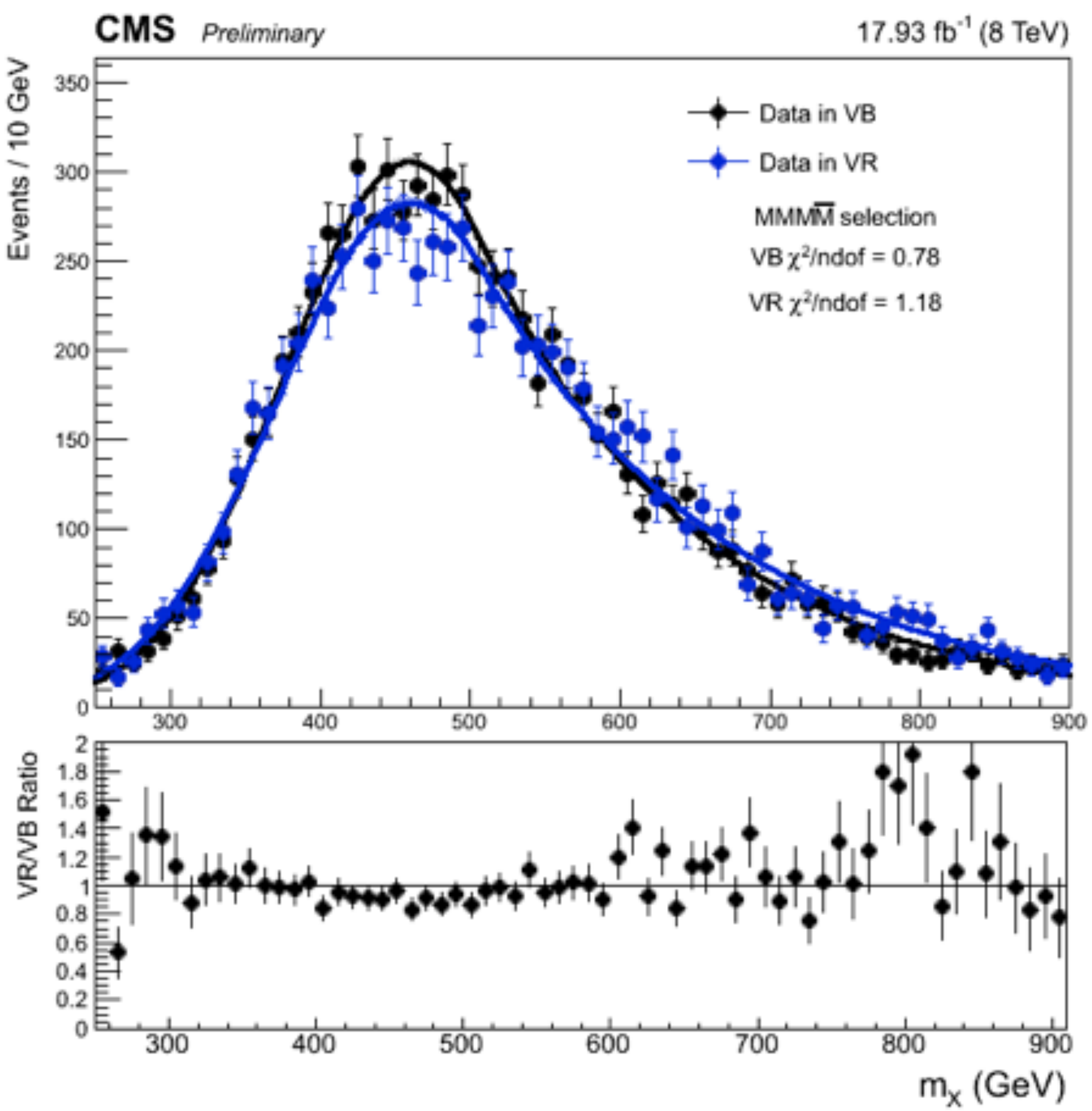

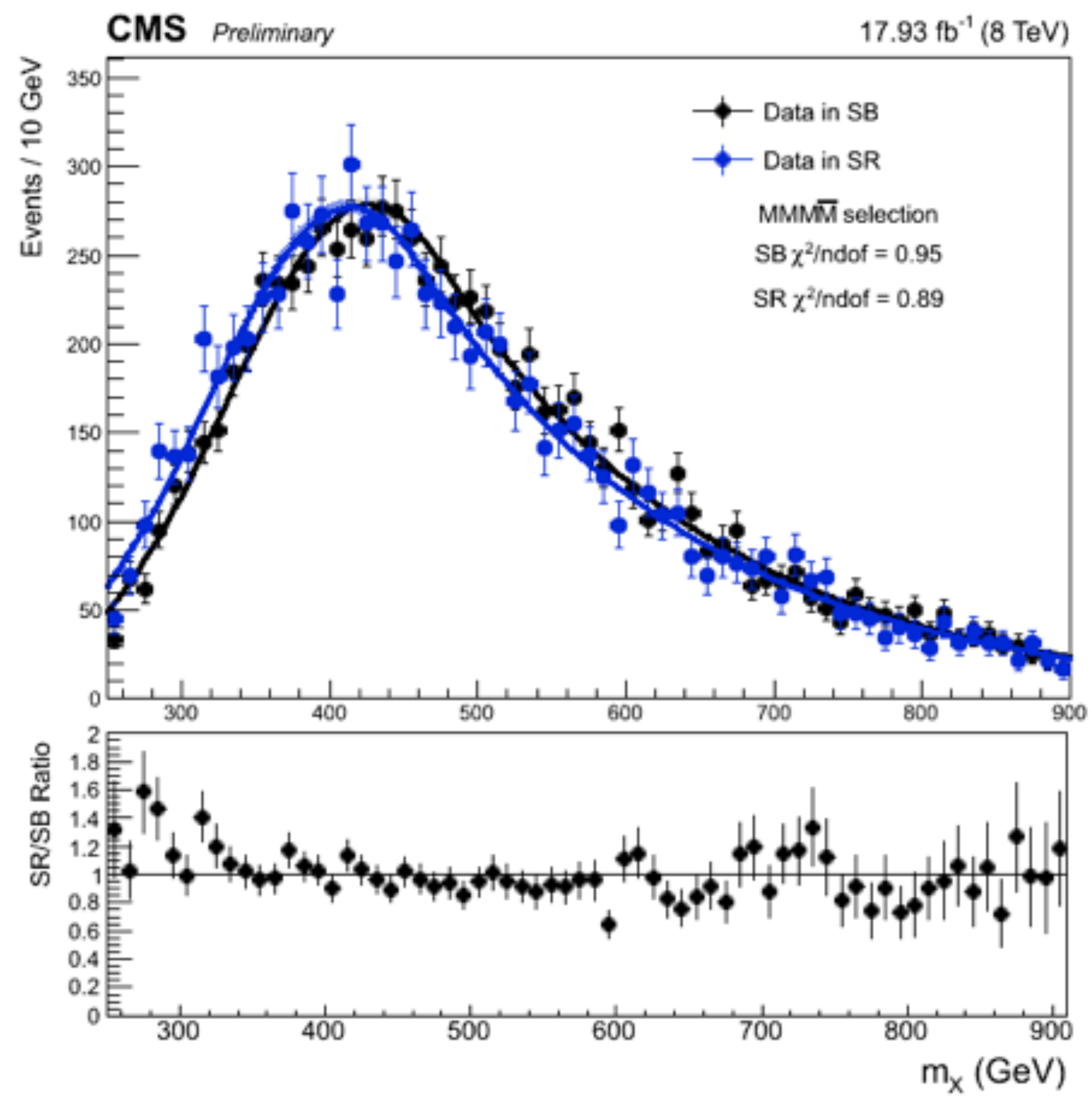

Low Mass Region, anti-btag Control Region: The m_X distributions of the QCD multi-jet component of the background in the Validation Region & Sideband (VR & VB) on the left and the Signal Region Sideband (SB) of LMR. The distributions are fitted to the GaussExp function.

$H(b\bar{b})H(b\bar{b})$: QCD Multi-jet Modeling

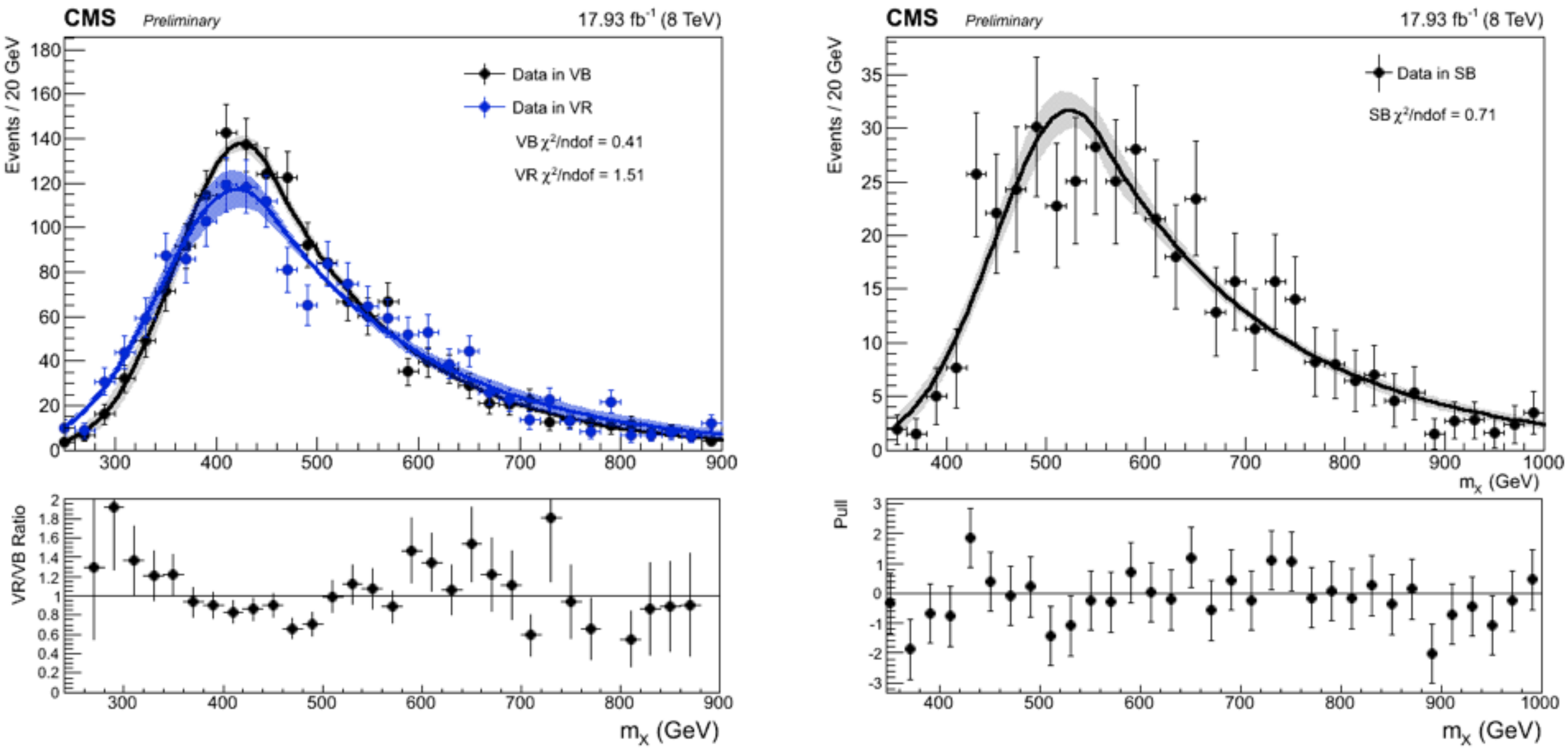

Medium Mass Region: The m_X distributions of the QCD multi-jet component of the background in the Validation Region & Sideband (VR & VB) on the left and the Signal Region Sideband (SB) of LMR. The distributions are fitted to the GaussExp function.

$H(b\bar{b})H(b\bar{b})$: QCD Multi-jet Modeling

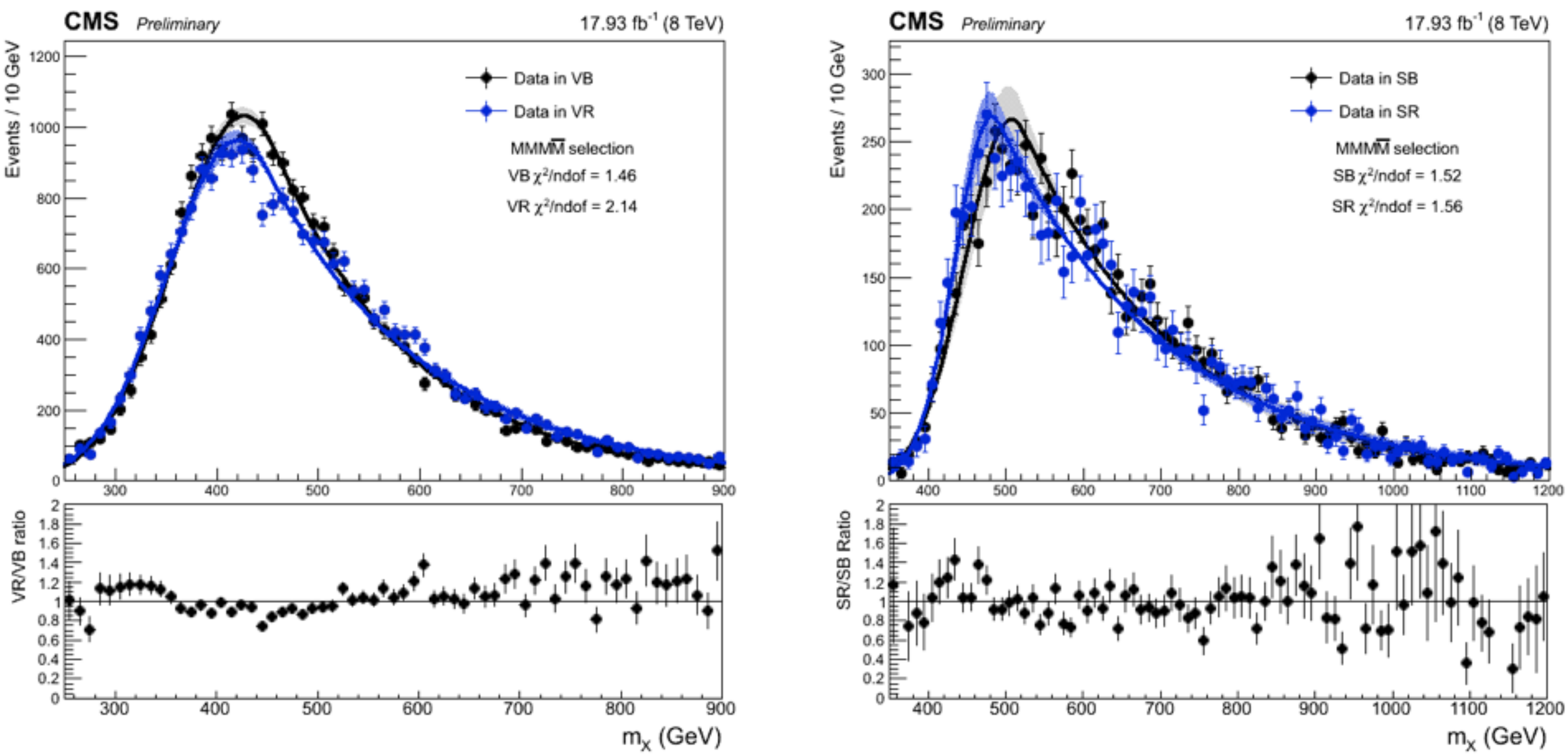

Medium Mass Region, anti-btag Control Region: The m_X distributions of the QCD multi-jet component of the background in the Validation Region & Sideband (VR & VB) on the left and the Signal Region Sideband (SB) of LMR. The distributions are fitted to the GaussExp function.

H($b\bar{b}$)H($b\bar{b}$): QCD Multi-jet Modeling

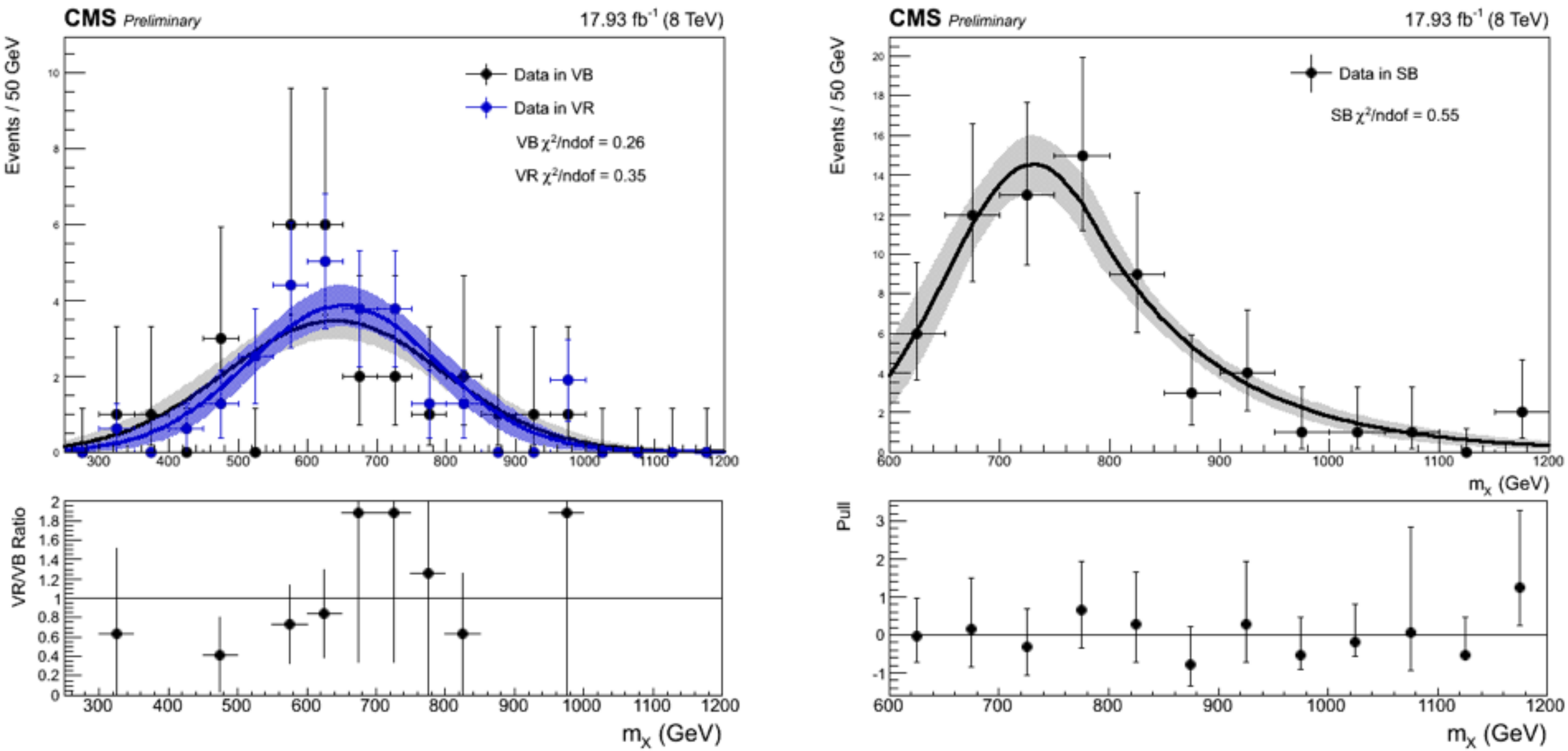

High Mass Region: The m_X distributions of the QCD multi-jet component of the background in the Validation Region & Sideband (VR & VB) on the left and the Signal Region Sideband (SB) of LMR. The distributions are fitted to the GaussExp function.

$H(b\bar{b})H(b\bar{b})$: QCD Multi-jet Modeling

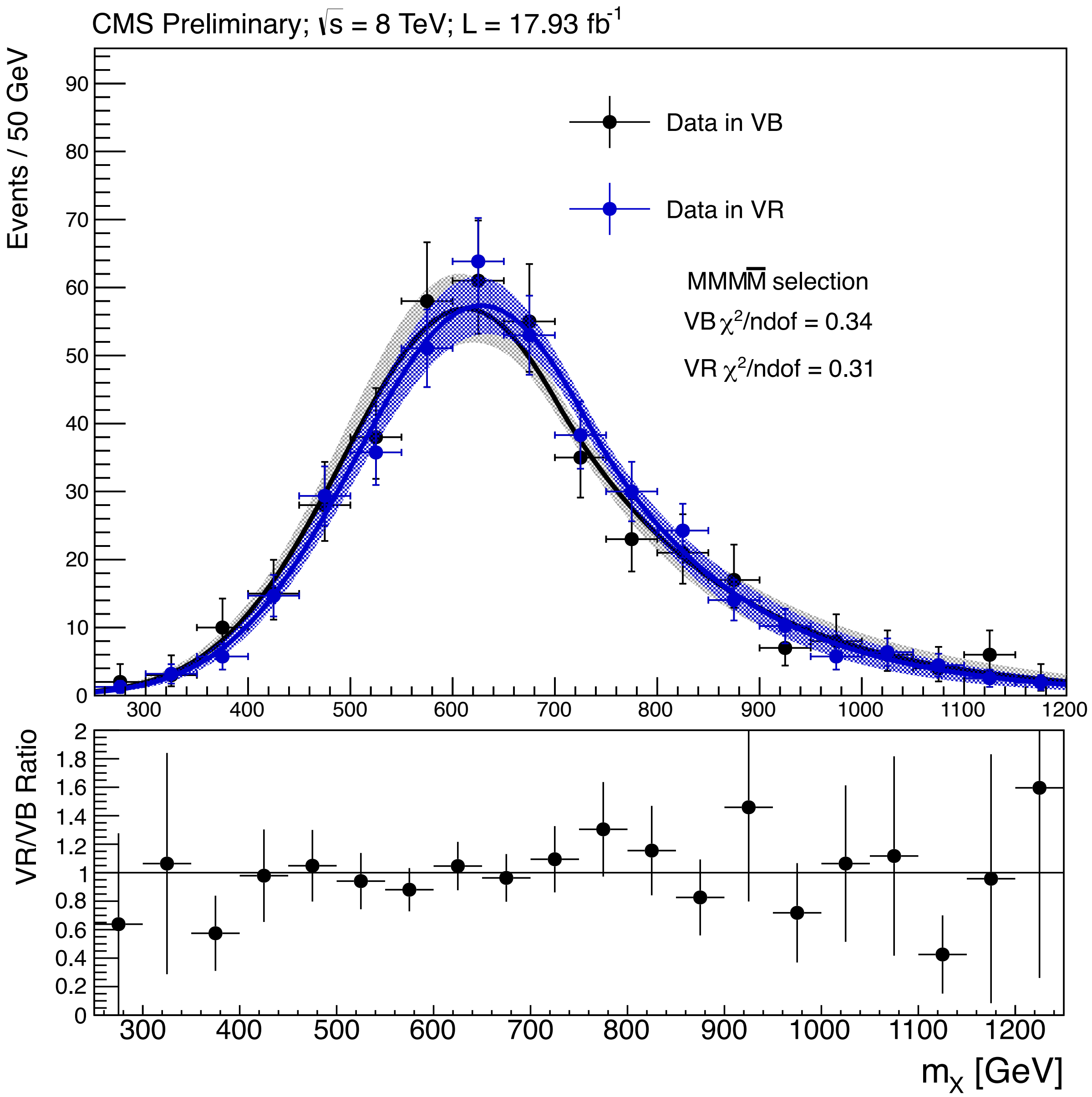

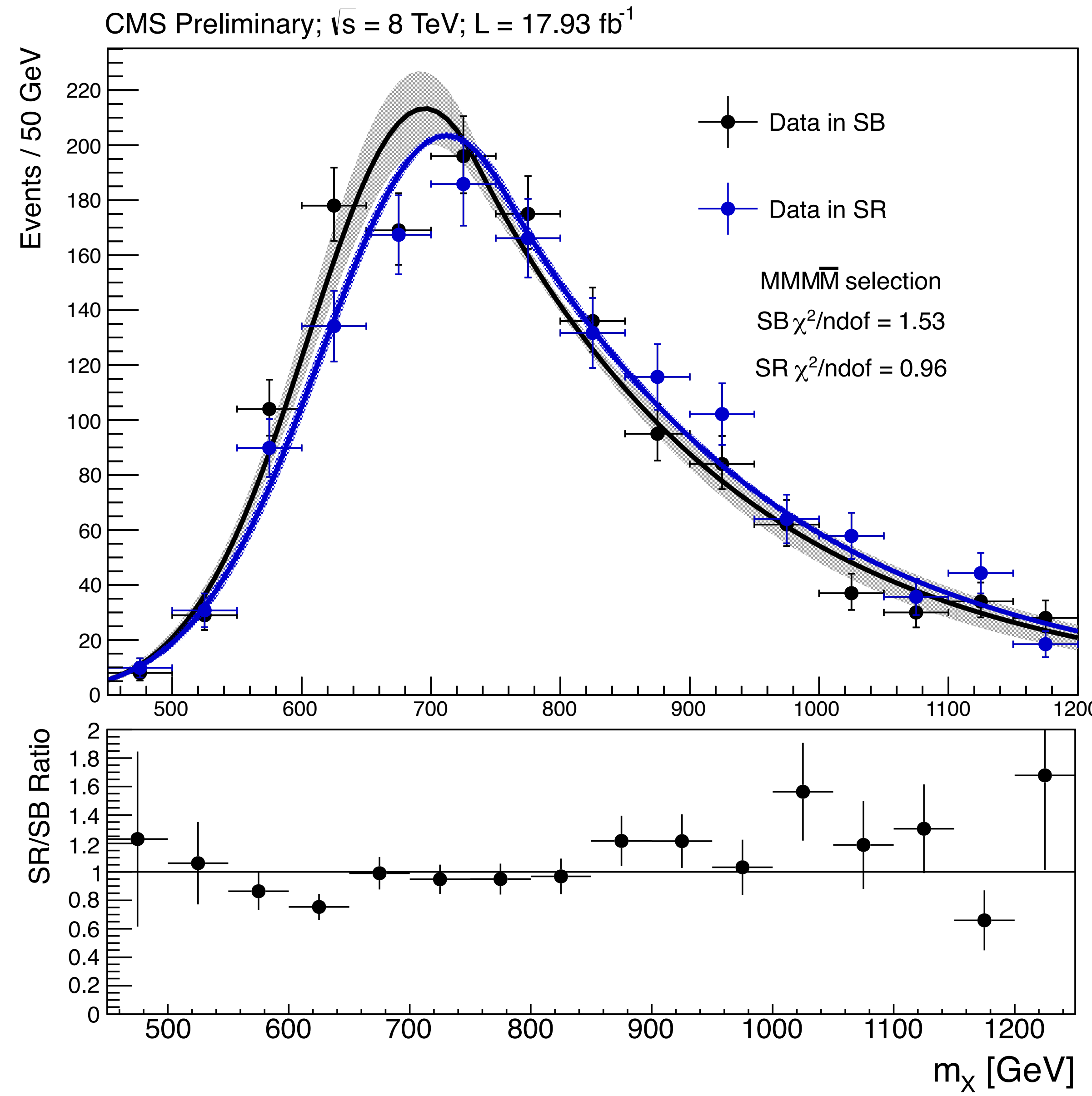

High Mass Region, anti-btag Control Region: The m_X distributions of the QCD multi-jet component of the background in the Validation Region & Sideband (VR & VB) on the left and the Signal Region Sideband (SB) of LMR. The distributions are fitted to the GaussExp function.

$H(b\bar{b})H(b\bar{b})$: Unblinded Data

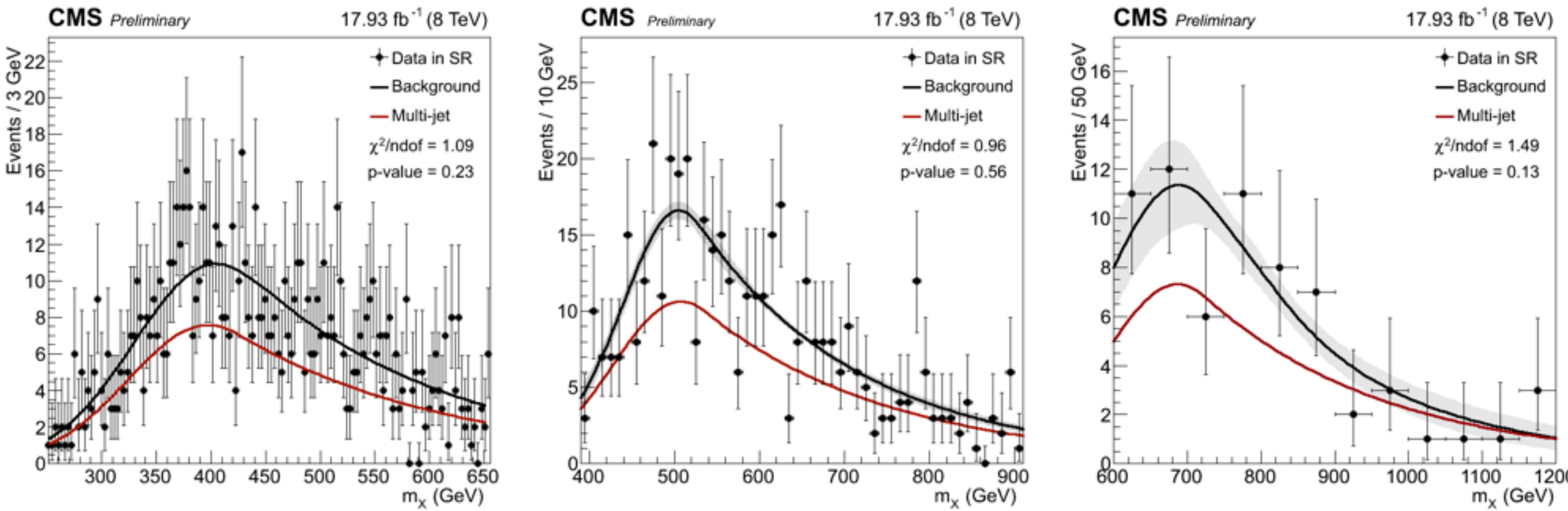

- Background-only fit shown to data in LMR, MMR and HMR. Red curve is the QCD multi-jet contribution. Black curve is QCD multi-jet + tt background.

- Shaded region corresponds to 1σ variation of parameterized fit. Number of degrees of freedom corresponds to the number of fit parameters subtracted from the number of bins in histogram

No clear deviation from background-only hypothesis. Compute upper limits.

$H(b\bar{b})H(b\bar{b})$: Radion Exclusion

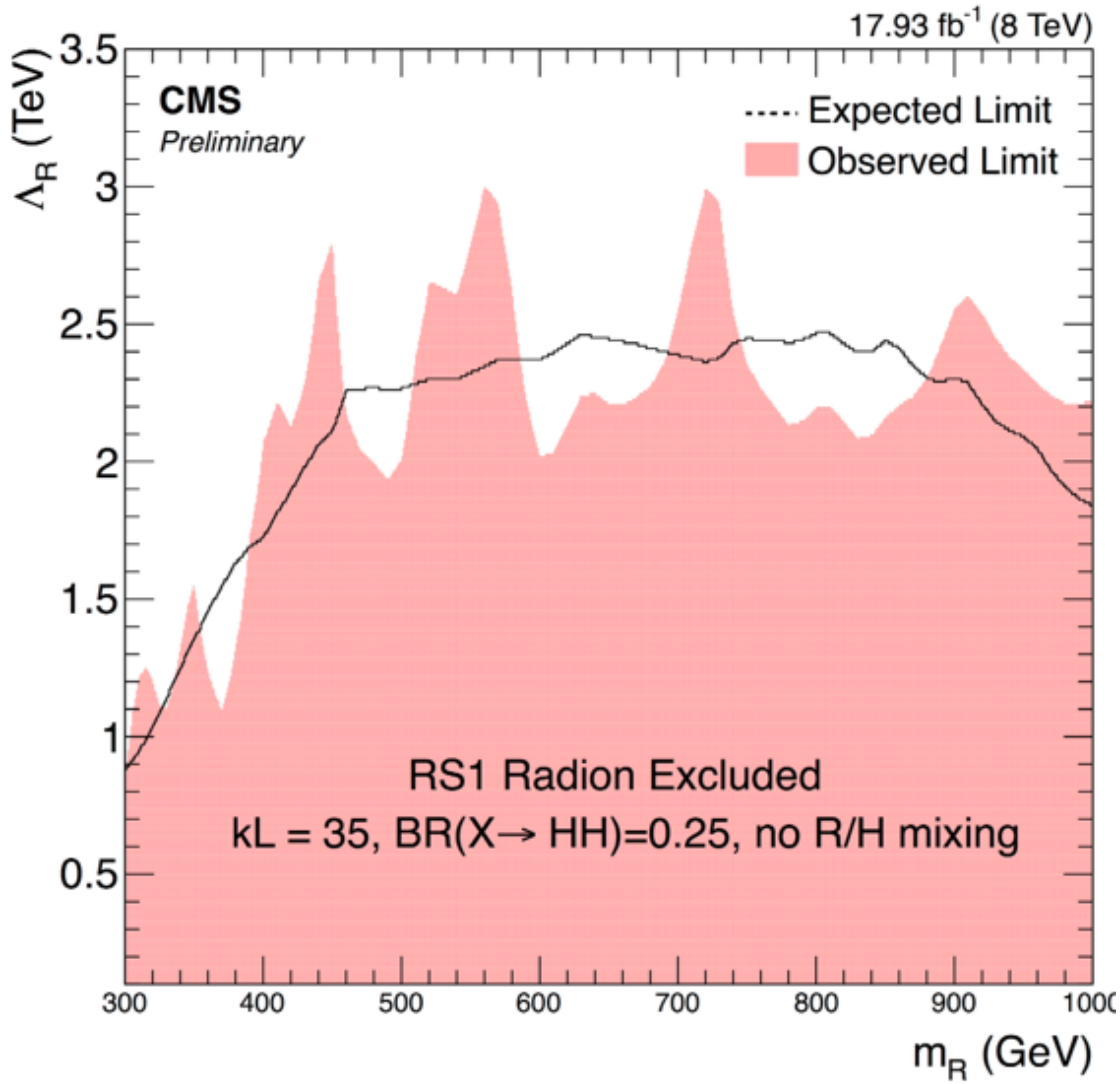

Cross sections of the radion assume *k*-factor for top-loop in gluon-fusion production of R to be identical to that of Higgs production. Also, $Br(R \rightarrow HH) = 0.25$

H($b\bar{b}$)H($b\bar{b}$): Graviton Exclusion

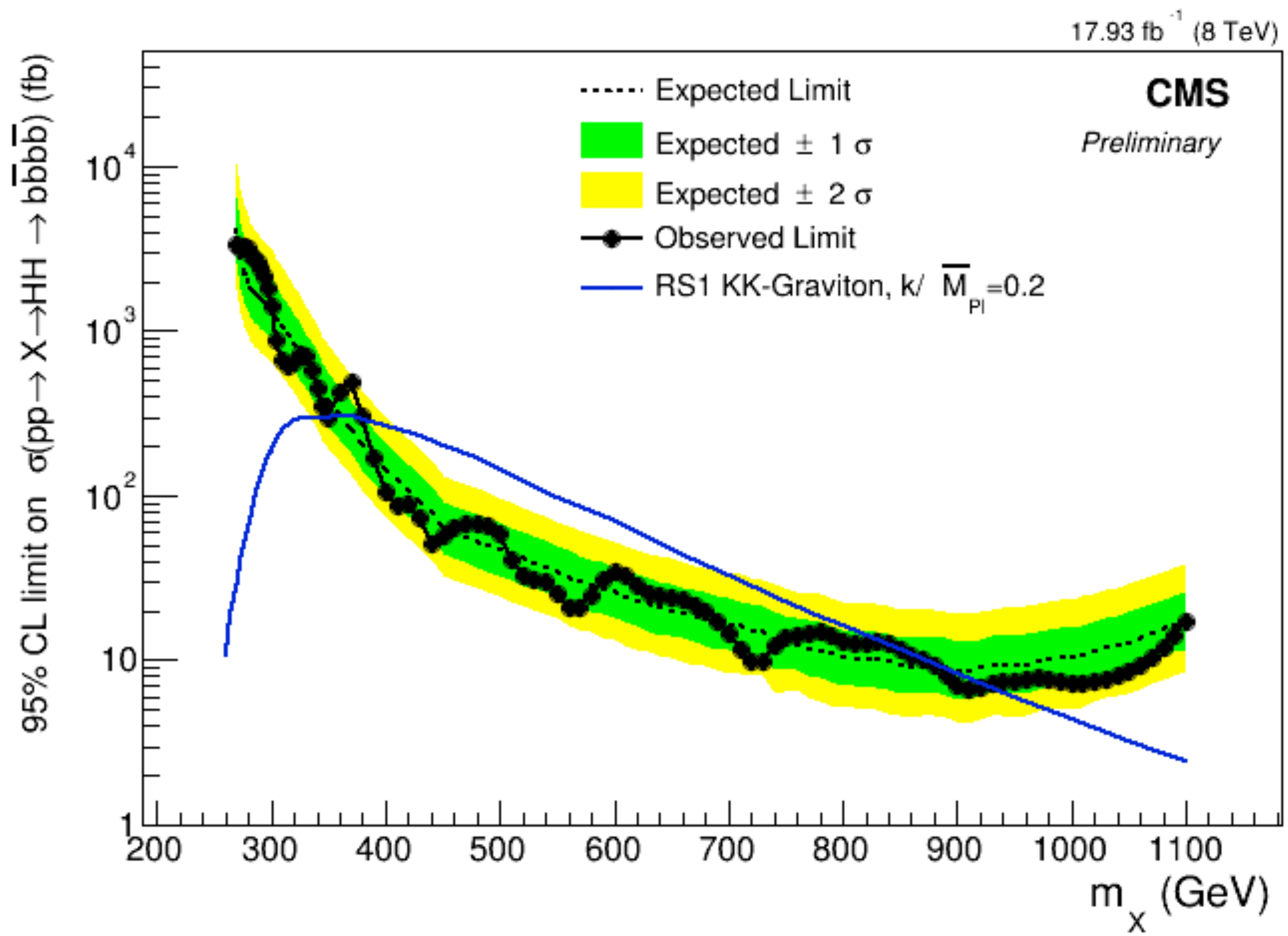

The results are interpreted as upper limit on the production cross section for a spin-2 particle. Signal efficiency is larger than for the spin-0 hypothesis. This results in the exclusion of a smaller cross section. The observed and expected upper limits on the cross section for a spin-2 X to H(bb)H(bb) at 95% confidence level using data corresponding to an integrated luminosity of 17.93/fb at sqrt{s} = 8 TeV using the asymptotic CLs method are shown. Theoretical cross sections for the RS1 KK-Graviton decaying to four b-jets via Higgs bosons are overlaid.

WED scenario: kL = 35, k/M_{Pl}=0.2

CMS double-Higgs: Graviton Exclusion

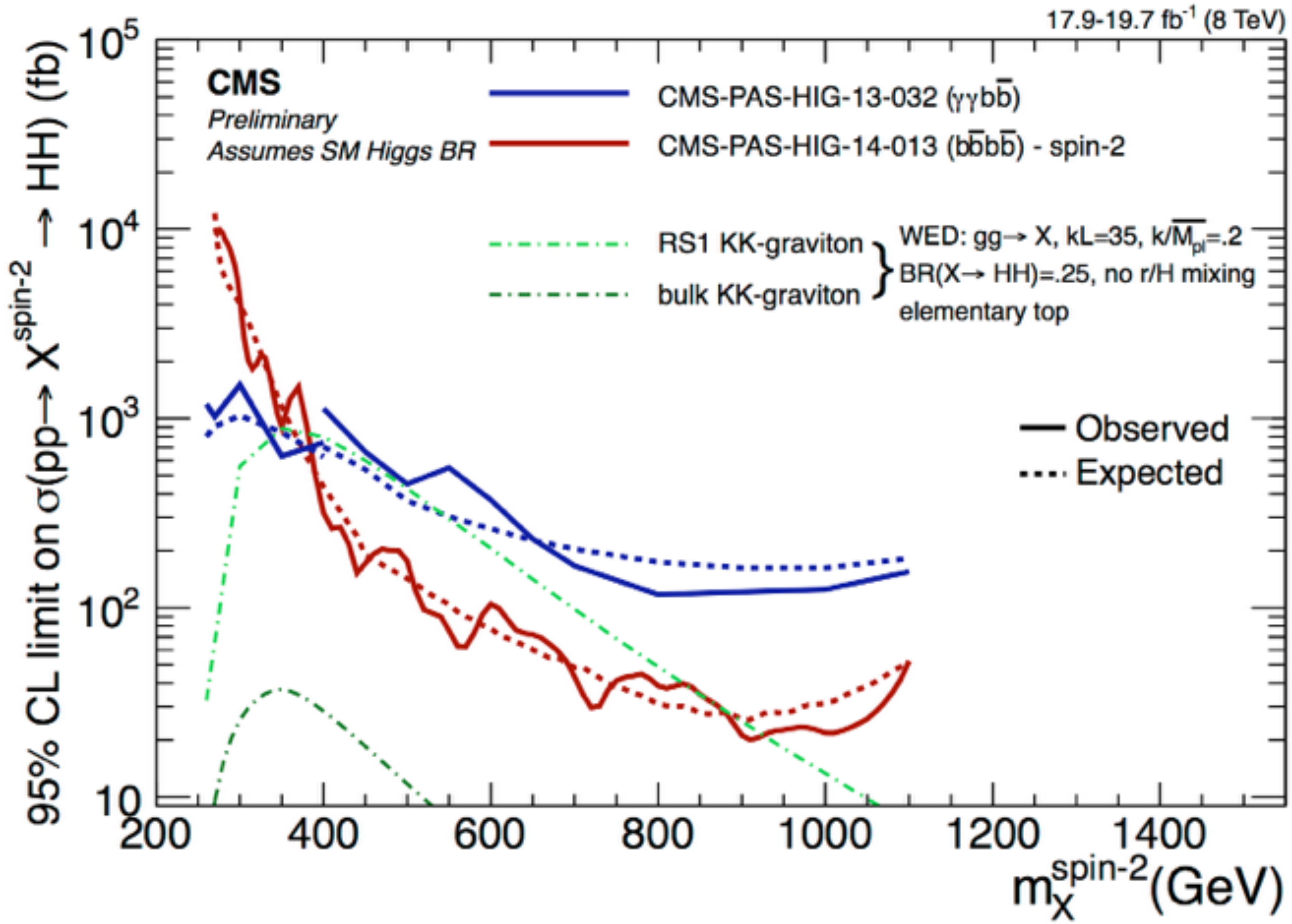

The expected and observed upper limit of spin-2 X to HH production at 95% CLs provided by combining the searches performed by the CMS experiment looking at the $b\bar{b}b\bar{b}$ (HIG-14-013), $b\bar{b}gg$ (HIG-13-032) final states.

WED scenario: kL = 35, k/M_{Pl}=0.2